Feedbacks between river morphodynamics and overbank flooding

Shelby Ahrendt

A dissertation
submitted in partial fulfillment of the
requirements for the degree of

Doctor of Philosophy

University of Washington

2023

Reading Committee:

Alexander R. Horner-Devine, Chair

Astrid Blom

Brian D. Collins

Program Authorized to Offer Degree:
Civil and Environmental Engineering

University of Washington

Abstract

Feedbacks between river morphodynamics and overbank flooding

Shelby Ahrendt

Chair of the Supervisory Committee:
Alexander R. Horner-Devine
Civil and Environmental Engineering

River morphodynamics (the way rivers adjust their shape and form) can affect overbank flooding if changes to cross-sectional area or roughness reduce the flow conveyance capacity of the channel. Extreme floods can also cause drastic adjustments to river morphology on relatively short timescales. The potential simultaneity of these processes raises the question: how do flood dynamics and river morphology co-evolve? Additionally, are river morphodynamics a substantial contributor to flood hazards?

Existing research on channel adjustment and recovery during a flood hydrograph has been limited by a paucity of field data recording river bathymetry during peakflows. Additionally, the computational expense of morphodynamic modeling has challenged the application of models to investigate feedbacks between morphodynamic river adjustments and flood hazard. This thesis seeks to fill the gaps in scientific knowledge about feedbacks between morphodynamics in flooding by (I) examining the importance of river morphodynamics in modifying flood hazards; (II) explaining causes of spatial variation in morphodynamic response to floods; and (III) investigating interactions between flood hydraulics and river morphodynamics during a flood event in a location with persistent overtopping during peak flows.

Part I investigates long-term changes to river channel conveyance in northwest Washington State, U.S., and compares the relative importance of these to shifts in moderate

flood streamflow using 50 long term river gaging datasets. River conveyance is unsteady in most rivers in western Washington, but its importance for modifying flood risk depends on the style of conveyance response. Conveyance responses can be linear, oscillating, punctuated by sudden sediment-supply events or influenced by flow regulation. The relative behavior and importance of conveyance and streamflow variability depends on flow regulation; moderate flood streamflows have increased in unregulated rivers, but this trend is suppressed and/or reversed in regulated rivers. Flow regulation does not necessarily reduce total flood hazard, because downstream channel conveyance losses can exceed reductions in flood flows. Part I concludes that channel conveyance unsteadiness is an important modifier of total flood hazard variability and incorporating this factor may improve flood risk predictions.

Part II explains the spatial variation of river bed response during floods and recovery during low flows in relation to floodplain geometry and topography using 20 years of bi-weekly bathymetry data from the Waal River, an engineered channel in the Netherlands. Bed response and recovery to peak flows are a result of floodplain geometry and topography that forces flood flows to enter or exit the main-channel including: 1) streamwise changes in floodplain width, and 2) topographic routing of floodplain flow that causes flow to plunge into and out of the main-channel during floods. The latter factor is primarily important for spatial variation in main-channel bed response and recovery to floods. Where floodplain flows enter the main-channel, erosion (deposition) occurs during floods (low flows) and where floodplain flows exit the main-channel, deposition (erosion) occurs during floods (low flows). Part II concludes that bed elevation within and between flood events may be understood by floodplain topography and geometry that results in flow exchange between the main channel and floodplain.

Part III applies a hydro-morphodynamic model to analyze hydraulic and morphodynamic feedbacks during the November 2021 flood in the Nooksack River, Washington

State–a system with persistent overbank flooding during peak flows at an historic avulsion node. Cross-sectionally averaged patterns of modeled bed elevation change suggest that meter-scale adjustments in bed elevation occurred during the flood. Bed elevation changes in the main-channel are commonly located where flow spatially accelerates or decelerates during the flood; in particular, flow deceleration is observed at locations of overbank flooding. At the historic overflow location, bed deposition co-occurs with abrupt flow deceleration related to overbank flooding. Part III demonstrates that the hydrodynamics of overbank flooding can cause channel adjustments that affect channel conveyance capacity for future floods.

These results augment our understanding of the importance of river morphodynamics in modifying overbank flooding and the feedbacks between overbank flooding and river bed response. The thesis concludes with a suite of possible questions and future research directions relating to: 1) the preferential style of morphodynamic adjustment to peak flows, 2) river bed response to climate variability, 3) feedbacks between floods, sediment supply, and channel response, and 4) compound channel structure as it relates to morphodynamic response to floods. Overall, this work furthers our understanding of fluvial response to floods with implications for improving flood safety of river-bounding communities.

TABLE OF CONTENTS

Page

LIST OF FIGURES

ACKNOWLEDGMENTS

I am profoundly lucky to have had so many support systems throughout this graduate research journey. This section would arguably be as long as the subsequent dissertation if it detailed all who shared seeds of wisdom and shoulders to cry on along the way.

My UW advisor, Alex Horner-Devine, is a tremendously talented mentor–I have so appreciated the chance to tackle riverine flood questions, face the challenges of research and academia, and grow as both a scientist and individual under his unwavering guidance. Alex–thank you for your kindness, patience, and support. I am so grateful for the opportunity to work with you, and I will always be game for roller-skiing up snowy canyons on conference mornings.

The UW Environmental Fluid Mechanics Group has been a supportive family during my time in graduate school. From afternoon gummy-bears in the office, to 11:30 Thursday seminars, to summer barbecues in the backyard of Harris Hydraulics–I would have never guessed that moving so far from my Minnesotan roots would have felt like moving home.

Many notes of thanks to my committee members: Brian Collins–thank you for teaching me the geologic history of the Puget Sound area, my regional geomorphic intuition is deeeply indebted to you; Jessica Lundquist–thank you for illuminating the art of stream-flow statistics; Allison Pfeiffer–thank you for paving my way into 'stage-residual-analysis' as a green graduate student; Alison Duvall–thank you for your excellent geomorphology courses which sparked my curiosity in river-hillslope interactions; Kate Huntington–thank you for jumping onboard with your keen insights into rivers, morphodynamics, and floods.

My warmest gratitude to Astrid Blom, who welcomed me into the Water Lab at TU

Delft in the Netherlands for a year abroad. Astrid–thank you for sharing your wealth of river engineering and sediment transport expertise, and for supporting me as a young scientist. From designing conceptual figures to hiking the Continental Divide, I have so appreciated your support over every rock in the trail. And to the wonderful humans of the TU Delft Water Lab–thank you for making life below sea level so darn fun.

To my late mentor Nirnimesh Kumar, who brought a bounty of light, laughter, and generosity wherever he went: thank you for your willingness and excitement to immerse yourself in the dingiest corners of my research. Be it afternoons coding hydrologic analyses at the round table in Harris or re-writing ocean-based spectral scripts for application to river beds, your passion and dedication will live on in the hearts of those you advised, taught, and collaborated with. We miss you, Nirni.

This work was supported by funding from the National Science Foundation as part of a PREEVENTS project and the Cascadia Coastlines and People project. The Valle Scholarship at the University of Washington supported the first year of my PhD. Nine months of funding were provided by a Fulbright fellowship sponsored by the Netherlands-America Foundation (NAF) for dissertation research abroad.

A particular thanks to the PREEVENTS team: Chapter 4 would not have been possible without Jacob Morgan, developer of the Delft3D Nooksack River model, and Wuming Ni who tirelessly ran simulations. Erkan Istanbulluoglu, Jeff Keck, Eli Schwat, & Dan Scott–thank you for the constructive science conversations that contributed to this work.

The Community Surface Dynamics Modeling System (CSDMS) team has been integral to my growth as a coder, and generously provided support for a summer in Boulder, CO through the OpenEarthscape visiting Summer Scholars program. Many thanks to Greg Tucker, Eric Hutton, Mark Piper, Irina Overeem, and Benjamin Campforts for their geomorphic wisdom and computational support in my modeling efforts: it is to you all that I owe my first git 'push' & 'pull'.

Streamflow data, digital elevation models, and river data were supplied by the U.S Geological Survey (Chs. 2 & 4) and the Dutch Water Ministry, Rijkswaterstaat (Ch. 3). To Scott Anderson at the Washington Water Science Center, along with Pepijn Van Denderen, and Ralph Schielen of HKV Consultants and Rijkswaterstaat in the Netherlands–a special thanks for your assistance with data access and thoughtful scientific insights.

Unending thanks to my family. To my parents–thank you for instilling my senses of adventure and independence, and for being my forever cheerleaders. I am so fortunate that your dream of a life in the Minnesota northwoods led to the coolest backyard wilderness a kid could ever hope to wonder about: my childhood questions about water and rocks are the foundation of those I get to explore in my research today. To my grandparents, Jane and Sheldon–you guys have humongous hearts and an unending capacity for love; what a treasure it's been to grow up with such cool and caring role models. To Kay Johnson & Joe Zunt–what a treat it was to spend a little slice of life together in Seattle; thank you for sharing your home. To my brother, Dan–I so appreciate both your humorous cackle and your sage wisdom on the rockier parts of life; thank you for the phone calls commiserating with my writing struggles and for the lessons on proper use of a cocktail shaker. To my partner, Garret–thank you for being my compassionate supporter and for reminding me of my basic needs when I get too deep in the data (e.g. food, water, fresh air, a hug). I am so lucky to have such a kindred soul with whom to trek through life.

LAND ACKNOWLEDGEMENT: In writing this dissertation and conducting this research, I have lived and worked on the unceded ancestral lands of of the Coast Salish peoples, including the tribes and bands of the Duwamish, Puyallup, Suquamish, Tulalip and Muckleshoot nations. These people's rich tradition of teaching through stories predate geologic investigations of this region; in some cases, their oral histories provide some of the only records of historic geomorphic events including volcanic lahars, river avulsions, and major floods. I honor that this way of knowing and passing knowledge is valuable in ways that supercede science. I recognize the Coast Salish peoples, their traditions, and the land with gratitude.

Chapter 1
INTRODUCTION

1.1 Motivation

River flooding occurs when flows exceed the conveyance capacity of the channel causing water to flood overbank. Conveyance capacity is set by river channel morphology, for example, cross-sectional geometry, planform, and roughness. However, river morphology is not static: changes in morphology, hereafter 'morphodynamics' can occur, often during floods capable of mobilizing substantial amounts of sediment (Fig 1.1). Morphodynamic adjustments affect how much flow can be transported through the channel, subsequently modifying flood risk (*Ahrendt et al.*, 2022; *Buffin-Bélanger et al.*, 2017; *Slater et al.*, 2015). Conceptually, this may be simple to understand, however, in practice, river morphodynamics are challenging to quantify and predict for reasons that are expanded upon in the following sections. With climate change affecting human exposure to flood hazard globally (*Arnell and Gosling*, 2016), understanding the variables contributing to flood risk has never been more imperative: river morphodynamics are foundational to this effort as they define the structure upon which flood models are built and hazard estimates are made.

1.1.1 Hydrogeomorphic Hazards Under Climate Change

Anthropogenic climate change is affecting global hydrology (*Fischer and Knutti*, 2015), modifying the flow regime in rivers across the world. Contemporary climate research often touts the concept: 'wet gets wetter', 'dry gets drier' in regards to expected hydrologic shifts under future climate scenarios (*Chou et al.*, 2013; *Hu et al.*, 2019; *Wasko et al.*, 2021), though this theory is modulated by the effects of terrestrial water storage (*Xiong et al.*, 2022)

and vegetation (*Lian et al.*, 2021; *Yang et al.*, 2019) convoluting its ubiquity. Nevertheless, in many regions precipitation events are becoming more intense under climate change including atmospheric rivers (*Gershunov et al.*, 2019; *Michaelis et al.*, 2022; *Payne et al.*, 2020), tropical cyclones (*Knutson et al.*, 2010; *Reyer et al.*, 2017), and prolonged rainstorms (*Kahraman et al.*, 2021; *Moyo and Nangombe*, 2015).

Heightened storm intensity under climate change poses a particular risk for hydrogeomorphic hazards (*AghaKouchak et al.*, 2020), which transport both fluid and sediment often suddenly and in high volumes. For example, the drought-flood cycle primes landscapes for post-wildfire-debris flows (*Cannon et al.*, 2008; *Diakakis et al.*, 2017); land- and rock instability is exacerbated by rapid warming in alpine regions (*Etzelmüller et al.*, 2022; *Petley*, 2022); and intense precipitation can trigger widespread landsliding (*Handwerger et al.*, 2019). Most important for this dissertation, intense storms can lead to river floods with massive and potentially widespread geomorphic consequences (e.g., *Mohr et al.*, 2023; *Observatory*, 2022).

Floods provide a high capacity for mobilizing sediment and reorganizing river channels. The effects of floods on river channel morphology can be immediate (e.g., *Li et al.*, 2020) as well as cumulative (e.g., *Guan et al.*, 2016) both of which can change the conveyance capacity for subsequent floods (Fig 1.1). Morphodynamic adjustments during floods are relevant for ecological reasons: floods can change bed texture (Fig 1.1a) in spawning habitats (*Saltveit et al.*, 2019), and recruit woody vegetation from proximal floodplains (Fig 1.1e), which can stabilize channels providing critical aquatic habitat (*Gurnell et al.*, 2005). Relevant for human safety, the relationship between floods and river morphodynamics has been recently recognized for its potential modification of anthropogenic flood risk (*Buffin-Bélanger et al.*, 2017; *Sofia and Nikolopoulos*, 2020). Indeed, an understanding of morphodynamic changes during floods has been highlighted as a critical gap in knowledge, particularly with increasing population density in river corridors (*Church and Ferguson*, 2015).

1.1.2 *River Engineering in the Anthropocene*

Most rivers across the globe reflect the results of human activity on the erosional capacity of the fluvial system and changes in sediment flux (*Milliman et al.*, 2008): river planforms have been fixed in place via levees and revetments to protect adjacent communities from flooding and longitudinal connectivity has been disrupted via dams for flood control and hydropower (*Wohl*, 2014). The imprint of human influence on rivers has driven scientists to document a period of morphologic responses associated with the Anthropocene (*Kelly et al.*, 2017; *Poff*, 2014; *Wohl*, 2020). While such anthropogenic development has substantially modified natural river dynamics, there is also a simultaneous push towards fundamental understandings of river morphodynamics (*Church and Ferguson*, 2015), in part, to develop adaptation and mitigation strategies under climate change (*Poff*, 2014). This imposes a semi-paradoxical demand of river scientists of the Anthropocene: research is dedicated towards detangling the natural morphodynamic response from the effects of interventions (e.g., *Ylla Arbós et al.*, 2023), and is then used towards the design of further interventions to harness river energy and protect against flooding and erosion.

This thesis caters to the contemporary requests of river science–it simultaneously seeks to further fundamental concepts of fluvial geomorphology and to inform current river engineering strategies as they relate to morphodynamics and flooding. The subsequent chapters investigate feedbacks between floods and morphology in both natural and engineered river systems.

1.2 *Outline*

- ***Chapter 1:*** revisits the fundamentals of river morphodynamics and the importance of floods in modifying river form. It additionally highlights existing challenges hindering the incorporation of feedbacks between these two processes into flood risk frameworks.

- ***Chapter 2 (Part I):*** quantifies the relative importance of channel conveyance vs streamflow variability for overbank flooding in the mountain-born channels of Western Washington State, U.S. using long-term river gaging data. This chapter has been previously published as:

  > Ahrendt, S., Horner-Devine, A. R., Collins, B. D., Morgan, J. A., Istanbulluoglu, E., "Channel Conveyance Variability can Influence Flood Risk as Much as Streamflow Variability in Western Washington State." *Water Resources Research* 58.6 (2022): e2021WR031890.

- ***Chapter 3 (Part II):*** traverses the globe to the highly engineered Waal River in the Netherlands. Here, we investigate the hydrodynamics of overbank flooding as it relates to persistent river bed adjustment during floods and bed recovery during low flows. This chapter draws on ideas from the previous publication:

  > Ahrendt, S., Blom A., Van Denderen, R. P., Schielen, R. M. J., Horner-Devine, A. R., "Geometric floodplain controls on riverbed elevation change within and between flood events." *River Flow 2022, The Eleventh International Conference on Fluvial Hydraulics*. (2022)

  and is in-prep for submission as:

  > Ahrendt, S., Blom A., Van Denderen, R. P., Schielen, R. M. J., Horner-Devine, A. R., "Floodplain geometry and floodplain-channel flow exchange explain main-channel bed elevation change within and between peak flow events in an engineered river."

- ***Chapter 4 (Part III):*** leverages intuition from Part II regarding morphodynamic responses to overbank flooding applied to a case study in the Nooksack River of western Washington State. We use a Delft3D hydro-morphodynamic model to investigate feedbacks between overbank flooding and bed elevation change in

a region with persistent, costly overbank flooding and active flood management needs.

- ***Chapter 5:*** synthesizes the main findings of Parts I-III and proposes future research directions based upon questions sparked during this investigation including ideas pertaining to: 1) river bed response to climate variability, 2) feedbacks between floods, sediment supply, and channel response, and 3) the effects of compound channel structure on morphodynamic response to floods.

1.3 Background:

1.3.1 River Morphodynamics: The Basics and The Challenges

Fundamentally, morphodynamic adjustment in rivers occurs where there are spatial gradients in sediment transport (*Parker*, 2008). At a given location, if there is a mismatch between incoming sediment flux and sediment transport capacity the channel will seek to evolve such that it is just capable of transporting this supplied sediment (*Blom et al.*, 2016), or that its longitudinal profile is in 'equilibrium' with the upstream flow regime and sediment supply (*Mackin*, 1948).

Rivers have several morphodynamic modes by which to adjust towards equilibrium, the predominant ones being changes in channel planform (e.g. width, sinuosity), bed slope, and bed texture (i.e. grain size). In engineered channels with a fixed planform, adjustments are reduced to slope and bed texture (e.g., *Harmar et al.*, 2005; *Ylla Arbós et al.*, 2021).

Substantial research has explored the concept of a morphodynamic 'equilibrium' discharge that replicates certain qualities of channel morphology (e.g., *Blom et al.*, 2017; *Castro and Jackson*, 2001; *Phillips and Jerolmack*, 2016; *Wolman and Miller*, 1960; *Wolman et al.*, 1957), yet in both natural and regulated channels, flow rate and sediment supply are rarely constant: they can change on slow time scales, for example with climate, (e.g., *Ylla Arbós et al.*, 2023; *Anderson and Konrad*, 2019), or on event time scales during seasonal

(e.g., *Plink-Björklund*, 2015) or singular (e.g., *Yousefi et al.*, 2018) floods. Channel response to such variation in controls has led to the delineation of a 'quasi-static' response (channel adjustments to controls operating on relatively long time scales) and 'dynamic' response (channel adjustments operating over relatively short time scales) (*Arkesteijn et al.*, 2021). This research points to a potentially distinct channel response to long-term changes in climate, along with intermediate time scale channel adjustments in response to discharge fluctuations and floods.

Morphodynamics are notoriously challenging to quantify, in part, due to the complexity of sediment transport. Sediment transported by rivers can be classified as 'wash load', finer sediments often derived from non-channel sources and transported within the water column, or 'bed material load', sediment often derived from the river bed and which can be transported along the river bed or in suspension depending on hydraulic conditions (*Rhoads*, 2020). Bed material load is often considered important for morphodynamics since it directly modifies the river bed, though wash load can also change the hydraulics of sediment transport (*Simons et al.*, 1963), indirectly affecting river form. Sediment can transition between different modes of transport locally, depending on the discharge magnitude (*Milhous*, 1973), or longitudinally, depending on particle attrition (e.g., *Pfeiffer et al.*, 2022).

Owing to its complexity, most equations for sediment transport have been derived empirically. Famously, the Shields curve representing incipient particle motion was obtained experimentally in 1936 (*Shields*, 1936). Foundational equations defining a relationship between discharge and sediment transport have been established using lab data for both sand- (e.g., *Engelund and Hansen*, 1967) and gravel-bedded rivers (e.g., *Meyer-Peter and Müller*, 1948). Field data for bedload sediment transport are exceedingly difficult to collect, and can vary by an order of magnitude (*Martin and Ham*, 2005), resulting in high errors when predicting total sediment transport in the field. As sediment transport varies nonlinearly with discharge (*Milhous*, 1973), sediment transport equations, which are typically developed under steady flow conditions, characteristically underestimate total

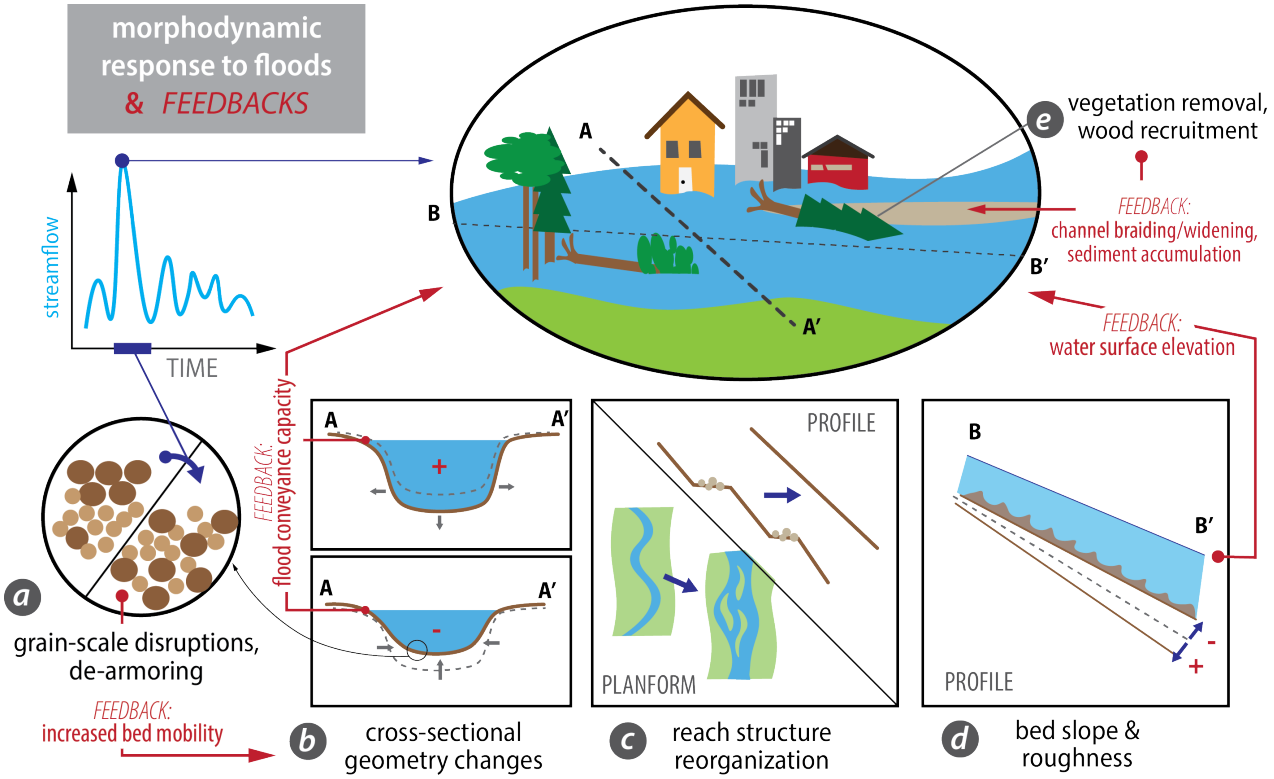

Figure 1.1: *A conceptual schematic of various morphodynamic responses to floods and prospective feedbacks into increased overbank flooding and/or further morphodynamic response. This includes a) disruptions to the grain matrix on the riverbed which affects bed mobility; b) changes to cross-sectional geometry which can affect flood flow conveyance; (c) reach scale reorganization of the river planform and profile; (d) changes to bed roughness and slope which can affect water surface elevation at flood stage; and (e) peak-flow removal of vegetation from channel-adjacent regions which can affect channel width and stability, along with large wood recruitment which can cause in-channel sediment accumulation.*

transport during unsteady flows (*Karimaee Tabarestani and Zarrati*, 2015). Thus, accurate predictions of sediment transport become especially difficult during floods.

1.3.2 Floods and Morphodynamics: A Dynamic Duo

Floods cause important morphodynamic responses in rivers across a range of adjustment scales. Importantly, many of these adjustments can feedback into further channel mobility as well as the degree of overbank flooding. At the grain-scale, floods can increase

sediment mobility by disrupting river bed armoring and grain interlocking that can occur in response to a period of low flows (Fig 1.1a) (*Masteller et al.*, 2019; *Milhous*, 1973; *Ockelford et al.*, 2019; *Reid et al.*, 1985).

Floods can locally deposit or erode sediment modifying channel cross-sectional geometry (Fig 1.1 b). Cross-sectional changes have been shown to feedback into changes in flow conveyance: channel narrowing and shallowing (Fig 1.1 b, lower-panel) has been shown to increase flood frequency (*Collins et al.*, 2019; *Stover and Montgomery*, 2001). Conversely, local scour and widening (Fig 1.1 b, upper-panel) can increase the channel conveyance for subsequent floods (e.g., *Guan et al.*, 2016).

Reach-scale patterns in river and profile can be substantially reorganized during floods (Fig 1.1 c). Floods can abruptly transform meandering channels to braided channels (*Brewer and Lewin*, 1998; *Erskine*, 2011), and disrupt keystone boulder clasts that define step-pool channels, completely re-arranging existing morphology (*Turowski et al.*, 2009). In some cases, floods have been shown to be essential for self-maintenance of certain longitudinal, morphological structures; for example, in riffle-pool sequences the relative change in flow velocity and sediment transport varies during peak flows between riffles and pools respectively and has been shown to reinforce their structure (*De Almeida and Rodríguez*, 2011).

River bedforms such as dunes can grow during floods in both gravel and sand-bedded rivers (Fig 1.1 d) (*Dinehart*, 1992; *Julien and Klaassen*, 1995). Bedforms modify hydraulic roughness along the channel, which affects stage increase and or decrease with discharge (*Paarlberg et al.*, 2010) (Fig 1.1 d). Namely, rougher channels tend to show higher water levels for the same discharge. River bed slope also sets water surface elevation; while channel slope (Fig 1.1 d) is less sensitive to abrupt changes in hydraulic controls, long term shifts in flood regime may change the shape of the flow duration curve, which can affect river profile (*Arkesteijn et al.*, 2019).

While floods are evidently important for river morphodynamics, and river morphodynamics can feedback into flood processes, predicting and understanding the relationship

between flood hazard and river morphodynamics is challenging to resolve for the following, non-exhaustive, reasons:

1. Sediment transport during a flood hydrograph is highly nonlinear and poorly predicted by existing transport equations as introduced in Section 1.3.1. In mixed-bed rivers, grain-size specific transport can be dependent on the flow magnitude: sand can be preferentially transported at low discharges (*Wilcock and Kenworthy*, 2002), whereas infrequently-mobile coarse bedforms may only be active during floods (*Wohl*, 2014).

2. Fine temporal resolution measurements of bed evolution throughout a hydrograph are sparse to nonexistent, hindering field verification of relationships between local sediment transport and river bed evolution during peak flows.

3. Channel-adjacent sediment storage can become mobilized during floods, causing a potentially abrupt shift in the relationship between river discharge, sediment supply, and morphodynamic response at certain water stages. Secondary channels that are only active once the water stage reaches a certain level can cause discrete, nonlinear steps in sediment transport. Floods may additionally affect sediment delivery from channel-bounding hill slopes that are being actively eroded by the river (e.g., *Scott and Collins*, 2021). Stage-dependent lateral sediment-supply further limits confidence in morphodynamic evolution during a peak flow at a given location.

4. The effects of floods on river morphology can vary in space depending on access to channel-adjacent sediment discussed above, and pre-existing channel morphology For example, channel confinement can drive reach-scale gradients in flow velocity and streampower affecting dynamic bed level response (*Arkesteijn et al.*, 2021; *Nanson and Croke*, 1992; *Sholtes et al.*, 2018).

5. Resolving morphodynamics at the spatially explicit 2- to 3-D scale used by hydraulic and hydrodynamic models to predict flood inundation area maps is also computationally expensive. While models have recently been adapted to incorporate 3-D morphodynamics (*Gessler et al.*, 1999; *Lesser et al.*, 2004), these simulations have yet to effectively reduce uncertainty in flood projections: sediment transport adds a degree of freedom to flood hazard resolution, and it is too computationally expensive to simulate the broad range of parameter space required to narrow these uncertainties (*Gilles and Moore*, 2010). Application of 2- to 3-D simulations over the decadal to centurial time scales typical for morphodynamic change often requires assumptions about sediment transport and channel conveyance adjustments that result in accumulating errors in morphological change (*Morgan et al.*, 2020) which may propagate into flood extent predictions.

Due to the aforementioned difficulty of measuring and predicting sediment transport during floods, this thesis seeks a systematic understanding of morphodynamic response to floods based upon channel form and how this affects spatial gradients in sediment transport (Part II). Since spatially explicit hydro-morphodynamic modeling is relatively complex and costly, we aim to identify when and where morphodynamic changes are important for modifying overbank flooding (Part I). We also distill complex results from a depth-averaged, Delft3D morphodynamic model during an extreme flood event to develop a process-based understanding for how feedbacks between overbank flooding can affect termporal and longitudinal patterns of morphodynamic response (Part III).

Parts I-III investigate morphodynamic changes focusing on planform and bed elevation adjustments in gravel-bed and mixed sand- & gravel-bed rivers across engineering time scales. In engineering time scales 'long-term' changes refer to multi-decadal to centennial trends and 'short-term' changes pertain to sub-annual, and event-scale adjustments. Both long- and short-term river conveyance changes are investigated in Part I and event-scale bed elevation changes are investigated in Parts II and III.

Part I

Chapter 2

CHANNEL CONVEYANCE VARIABILITY CAN INFLUENCE FLOOD RISK AS MUCH AS STREAMFLOW VARIABILITY IN WESTERN WASHINGTON STATE

2.1 Abstract

Changes in the severity and likelihood of flooding events are typically associated with changes in the intensity and frequency of streamflows, but temporal adjustments in a river's conveyance capacity can also contribute to shifts in flood hazard. To assess the relative importance of channel conveyance to flood hazard, we compare variations in channel conveyance to variations in the flow magnitude of moderate (1.2 year) floods at 50 river gauges in western Washington State between 1930 and 2020. In unregulated rivers, moderate floods have increased across the region, but in regulated rivers this trend is suppressed and in some cases reversed. Variations in channel conveyance are ubiquitous, but the magnitude and timing of adjustments are not regionally uniform. At 40% of gages, conveyance changes steadily and gradually. More often, however, conveyance variability is nonlinear, consisting of multi-decadal oscillations (36% of gages), rapid changes due to unusually large sediment-supply events (14% of gages) and increases or decreases to conveyance following flow regulation (10% of gages). The relative importance of conveyance variability for flood risk depends on the mode of adjustment; in certain locations with historic landslides, extreme floods, and flow regulation, the influence of conveyance changes on flood risk matches or exceeds that of streamflow at the same site. Flood hazard management would benefit from incorporating historic long- and short-term conveyance changes in predictions of future flood hazard variability.

2.2 *Introduction*

Damages and costs of river flooding have increased globally in recent decades (*Ward et al.*, 2017; *Winsemius et al.*, 2016). The frequency and magnitude of heavy precipitation is projected to increase as climate changes in the 21st century in many areas of the world (*Murray and Ebi*, 2012), substantially increasing human exposure to flood hazard (*Arnell and Gosling*, 2016). As more people live in flood risk zones, there is a pressing need for accurate flood risk predictions to foster human safety (*Jongman et al.*, 2012).

Flooding occurs when streamflow exceeds a channel's conveyance capacity, driving flows overbank. Increases in overbank flow intensity and frequency can be driven by increases in streamflow or losses to channel conveyance capacity (Fig 2.1); however, flood risk assessments have generally focused on systematic increases in streamflow through time rather than conveyance changes. Streamflow data are hence used to understand changing flood potential with trends in flood hazard inferred from trends in peakflows (e.g., *Hodgkins et al.*, 2019; *Mastin et al.*, 2016), and frequency and intensity of floods estimated from mean daily discharge data (e.g., *Hamed and Rao*, 2019; *Kjelstrom*, 1998; *Pilgrim and Cordery*, 1975).

Recent studies of flood risk, however, focus on river morphodynamics as an important control on flooding (e.g., *Li et al.*, 2020; *Slater et al.*, 2015; *Sofia and Nikolopoulos*, 2020). A decrease in channel cross sectional area or an increase in roughness can increase water stage for a given discharge, resulting in channel overflow at discharges that were once within bank (Fig 2.1 b). Indeed, case studies show that reductions in local river conveyance capacity can increase flood frequency without a change in peak flows (*Collins et al.*, 2019; *Stover and Montgomery*, 2001); flooding on the Missouri River now occurs at flows that were entirely in-bank in the early 20th century (*Pinter and Heine*, 2005).

To quantify the influence of morphodynamics on flooding, *Slater et al.* (2015) developed a method for separating the relative contributions of channel conveyance and mean daily streamflow changes to trends in flood frequency. They used this method to search for

monotonic trends in flood hazard from 1950 to 2013 in 401 river gauges across the United States and found that more than half the sites had a non-stationary flood frequency, with significant changes in channel conveyance contributing to trends at just under half of the stations.

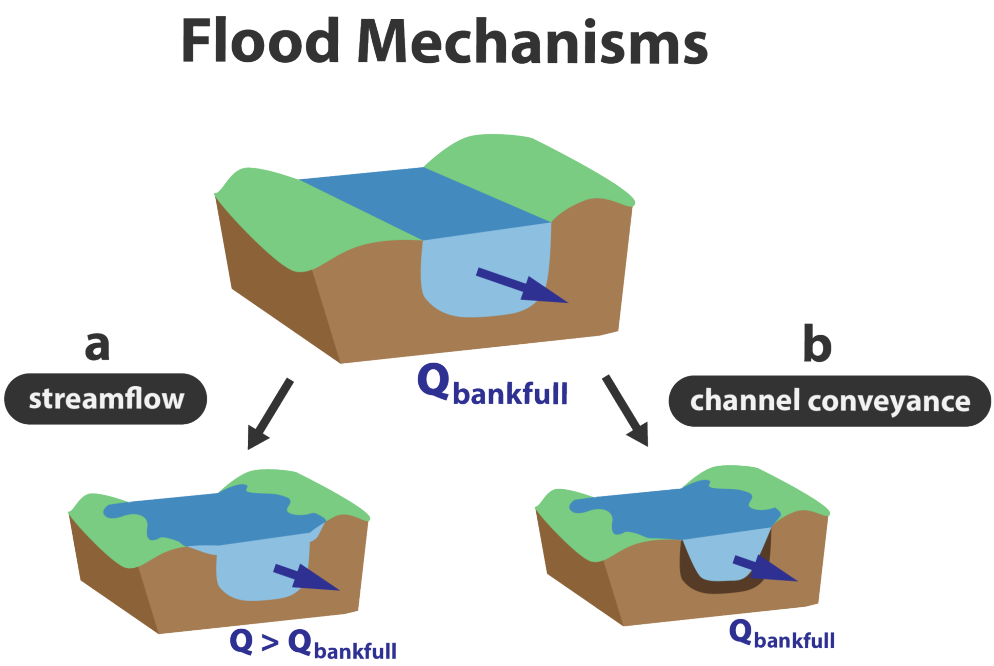

Figure 2.1: *A conceptual understanding of flooding driven by (a) streamflow vs. (b) channel conveyance: (a) Streamflow-driven flooding results from runoff events inducing channel flows (Q) that exceed the bankfull flow capacity ($Q_{bankfull}$) of the channel. (b) Channel-driven flooding results from reductions in the conveyance of the channel through mechanisms such as sediment aggradation, channel narrowing, or increases in roughness. This leads to flooding at flows that were previously in-bank.*

However, both changes to channel conveyance capacity and streamflow regime can be non-monotonic, and neglecting this can obscure short-term changes in flood hazard as well as climatic and geomorphic processes that drive such trends. For example, comparing monotonic trends in streamflow and channel conveyance fails to account for the importance of abrupt geomorphic changes occurring during tropical cyclone events in

Puerto Rico, where short-term conveyance capacity changes can exceed peak streamflow changes (*Li et al.*, 2020). Additionally, climate variability can simultaneously affect patterns of streamflow and channel conveyance change, where discharge and channel form adjust to cycles of increases in precipitation and sediment supply (*Anderson and Konrad*, 2019; *Rumsby and Macklin*, 1994; *Slater et al.*, 2019). Fitting long-term, monotonic trends to cyclic patterns of streamflow and channel-conveyance change can overlook short term hydrologic and morphologic behavior that could amplify or offset flood-hazard.

Here, we modify the approach of *Slater et al.* (2015) by considering monotonic, non-monotonic, short-term, and long-term changes to flood hazard. We focus on western Washington State, a region in the northwestern United States where recent floods have been attributed to conveyance capacity losses; extensive flood damages caused by the White River during January 2009 occurred after a 25% channel conveyance reduction during a two-month period between winter storms (*Czuba et al.*, 2010; *Green*, 2009). *Slater et al.* (2015) also document channel capacity decreases across the northwestern United States that increased flood hazard, although relatively few sites were analyzed in western Washington. We separate the influence of channel conveyance and streamflow variability by analyzing the relative magnitude of flow displaced by channel conveyance adjustments vs. changes in the streamflow rate of 1.2 year recurrence interval floods over time, which is the typical frequency of bankfull flow for alluvial rivers in western Washington (*Castro and Jackson*, 2001). While channel conveyance and moderate floods are not mutually exclusive (e.g. conveyance may change in response to floods), we consider both factors as simultaneously influencing the potential for overbank flooding at a given location. We apply the method to 50 river gages in western Washington State using field measurement and mean-daily flow data over the last 30-90 years to better understand the causes of flooding and how and why it may change in the future. This analysis resolves the temporal variability of conveyance changes. Spatial variability is addressed by comparing responses in rivers across the region and, where possible, by comparing gages on the same river.

Specifically, we ask: 1) what are the magnitudes and time scales associated with both monotonic and non-monotonic changes in moderate flood streamflows and channel conveyance and how do these compare to one another? 2) are there regional patterns to changes in flood risk driven by streamflow and/or channel-conveyance change? and 3) how do flood risk changes in regulated rivers that have had substantial modifications to water and sediment continuity compare with changes in unregulated rivers?

2.3 Study Area

Rivers in western Washington head in the Olympic Mountains and the Cascade Range (Fig 2.2). The Cascade Range, where most of our study sites are located, hosts alpine proglacial zones, which deliver sediment to proximal channels through rockfall and proglacial debris flows particularily from Quaternary volcanoes (e.g., *Anderson and Pitlick*, 2014; *Czuba et al.*, 2012). The episodic nature of this delivery is associated with high variability in river bed elevation downstream of glaciated basins (*Pfeiffer et al.*, 2019), and downstream-propagating bed waves (*Anderson and Konrad*, 2019). However, pro-glacially derived sediment can also remain stored in upland valley floors (*Anderson and Jaeger*, 2020) and sediment transit times in headwater channels can be on the order of 10^3 years (*Lancaster and Casebeer*, 2007); as a result, the connectivity between proglacial areas and downstream channels is not well understood.

The Cascade and Olympic ranges are bisected north to south by the Puget Sound lowland which includes a sedimentary fill of lacustrine silts and clays, outwash sands, and gravels from successive advances and retreats of the Puget Lobe of the Cordilleran ice sheet (*Booth*, 1994). Post-glacial fluvial incision into the lowland fill has created terraces prone to channel-adjacent landsliding (*Booth et al.*, 2017; *LaHusen et al.*, 2016) which contribute substantial coarse sediment low in the channel network (*Scott and Collins*, 2021). While the extent to which mass flux from glacial terraces contributes sediment directly to the channel varies between rivers, the grain size and lithology of these sediments suggest their potential importance for downstream sedimentation (*Scott and Collins*, 2021).

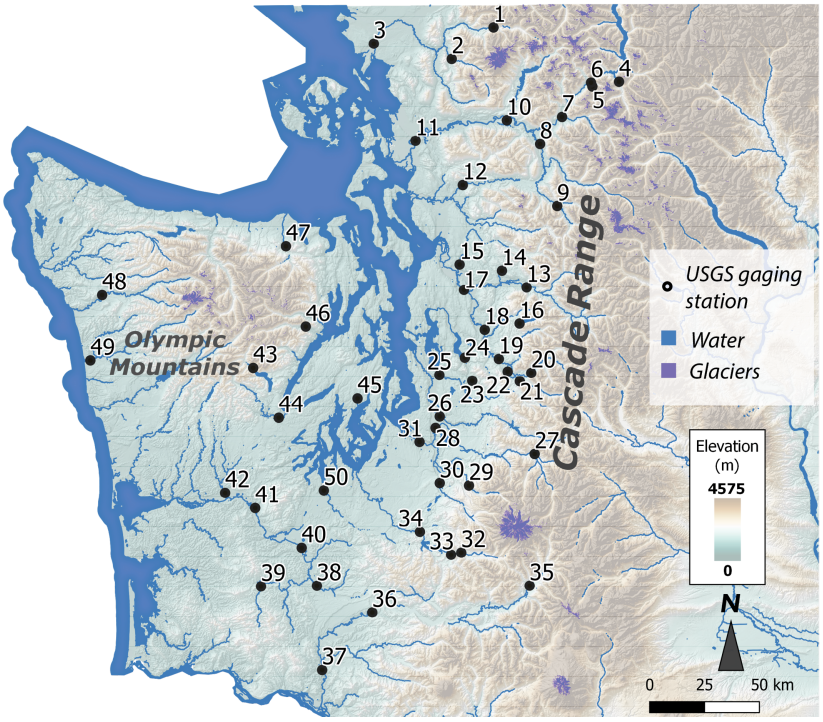

Figure 2.2: *Map of study region. Alpine glacial coverage is highlighted in purple, and the location of United States Geological Survey gaging stations (USGS) used in this study are marked and numbered. Corresponding gage names and information may be found in supplemental dataset S1. Site numbers correspond to those in Figs 2.6, 2.7 and 2.8. Elevation data is from a 30m mosaicked DEM of Washington (UW Geomorphological Research Group) resampled from USGS 10m DEM products (USGS, 2017).*

Within the Puget Sound region, rivers are still responding to relict Pleistocene glacial and volcanic landforms; rivers are aggrading where they flow through valleys carved by subglacial processes during the last ice age and incising in valleys downcut by Holocene fluvial activity, post-glaciation (*Collins and Montgomery*, 2011). Human engineering has in some cases exacerbated Holocene sedimentation; for example, in the Puyallup system engineered rerouting of the White River channel has increased sedimentation (*Anderson and Jaeger*, 2020) in locations prone to severe flooding (e.g., *Czuba et al.*, 2010; *Green*, 2009).

Western Washington rivers have been dammed for flood control, water supply, and hydroelectricity generation (*Gendaszek et al.*, 2012; *Lee et al.*, 2016), modifying connectivity with upstream sediment supply and streampower available for downstream sediment transport, the balance of which determine whether rivers downstream of dams aggrade or degrade (*Grant*, 2012). Aggradation happens when flow regulations reduce competence for transporting sediment delivered by tributaries (e.g., *Andrews*, 1986; *Van Steeter and Pitlick*, 1998; *Wilcock et al.*, 1996) or when coarse, bed-sized sediment is eroded from downstream banks (e.g., *Gaeuman et al.*, 2005). In the eastern Puget Lowland, coarse sediment eroded from terraces is mostly downstream of dams (*Scott and Collins*, 2021). On the Skokomish River, dam reductions in discharge in concert with continued, high sediment supply from a downstream tributary caused drastic conveyance losses in the lowland mainstem channel (*Collins et al.*, 2019).

Both sediment supply and streamflow are sensitive to variations in climate. In proglacial basins, annual sediment yield has been correlated to annual precipitation and runoff (*Hicks et al.*, 1990) with high sedimentation also related to periods of glacial advance and succession (*Leonard*, 1997). Mean monthly streamflow fluctuates on annual to multi-decadal time scales in relation to climate cycles that include the El Nino/Southern Oscillation (ENSO) (*Kahya and Dracup*, 1993) and the Pacific Decadal Oscillation (PDO) (*Mantua et al.*, 1997). Flood insurance claims are positively correlated with La Nina cycles of ENSO in the Pacific Northwest (*Corringham and Cayan*, 2019). Warming winter temperatures have decreased snowpack storage, resulting in higher fall and winter peak

flows in basins with a high fraction of elevation above historic snowpack lines (e.g., *Mote et al.*, 2018; *Neiman et al.*, 2011). Atmospheric river events were responsible for 96% of peak annual daily streamflows in the region between 1998 and 2009 (*Neiman et al.*, 2011) and are forecasted to increase the frequency of days with heavy and severe precipitation over the next century (*Gershunov et al.*, 2019).

That climate influences both streamflow and sediment supply highlights the need for understanding the corresponding effects of climate on channel morphodynamics and flooding. *Pfeiffer et al.* (2019) suggest that in this region, river bed variability is driven by changes in sediment supply rather than peak flows resulting in regionally asynchronous variation in bed elevation. *Anderson and Konrad* (2019) demonstrate river bed patterns that are lag-correlated to the PDO as a sediment disturbance propagating downstream from proglacial regions on Mt. Baker. However, *Slater et al.* (2019) presents a correlation between climate signals and adjustments to channel capacity across the United States under the assumption that changes in river form occur synchronously with climatic shifts. Understanding whether channel conveyance responds to climate-driven changes as a propagating downstream signal, a system-wide adjustment in channel form, or in other ways is important for understanding how flood hazard will change in the future.

2.4 Methods

2.4.1 Analysis of Channel Conveyance Change:

We include 50 USGS river gages spanning sites from steep mountain headwaters to lowland, managed channels (Fig 2.2). Gage elevations range from sea level to 536 m, contributing drainage areas range from 16 to 5774 km^2, and mean basin slopes range from 4 to 59% (GAGES-II dataset: *Falcone* (2011)). To analyze channel conveyance variability, we use USGS field records of simultaneous stage and discharge measurements (*Sauer*, 2002); discharge is measured by combining measurements of cross-sectional area and velocity and is typically used to estimate streamflow to continuous measurements of

water stage. These data are accessed from the National Water Information System (NWIS) web interface (*USGS-NWIS*). We limit our study to gages with long, relatively continuous records that extend to within five years of the present year (2020); we include gages with a minimum of 30 years of data with measurement gaps less than 20 years. Some gages have a shift in datum as the gaging location was moved upstream or downstream from its original location. Where the USGS has published values for this shift, we use this value to adjust our data to a unified datum by offsetting the data with the minority number of stage measurements on one side of the shift to match the majority of the record. We implement this shift for three gaging sites. At 13 gages where published datum shifts are not available, we trim gage data records to exclude measurements made prior to the shift. The resulting gage records range from 30 to 92 years and average 59 years.

We infer changes in channel conveyance capacity from shifts in the stage-discharge relationship at a gaging station as the difference between the field-measured flow and the flow predicted by a static rating curve (Fig 2.3 a and b). This method, conventionally termed "specific gage analysis" (*Blench*, 1969), has long been used to detect how geomorphic changes affect river water level heights and corresponding flow capacity (e.g., *Biedenharn et al.*, 1997; *Gilbert*, 1917; *Jemberie et al.*, 2008; *Pinter and Heine*, 2005). In our application of specific gage analysis, we use a rating curve for the channel near its maximum capacity to avoid limitations imposed by using the most recent (e.g., *Anderson and Konrad*, 2019; *Pfeiffer et al.*, 2019) or time-averaged (*Slater et al.*, 2015; *Slater*, 2016) ratings: in rapidly aggrading channels, the most recent rating curves cannot accommodate flow-residual values for stages below the current channel bottom; at sites with sudden changes to channel capacity, or an uneven sampling record, a time-averaged rating can be unusually skewed and misrepresent channel change over time.

We create rating curves for the channel near the maximum capacity using the BaRatin method and software (*Le Coz et al.*, 2014). This approach combines hydraulic channel geometry data and stage-discharge field gagings to create rating curves and is beneficial because it allows for a physically-based estimation of discharge above the range provided

in the field gagings (*Lundquist et al.*, 2016). We obtain cross-sectional geometry and channel slope for these calculations from a 0.5-2km reach around each gaging station using 1m resolution LiDAR-derived DTMs and USGS stage-discharge measurements for a five-year time span when the channel was vertically stable. A detailed account of rating curve data selection and processing is available in the supporting information (Text S1). This method of rating-curve formulation ensures that 1) all flow-residual values representing channel conveyance change can be predicted by the current rating curve (i.e. no values fall below the minimum stage value in the rating curve), 2) the rating curve represents a single channel geometry for a broad range of flows, and 3) we can compare morphologic changes between sites with respect to a stable, near-maximum channel conveyance.

We confine our channel conveyance analysis to high flows to focus on changes relevant to flooding by using measurements made around the "flood flow" (Q_{flood}) or the discharge at which flows begin to overtop the banks. We obtain an estimate for this discharge based upon the 1.2 year return period flow computed from a flow-duration curve using the Weibull plotting position formula (*Helsel and Hirsch*, 1992; *Weibull*, 1939) with 10 years of mean daily flow data bracketing the time for which we create a site's rating curve. The 1.2 year flow is chosen as a representative flow based upon *Castro and Jackson* (2001) who computed return periods of bankfull flow from field measurements of hydraulic geometry and stream statistics for the Pacific Northwest. A mean bankfull return period of 1.2 years was reported for the Pacific Maritime Mountains where the majority of our study gages are located. While variations in bankfull channel geometry resulted in a return period range of 1-1.5 years reported for the sites consistent between our study and *Castro and Jackson* (2001), using a single return period allows us to also compare streamflow statistics consistently across stations. We trim our data to analyze measurements made to one-half of the "flood depth" on either side of flood stage, where flood stage is interpolated from a site's rating curve as the stage predicted for Q_{flood}, and flood depth is calculated as the difference between flood stage and the minimum measured stage within the field data.

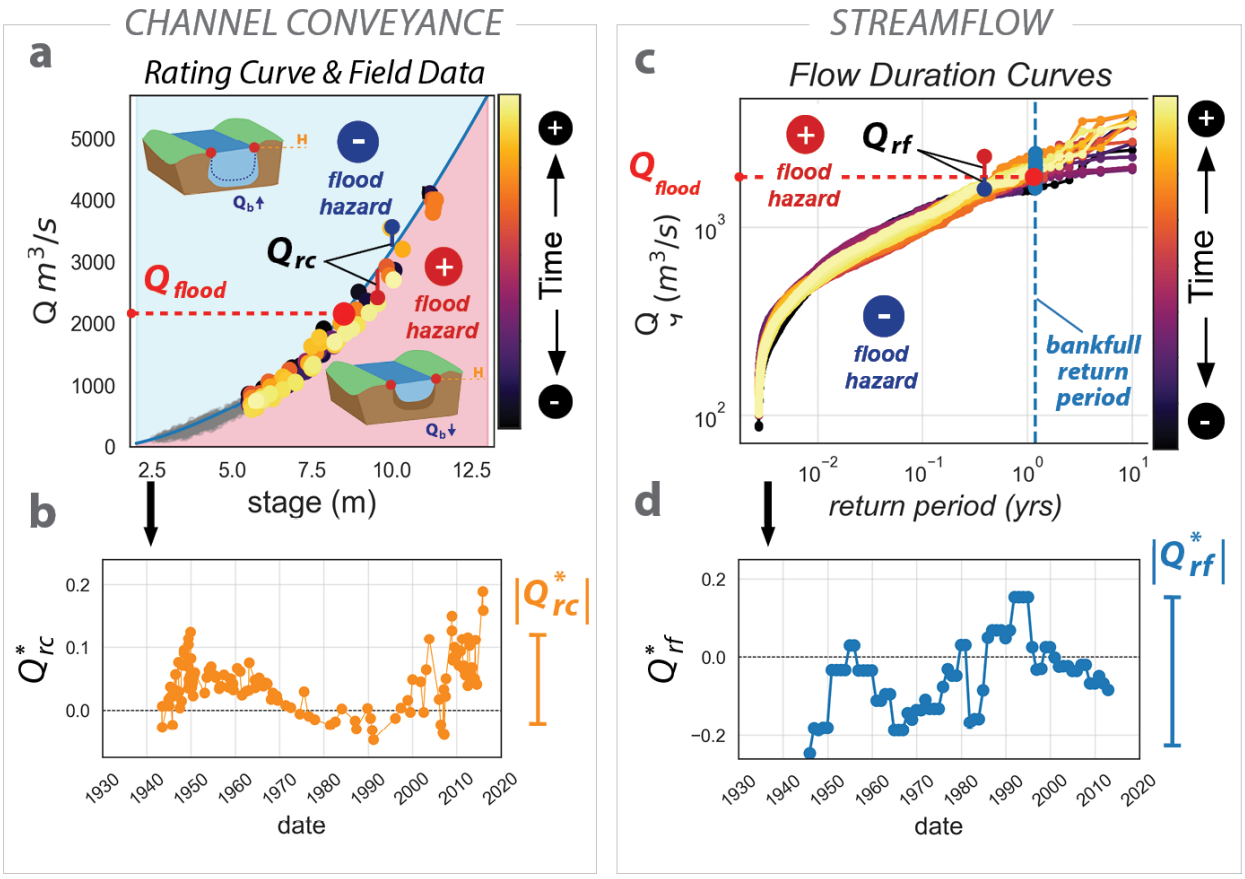

Figure 2.3: *Methods for calculating (a) channel conveyance changes and (b) moderate flood streamflow changes at a representative USGS gauging station. (a) the calculation of Q_{rc} as the difference between field measurements of river stage and discharge and a rating curve representing the hydraulic relationship between flow and depth for a static time. Q_{flood} denotes the flood flow. (b) Q^*_{rc} represent normalized channel conveyance change over time. Data are normalized as Q_{rc}/Q_{flood}. $|Q^*_{rc}|$ represents the range calculated from a 5-point moving median across the Q^*_{rc} time series and is considered "potential" for change in channel conveyance altering Q_{flood} at a site. (c) calculation of Q_{rf} as deviations from Q_{flood} at the bankfull return period (1.2 yrs). Q_{rf} are interpolated flows at the bankfull return period from flow duration curves built from a 10-year moving window of mean-daily flow data. (d) shows normalized Q^*_{rf} over time ($Q^*_{rf} = Q_{rf}/Q_{flood}$) which are interpreted to indicate hydrologic changes in high-flow regime such as peakflow magnitudes and flood duration that would cause streamflow driven flooding. $|Q^*_{rf}|$ represents the range of the Q^*_{rf} time series and is considered to represent the "potential" for changes in Q_{flood} driven by streamflow at a site.*

We quantify channel conveyance variation over time by calculating flow residuals as the difference between flows predicted by our rating curve and measured flows (Fig 2.3 a). We refer to these as Q_{rc}, or flow residuals associated with conveyance change. Q_{rc} represent temporal changes in channel conveyance at a gaging station that result from adjustments in channel cross-sectional area or hydraulic roughness. Positive Q_{rc} indicate conveyance losses with respect to the capacity predicted by the rating curve and result in excess overbank flow. To assess the influence of channel conveyance variability on flooding and to compare results between rivers of different sizes, we normalize Q_{rc} by a site's "flood flow" (Q_{flood}) to obtain Q^*_{rc}.

To identify outliers due to errors in field measurement data, we fit a ten-point moving median to the time series of Q^*_{rc} and ignore data that falls outside three standard deviations of this moving median. This resulted in a mean of three points and median of one point being removed from each gage data record. We quantify the magnitude of variability in channel conveyance by taking the range of the moving median Q^*_{rc} as: $|Q^*_{rc}| = \max(Q^*_{rc}) - \min(Q^*_{rc})$ (Fig 2.3b). Since temporal trends in Q^*_{rc} were often non-monotonic resulting in equal amounts of channel conveyance gain and loss over time (e.g. Fig 2.3b), we consider $|Q^*_{rc}|$ to represent the *potential* for conveyance driven flood hazard at a given site rather than magnitudes of change from a single trend.

2.4.2 *Analysis of Streamflow Change:*

We analyze time series of streamflow variability at the bankfull return period to quantify how hydrological changes such as shifts in precipitation and runoff rates affect overbank flood flows over time. We use the mean daily discharge record at USGS gaging sites, trimmed to the same length as the field measurement data, to build flow duration curves and quantify increases and/or decreases in the high-flow regime over time (Fig 2.3c). Changes in this part of the flow duration curve tend to represent a range of drivers of streamflow change including shifts from snowmelt- to rain-dominated floods and changes

in the influences of flow regulation on hydrologic storage (*Searcy*, 1959). While many flood risk analyses use peakflows to characterize hydrologic trends, this can neglect flood severity that arises from a moderate flood extending through multiple days and will not account for the occurrence of multiple flood events of lesser magnitude within the year (*Slater et al.*, 2015). Using flow-duration curves built with mean daily flows accounts for flood intensity, frequency and duration. Our analysis ultimately aims to quantify shifts in moderate flood streamflows that *persistently* affect overbank flooding rather than trends in the highest flows which may be rare and short-lived.

To compute streamflow variability over time, we hold the bankfull return period constant, and calculate the flow predicted by a suite of flow-duration curves built with a ten-year moving window of mean daily flow data offset by yearly increments (Fig 3 b). By testing the sensitivity of the interpolated bankfull discharge to data windows from three- to 25-yrs (supporting information Fig S1), we determine that ten years of mean-daily flow data is long enough to represent return-periods on the one- to three-year scale with reasonable confidence and short enough to capture changes in hydrological forcings driven by climatic and basin processes. The residuals, which we term Q_{rf}, quantify the difference between calculated flow values and Q_{flood} (Fig 2.3 b and c). The temporal pattern Q_{rf} agrees well with estimates of flood flow over time for a test gage on the Skagit River (supporting information Fig S2). An increase to Q_{rf} over time means that higher discharges are occurring for the same return period and indicates increased potential for flooding. To obtain a normalized Q^*_{rf}, we divide the change in Q_{rf} by Q_{flood}, as we normalized Q_{rc}. We calculate the range of Q^*_{rf} ($|Q^*_{rf}|$) similarly to the range of Q^*_{rc} to quantify the degree of variability in near-bankfull streamflows over the temporal record. To asses the relative influence of streamflow vs. channel conveyance variability on flood magnitudes we compare $|Q^*_{rf}|$ to $|Q^*_{rc}|$.

2.4.3 *Analysis of Combined Changes in Flood Hazard:*

To analyze cumulative change in flooding as a result of both channel conveyance and flow regime changes, we add the time series of Q^*_{rc} and Q^*_{rf} to estimate combined changes in Q_{flood} over time (hereafter Q^*_{rcomb}). Computing both effects independently allows us to consider potential interactions between channel conveyance and streamflow driven effects on long-term flood risk; for example, long-term increases in Q^*_{rf} may be offset by equivalent increases in the channel conveyance represented as negative Q^*_{rc}, resulting in lower Q^*_{rcomb}. Conversely, if increases in Q^*_{rf} and Q^*_{rc} occur in tandem, Q^*_{rcomb} can be higher than either effect alone.

Because the sampling frequency of Q^*_{rc} depends on the frequency of field observations whereas Q^*_{rf} are regularly spaced at one-year intervals, we linearly resample Q^*_{rf} to match the frequency of Q^*_{rc}. We subsequently add the time series together and fit a ten-point moving median to the data as we fit to the time series of Q^*_{rc}. We interpret the range of the moving median of Q^*_{rcomb} across the time series, $|Q^*_{rcomb}|$, to indicate combined potential for changes in Q_{flood} due to both channel conveyance and streamflow driven changes.

2.4.4 *Identifying Gage Characteristics and Regional Patterns:*

We use published basin statistics for gages including watershed mean elevation, mean slope and drainage area (GAGES-II dataset: *Falcone* (2011)) to identify whether these are predictive characteristics for certain types of channel conveyance responses. We additionally separate gages at locations with minimal to no flow regulations from regulated locations by consulting the USGS NWIS "Water-Year Summary" which notes whether there are regulations or diversions upstream from a station. If regulations are characterized as "some" or "minor" on the USGS Water-Year Summary, we assess whether these are significantly affecting the flow by calculating what percent of the average published value for diverted flow is of Q_{flood}. We consider sites where this fraction is less than 3%

of Q_{flood} to be characterized as unregulated since such changes to a small fraction of flow are unlikely to substantially influence variability in Q_{flood}.

To investigate regional temporal patterns in channel conveyance and streamflow change, we calculate the three-year average of the time series of Q^*_{rc} and Q^*_{rf} across the study domain. We choose a three-year average because this falls on the lower bound of the period of fluctuations in precipitation and temperature conditions in response to ENSO which typically range from three to seven years (*Halpert et al.*, 2016). We take the median of the three-year time series average for both Q^*_{rc} and Q^*_{rf} to aggregate time series across the region for unregulated and regulated gage sites respectively. Non-zero median values indicate consistency in behavior between sites across the study area.

2.5 *Results*

2.5.1 *Overall Variability of Channel Conveyance, Streamflow, and Cumulative Flood Hazard*

The median magnitude of temporal variation in channel conveyance is about half of the magnitude of streamflow variation. The median $|Q^*_{rc}|$ at our 50 gages is 0.24 (Fig 2.4a), indicating a median channel conveyance variability of 24% of flood capacity, Q_{flood}. The distribution of Q^*_{rc} is skewed towards low magnitude conveyance changes with a modal $|Q^*_{rc}|$ of 0.19. Changes in the streamflow of moderate floods over the same time period are greater than than channel conveyance changes, with a median $|Q^*_{rf}|$ of 0.49 (Fig 2.4b). At 40 of the 50 sites, $|Q^*_{rf}|$ is higher than $|Q^*_{rc}|$, however one river shows high magnitude changes in channel conveyance that exceed the highest values of $|Q^*_{rf}|$ (Fig 2.4 a and b). In comparison to $|Q^*_{rc}|$, the distribution of $|Q^*_{rf}|$ is less skewed with a greater range, and fewer outliers. This is likely because we did not focus on the most rare and extreme floods in favor of discharge changes for moderate floods, which persistently affect overbank flooding.

The median of combined channel conveyance and streamflow variability, $|Q^*_{r,comb}|$, at the 50 gages is 0.47 (Fig 2.4c). If both Q^*_{rc} and Q^*_{rf} were consistently additive (e.g.

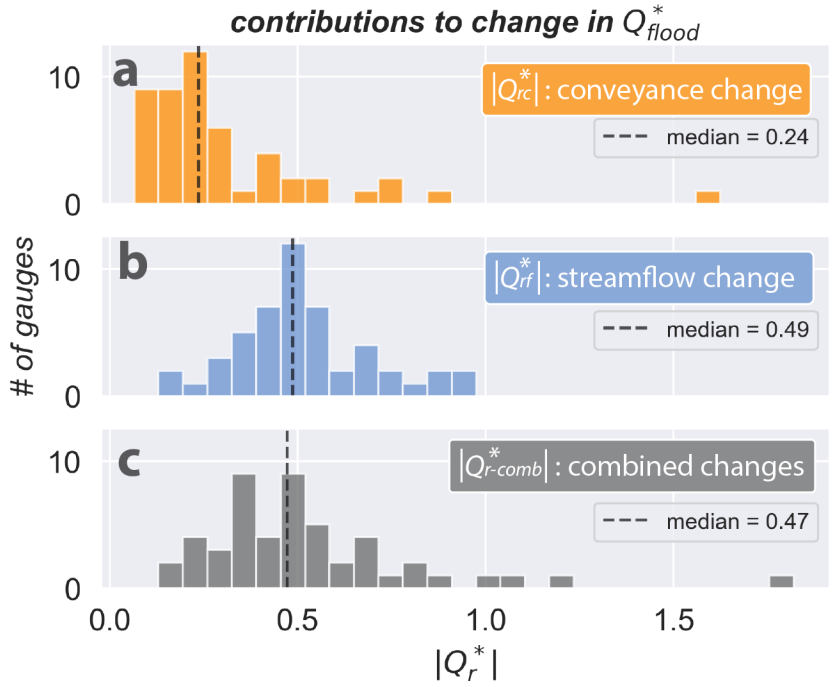

Figure 2.4: *Distribution of magnitude changes in Q_{flood} influenced by (a) channel conveyance changes represented by $|Q^*_{rc}|$, (b) streamflow changes represented by $|Q^*_{rf}|$ and (c) combined change in flood risk incorporating both factors represented by $|Q^*_{r,comb}|$. Dashed lines note the median value for each distribution.*

channels were losing conveyance in concert with increasing discharge) we would expect a median $|Q^*_{r,comb}|$ of 0.65. Instead, median $|Q^*_{r,comb}|$ is slightly lower than $|Q^*_{rf}|$. This indicates that in some cases, changes in channel conveyance and streamflow must offset the change in Q_{flood} imposed by each factor alone and occurs because channel conveyance and streamflow variability are often temporally asynchronous.

2.5.2 *Temporal Patterns in Channel Conveyance and Streamflow Variability*

Channel conveyance changes typically do not occur at the same time across the region; the median of the time series of Q^*_{rc} shows a near-zero trend for unregulated sites (Fig 2.5a) and a slightly positive trend for regulated sites (Fig 2.5b). There are small fluctuations (3-5%) in median channel conveyance in unregulated channels on multi-decadal time scales,

although this is substantially less than the spread of the data (Fig 2.5a). Regulated rivers tended to lose conveyance across the period of record (Fig 2.5b) with median conveyance losses of 10% extending to 70% on the upper bound. Two sites on regulated rivers showed steeper loss trends than this for shorter records; however, other sites showed minimal change to slight gains in channel conveyance (Fig 2.5b).

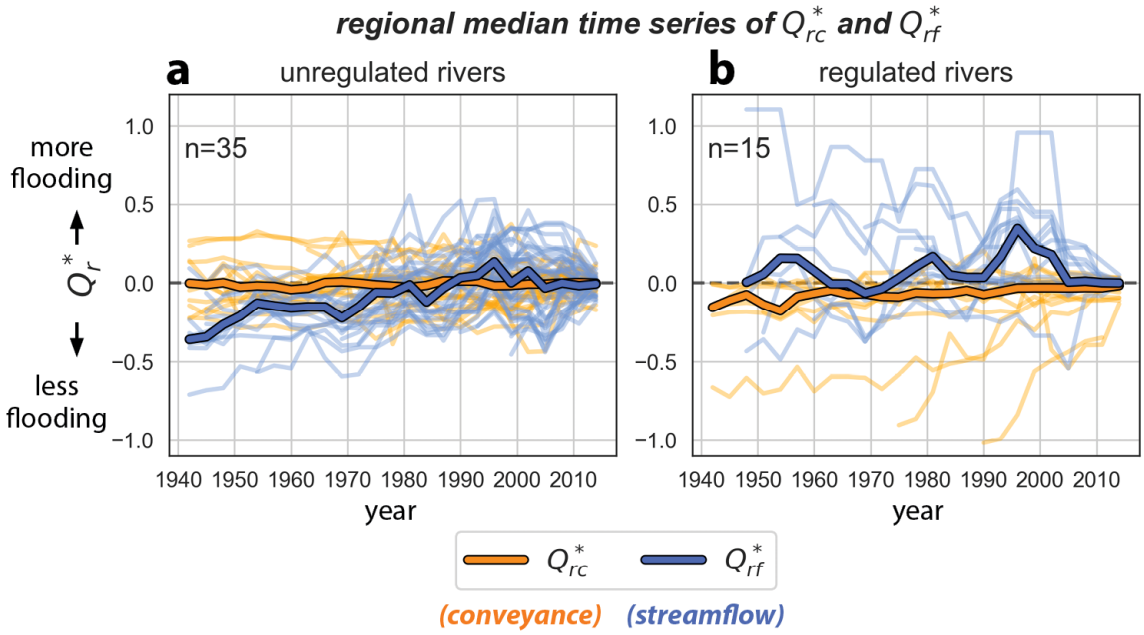

Figure 2.5: *Change in conveyance and streamflow through time at study gages. Medians of the time series for channel conveyance (Q^*_{rc}: orange curve) and streamflow regime variations (Q^*_{rf}: blue curve) with respect to 2015 are shown for (a) unregulated and (b) regulated channels. Data is aggregated into three-year median Q^*_{rc} and Q^*_{rf}. Q^*_{rc} and Q^*_{rf} time series for all study sites are plotted as the light orange and blue curves respectively.*

In contrast, streamflows at sites on unregulated rivers increased over time; median Q^*_{rf} increases by 0.4 between 1940 and 2000 at unregulated sites (Fig 2.5 a). A majority of sites on unregulated rivers show a steepening of the flow duration curve for 0.5-10 year return periods reflecting the increase in the magnitude of moderate floods and Q_{rf} (Fig 2.6 a). The generally positive trend in Q^*_{rf} shown in Fig 2.5 a becomes a noisy, near-zero trend between 2000 and 2015.

In regulated rivers, streamflow does not consistently increase. In contrast to unregulated rivers, seven of the Q^*_{rf} time series on regulated rivers show net negative changes in streamflow on the upper bound of the distribution (Fig 2.5 b) with the largest negative trends being comparable in magnitude to the most positive changes in streamflow on unregulated rivers (Fig 2.5 a). Gages with decreasing trends tended to show a flattening in the high flow regime resulting in a reduction in 2-10 year return period flows (Fig 2.6 b). In some sites such as the example shown in Fig 2.6 b, a reduction in infrequent flows imposed by flow regulations is compensated by relatively higher flows at the 0.5-1 year return period.

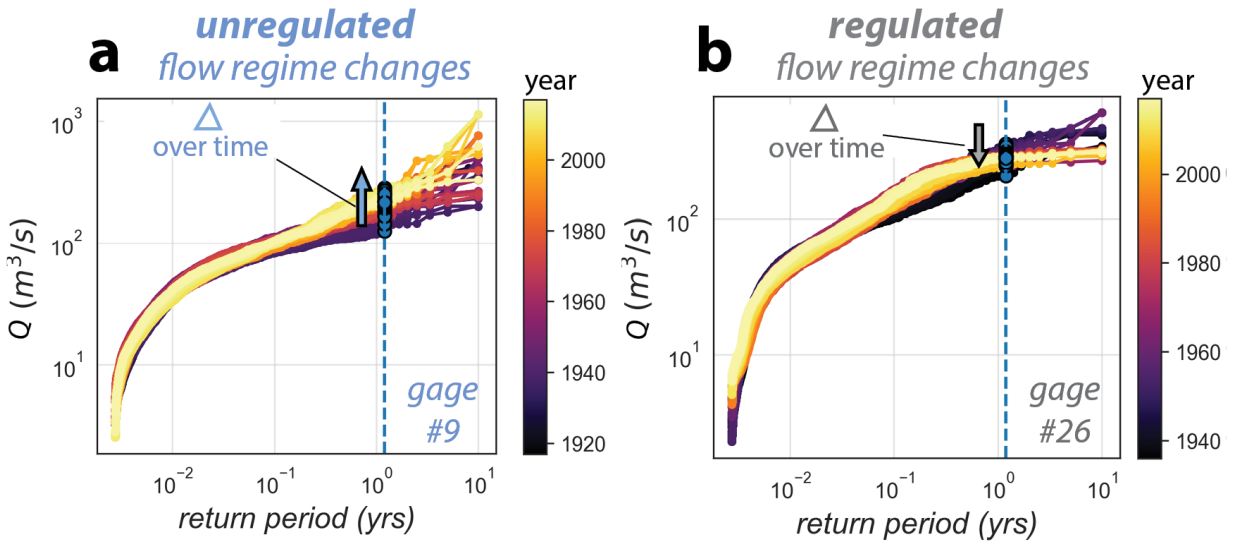

Figure 2.6: *Examples of the ensemble of flow duration curves showing flow regime changes in an (a) unregulated and (b) regulated site. Flow duration curves are colored by time and the bankfull return period of 1.2 years is noted by a vertical dashed line. The interpolated flows are represented as dots on the bankfull return period line, and the overall change in Q_{rf} with time is noted by an arrow.*

Streamflow decreases the most at gages 6, 16, 36, and 34 (Q^*_{rf} decreases ranging from -30% to -97%) which are located relatively close to the dam (within 10km downstream)

in comparison to other sites (ranging between 18 and 116 km downstream). These sites also do not have major tributary input between the gauging site and the dam. In contrast, gages with major upstream tributary input between the gauging site and the dam, including sites 31, 11, 17 and 44, show a near-zero or positive change in Q^*_{rf} of up to 40% across the study period. This suggests that the influence of flow regulations on streamflow at a given gauging location, in particular, the degree of streamflow decrease, is likely a function of the fraction of flow that is regulated. This may also explain why the median Q^*_{rf} for regulated sites does not reflect the decreases in streamflow observed in many individual time series since trends are affected by input from unregulated tributaries.

2.5.3 *Modes of Channel Conveyance Change and Interactions With Streamflow Change*

Channel conveyance and flow regime changes do not interact consistently across western Washington due to regionally asynchronous Q^*_{rc} time series. Additionally, patterns in channel conveyance often display variability that is not captured by a linear trend (Fig 2.5). We distinguish sites with monotonic trends by testing the Q^*_{rc} time series for linearity and identifying sites that do not have significant lag-1 autocorrelation. We use this autocorrelation test in combination with flood and sediment records and history of flow regulations to subset the results into four modes of conveyance change: monotonic changes, multi-decadal oscillations, sudden sediment-supply events and regulated conveyance responses. In what follows, we describe these patterns of behavior and investigate how and why $|Q^*_{rf}|$, $|Q^*_{rc}|$, and $|Q^*_{r,comb}|$ vary between modes of conveyance variability.

2.5.4 *Channels Conveyance Change: Linear vs Nonlinear Behaviors and Relative Magnitudes of Adjustment*

Trends in residuals are monotonic at 20 gages (Fig 2.7 a) and non-monotonic at 30 gages (Fig 2.7 b-d). Of the records with monotonic trends, trend slopes ranged from +3.5% to -2.8% channel conveyance loss per decade, with ten sites showing conveyance loss of 1% or more per decade (gages 15, 50, 29, 49, 45, 41, 7, 13, 14 and 31) and five sites showing conveyance increase of 1% or more per decade (gages 17, 19, 2, 22, and 24) (Fig 2.7 a). The median $|Q^*_{rc}|$ for monotonically changing channels is 0.14 (Fig 2.7 e) which is lower than the overall median $|Q^*_{rc}|$ of 0.24 and the median $|Q^*_{rc}|$ of 0.24 for gauges with non-linear modes of change (Fig 2.7 b-d).

In the majority of gages (18 out of 30) with Q^*_{rc} that change non-monotonically, channel conveyance oscillates at periods ranging from 30 to 70 years (Fig 2.7 b). The median $|Q^*_{rc}|$ for these sites is 0.24 and indicates a median amplitude of conveyance oscillations (Fig 2.7 f). Since these sites underwent periods of both channel conveyance gain and loss, $|Q^*_{rc}|$ is often much higher than the net change between the beginning and end of the record. At many gages, the change in conveyance between the beginning and end of the record is near zero; however, short-term trends in conveyance tend to be of greater magnitude than channels that are changing monotonically resulting in a relatively higher $|Q^*_{rc}|$ for gages showing oscillations in conveyance vs. steady shifts (Fig 2.7 f vs. e). Oscillatory conveyance behavior occurred across a broad range of channel elevations, slope and drainage areas when considering the basin statistics of all gages (Fig 2.9 b-d).

Large, rapid changes in channel conveyance capacity occurred on instantaneous to annual scales in seven sites in response to extreme events capable of delivering a high volume of sediment to the river nearby a gaging station. These events include lahars from the 1980 Mt. St. Helens eruption (gage 37) (*Major et al.*, 2019), intermittent debris flows in proglacial streams (gage 1 and 32) (*Czuba et al.*, 2012; *Tucker et al.*, 2014), a landslide on the NF Skokomish River (gage 43, USGS Water Year Summary) and a 2003 peakflow

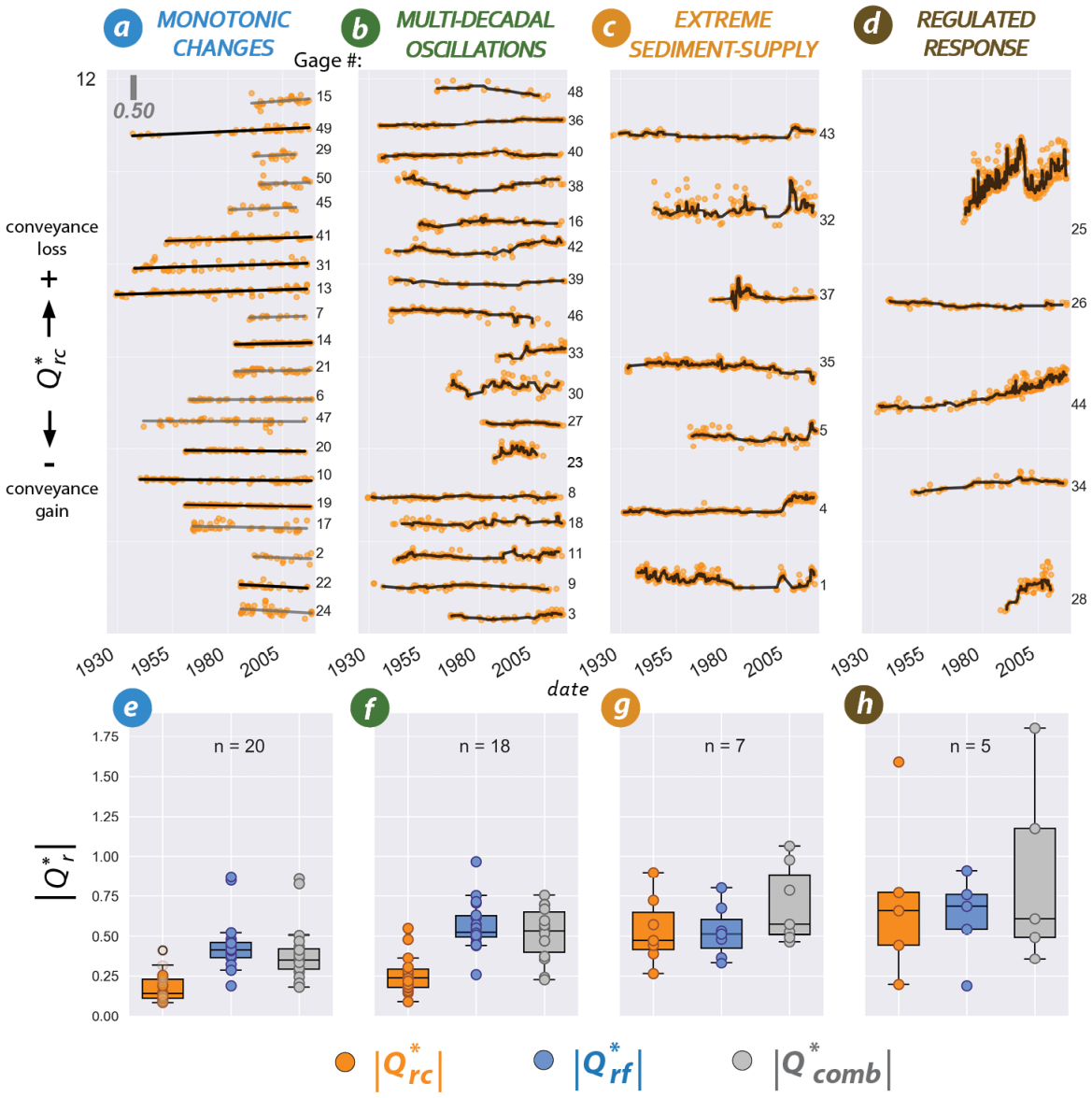

Figure 2.7: *Comparing temporal patterns and magnitudes of change for different styles of channel conveyance adjustment. (a-d): channel conveyance patterns from each of the four styles of channel change. Channel conveyance data for monotonic changes are plotted with a linear fit. Bold trend lines represent statistically significant trends ($p < 0.05$). Channel conveyance data for other categories are plotted with a 5 point moving median. The vertical scalebar in the top left of the plot represents the magnitude of a 50% change in channel conveyance. Gage numbers correspond to Fig 2.2. (e-h): box-plots representing the normalized magnitude of channel conveyance changes ($|Q^*_{rc}|$), streamflow changes ($|Q^*_{rf}|$), and cumulative flood risk changes ($|Q^*_{r,comb}|$) for the four categories of morphological response. $|Q^*_{rc}|$ values for monotonic changes in channel conveyance that are not statistically significant are shown on the boxplot as light colored dots.*

event in Thunder Creek delivering 1.2 times the discharge of the next highest flood on record (gage 4) (Fig 2.7 c). These sites have a median $|Q^*_{rc}|$ of 0.47 (Fig 2.7 g), which is two and three fold higher than the median $|Q^*_{rc}|$ for conveyance oscillations and monotonic changes respectively. These modes of responses tend to occur in headwater rivers with higher mean basin elevation and slope and smaller drainage areas (Fig 2.9).

Some of the largest non-linear channel conveyance changes occured in mainstem channels affected by flow regulation with a median $|Q^*_{rc}|$ of 0.66 (Fig 2.7 d and h). Here we highlight five sites, based upon existing literature (Gages 25, 44, 28, (*Gendaszek et al.*, 2012; *Collins et al.*, 2019; *Anderson and Jaeger*, 2020)), observable conveyance changes concurrent with dam installation (Gage 34) or conveyance changes consistent with the magnitude and time scales of typical geomorphic responses to dams (Gage 26). Four of these sites lost conveyance (gages 24, 44, 34, and 28) and one gained conveyance (gage 26) across the measured record. Conveyance losses were greater than conveyance gains, and in three of the sites, conveyance loss occurred relatively steadily over prolonged periods of time ranging from 30-80 years (gages 25, 44, 28) (Fig 2.7 d). In the Cedar River (gage 25), conveyance losses were so extreme resulting in periodic channel dredging to reduce flood risk (*Gendaszek et al.*, 2012), which is why the channel conveyance shows an abrupt increase in the late 90s followed by continued loss (Fig 2.7 d).

The presence of both conveyance gain and loss indicates that flow regulation does not affect conveyance changes universally across the region. At gage 26 (Fig 2.7 d), regulations suppressed the magnitude of the most infrequent flood flows, but augmented flows at lower return periods (Fig 2.6 b). An increase in frequency of flows around the threshhold of sediment mobilization in concert with sediment deficit is predicted to cause channel degradation (*Grant*, 2012). Lateral mass failures between 2002 and 2016 were less numerous between the dam and gage location in comparison to the sites where channels lost conveyance (*Scott and Collins* (2021): Supplemental Data). Thus, the particular effects of dam influence on sediment-supply and streamflow are necessary to consider when predicting whether channels will respond through conveyance increases or decreases.

2.5.5 *Comparing Conveyance vs. Streamflow Variability and Combined Influence on Flood Hazard*

The relative contribution of conveyance variability ($|Q^*_{rc}|$) and streamflow variability ($|Q^*_{rf}|$) to flood hazard varies with the mode of conveyance change (Fig 2.7 e-h). Median $|Q^*_{rf}|$ was more similar between modes than median $|Q^*_{rc}|$ indicating that the degree of streamflow variability alone does not account for differences in the degree of channel stability. Monotonic and oscillating conveyance variations have median $|Q^*_{rf}|$ values of 0.42, and 0.52 respectively, which are higher than $|Q^*_{rc}|$ for both styles of conveyance change (Fig 2.7 e and f) indicating that streamflow variability typically contributes more to total flood hazard variability for these modes of channel response. In channels responding to extreme sediment-supply events, the degree of streamflow and channel conveyance variability are similar, with the median $|Q^*_{rf}|$ of 0.51 falling within the upper quartile of the $|Q^*_{rc}|$ distribution (Fig 2.7 g) indicating conveyance and streamflow variability typically contribute similarly to total flood hazard variability. The magnitude of streamflow change is highest at sites in regulated rivers (median $|Q^*_{rf}|$=0.69; which is comparable to the median changes to channel conveyance ($|Q^*_{rc}|$=0.66) in the same systems (Fig 2.7 h), indicating conveyance variability can play a comparable role to streamflow variability in total flood hazard variability in some regulated systems.

In sites with monotonic trends in Q^*_{rc}, channel conveyance changes are most likely to offset the pattern of Q^*_{rf} across the study region, resulting in a value of the median $|Q^*_{r,comb}|$ of 0.35, which is lower than that observed in all the other modes (Fig 2.7e); for example, in the Snoqualmie River (gage 19; Fig 2.8 a) increasing streamflows (Q^*_{rf}) are offset by channel conveyance gain (decreasing Q^*_{rc} values), resulting in a reduced impact on flood risk (lower $|Q^*_{r,comb}|$). Nonlinear changes to channel conveyance had higher relative contributions to total flood hazard variability. Oscillating channel conveyance most commonly combines with streamflow regime changes to cause higher changes in Q_{flood} than each effect alone, and resulting in a $|Q^*_{r,comb}|$ of 0.53 (Fig 2.7 f). This is because decadal-scale peaks in

Q^*_{rc} (channel conveyance minimums) and Q^*_{rf} (streamflow maximums) often occur in tandem resulting in additive channel conveyance and streamflow influences on $Q^*_{r,comb}$ (e.g. Chehalis River gage 42, Fig 2.8 b). Since extreme sediment-supply events are also often independent of concurrent streamflow behavior, Q^*_{rc} and Q^*_{rf} are also additive for this mode of conveyance change resulting in a relatively higher value of $|Q^*_{r,comb}|$=0.57 (Fig 2.7 g); for example, gage 32 on the Nisqually River is located downstream of a proglacial debris flow zone (*Czuba et al.*, 2012) where punctuated losses in channel conveyance are superimposed on a generally positive Q^*_{rf} trend, exacerbating changes in $Q^*_{r,comb}$ (Fig 2.8 c). In regulated channels, temporal changes in Q^*_{rf} offset some of the losses in channel conveyance resulting in a $|Q^*_{r,comb}|$=0.61 (Fig 2.7 h); for example, in gage 34 on the Nisqually River (Fig 2.8d), Q^*_{rf} decreases offset channel conveyance losses (increasing Q^*_{rc}).

The differences in median total variability in flood hazard ($|Q^*_{r,comb}|$) vary between modes of conveyance adjustment due to the differences in the ways short- and long-term changes in Q^*_{rc} and Q^*_{rf} combine or offset temporally (Fig 2.7 e-h). This demonstrates that in order to accurately quantify variability in total flood hazard, it is important to consider short-term trends in channel conveyance and streamflow data which can change in magnitude or direction over time.

2.6 Discussion

Our primary goal is to characterize the relative magnitudes and time scales of channel conveyance- and streamflow-driven changes to flood risk in western Washington State, considering both monotonic and non-monotonic temporal changes. We find that the magnitude of flood flow variability is about twice the magnitude of channel conveyance variability, although in some cases variation in channel conveyance is equal to or greater than that of streamflow. These findings are consistent with *Slater et al.* (2015) who, in their analysis of monotonic trends between 1950 and 2013 across the U.S. also showed that hydrologic change was typically a greater contributor to temporal changes in flooding

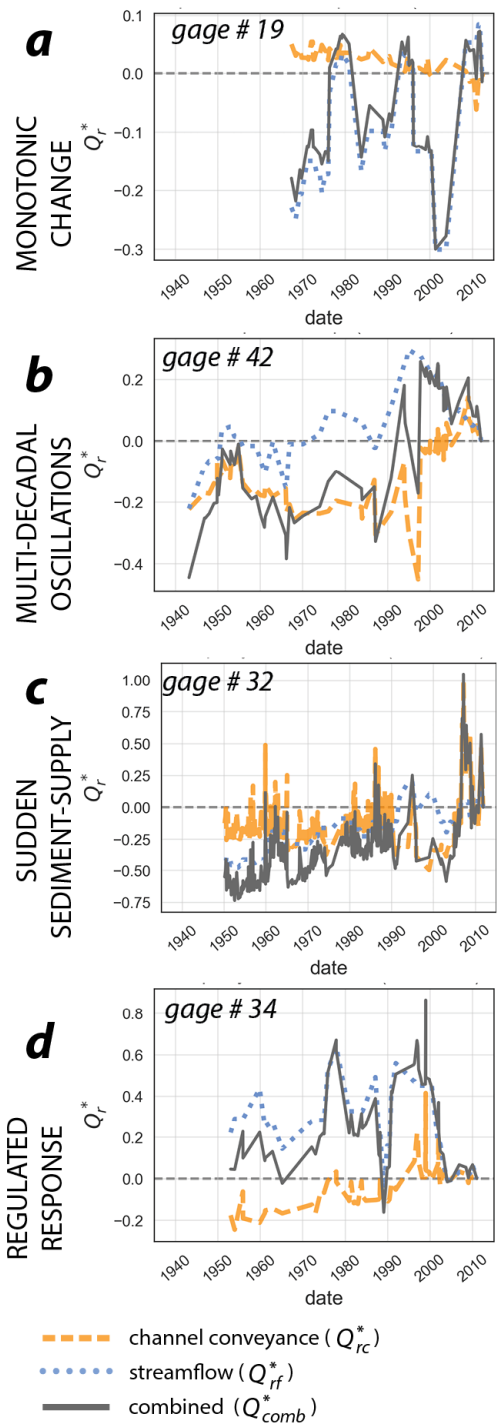

Figure 2.8: *Differing interactions between conveyance, streamflow, and combined flood hazard variability for (a) monotonic (b) oscillating (c) sudden sediment-supply events, and (d) regulated modes of channel conveyance change.*

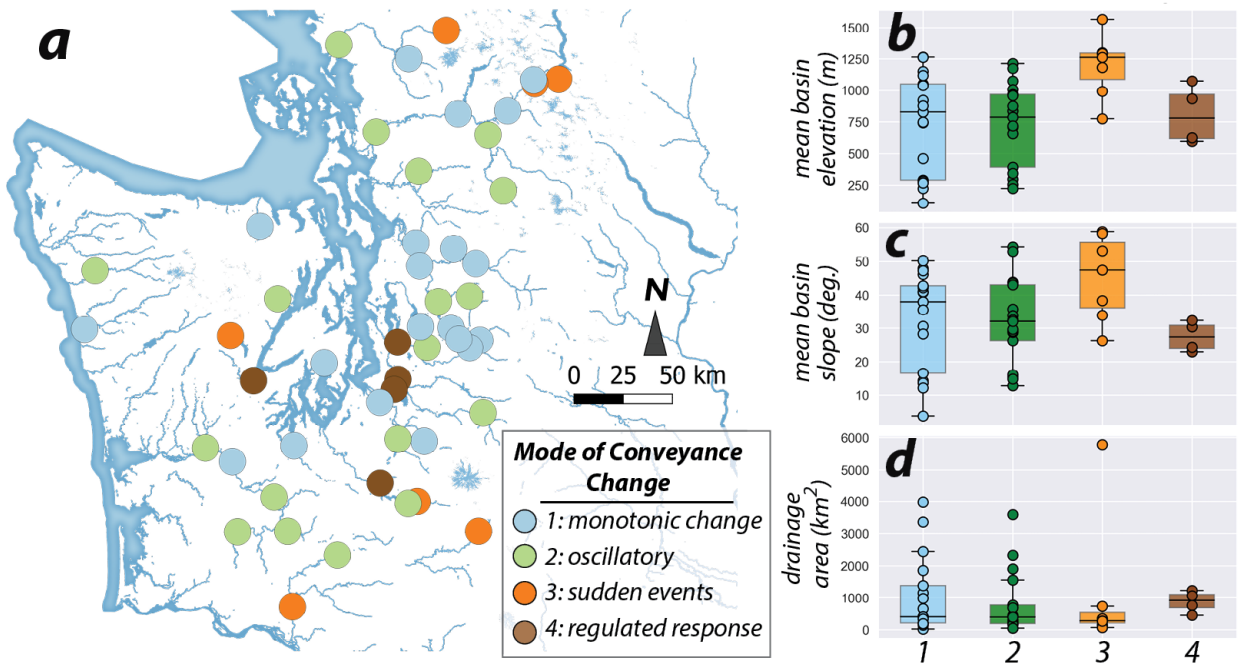

Figure 2.9: *Spatial distribution of channel conveyance modes and basin statistics within each category. (a): USGS river gauging sites included in the study colored by mode of channel conveyance change. (b, c, and d): Basin statistics for each category including mean elevation, mean slope, and drainage area respectively.*

than morphologic change. However, conveyance change is non-steady at nearly all the gages in western Washington. Since USGS gages are intentionally located at stable sites, this analysis likely underestimates the importance of conveyance changes. While at seven gage locations conveyance changed gradually and slowly ($< 1\%$ per decade), at most gages the variability in conveyance was substantial (median of 24% at all gages in the last 30-90 years) and in some cases occurred rapidly, indicating that conveyance unsteadiness is an important contributor to variability in flood hazard.

Nonlinear conveyance changes are important to consider in order to capture total variability in flood hazard because they occur at over half the gages (60%). Not only were nonlinear conveyance changes more common, but total variability and short-term trends at sites with nonlinear adjustments were of higher magnitude than long-term, linear

trends (Fig 2.7 f-h vs. e respectively). For example, had we considered only monotonic trends, many of the gage locations with oscillating conveyance would have shown a trend of zero slope since there were equal amounts of conveyance loss and gain; however, the magnitude of conveyance gains and losses over the course of an oscillation (about one to two decades) at these locations are typically greater than the total conveyance adjustment in locations with steady monotonic change (Fig 2.7 f vs. e). *Li et al.* (2020) showed that short-term, transient capacity change due to tropical storms in Puerto Rico was frequently higher magnitude than long-term trends. Here, we find that rapid and nonlinear conveyance changes are also widespread in space and time in a temperate zone. We also find that fitting monotonic trends to non-linear conveyance records would have smoothed out rapid or cyclic changes to capacity and resultant influence on flood hazard variability. Thus, the methods used in this analysis of flood hazard shifts driven by streamflow vs conveyance *variability* are a necessary and important improvement to previous approaches that assume monotonic change (e.g., *Slater et al.*, 2015; *Slater*, 2016).

Instead of fitting monotonic trends to the gage time series of conveyance capacity variation, we identify four temporal modes of conveyance change in an effort to describe total variability in flood hazard (Fig 2.7). While these modes are not exhaustive representations of the ways rivers might adjust in other areas of the world, this type of analysis provides useful information on reach-scale conveyance changes that can affect overbank flooding at USGS gages. Adding recent conveyance adjustments to the daily and long-term flood forecasting at USGS gages which are presently computed using streamflow and precipitation data (*NOAA*) could improve local flood hazard predictions. For example, gage 3 on the Nooksack River has multi-decadal oscillations in conveyance and presently has around 15% less capacity than it did in 1990 but relatively similar capacity to the mid 1960s. There has been recent debate amongst stakeholder groups about whether flood prevention actions in the Nooksack River should involve sediment removal (*Kempe*, 2021). Considering that channels can locally be in phases of conveyance loss would be valuable for forecasting local flood hazards and could facilitate development of sediment-removal

plans that strategically interrupt short-term minimums in conveyance. In what follows, we discuss the implications of different modes of conveyance variability for flood hazard and investigate potential drivers of these patterns in an effort to predict when a given mode is expected to arise.

2.6.1 *Are increases in streamflow-driven flood hazard being moderated by increases in conveyance capacity?*

While channel conveyance is changing in many systems, regional trends in flooding are better predicted by streamflow behavior. Shifts in moderate flood flows in unregulated rivers are generally positive in western Washington (Fig 2.5 a). However, channel conveyance variability in western Washington State does not alter flood risk uniformly or simultaneously across the region (Fig 2.5 a). This is at odds with some studies that suggest channels adjust coherently to changes in climate; *Slater et al.* (2019) found that across the United States, two thirds of 67 USGS study gages showed correlation between channel capacity and climate indicators representative of patterns in regional rainfall and temperature. *Rumsby and Macklin* (1994) found that channels in northern England had widespread, alternating phases of channel incision and stability in response to decadal-scale fluctuations in flood frequency.

However, asynchronous channel bed adjustments have been previously documented in western Washington and attributed to variation in sediment supply rather than streamflow (*Pfeiffer et al.*, 2019). Studies of individual western Washington rivers have demonstrated that sediment supply alters channel bed morphology as downstream-propagating disturbances over multi-decadal time scales with behavior similar to a Gilbert Wave (*Nelson and Dubé*, 2016) or a non-diffusive series of river bed elevation changes with celerity related to slope (*Anderson and Konrad*, 2019). Presumably, increases in runoff and temperature also activate delivery of sediment from proglacial, alpine regions (*Costa et al.*, 2018) and an increase in the magnitude of moderate floods could increase sediment delivery from

channel-adjacent terrace failures that are predominantly triggered by lateral fluvial erosion (*Scott and Collins*, 2021). Intermittency in magnitude and timing of sediment delivery is likely to add noise to a climate-driven signal (*Jerolmack and Paola*, 2010) and could obscure or dominate over the influence of climate on river adjustment in this region.

While the magnitude and intermittency of sediment supply likely contribute to observed asynchronous conveyance changes, differences in routing between systems likely affect the propagation of sediment signals downstream. Gage locations downstream from extreme sediment-supply type responses do not necessarily show the same response mode; they can show both monotonic shifts and multi-decadal oscillations in conveyance (Fig 2.9a). Conversely, common downstream responses don't correspond to common upland inputs. For example, channel conveyance variations at gages on low-elevation reaches of the Skagit and Nooksack Rivers show very similar behavior despite differing degrees of headwater conveyance change (Fig 2.10), the headwater Nooksack gage being relatively more active than high-elevation Skagit gages. Thus, we do not observe clear connectivity between the conveyance responses in headwater and lowland reaches based upon the sites analyzed in this study.

Overall, regional flood hazard is increasing in unregulated rivers, but this trend is dominated by regional streamflow patterns rather than conveyance patterns (Fig 2.5 a). Steepening of the high flow region of the flow duration curve in unregulated sites (Fig 2.6 a) is typical in rivers transitioning from snowmelt- to rain-dominated floods (*Searcy*, 1959). Previous studies have shown dramatic declines in western United States snowpack (e.g., *Mote*, 2003; *Mote et al.*, 2018) in concert with regional warming over the last century (*May et al.*, 2018). This results in statistically significant increases in winter maximum streamflows as previously snow-dominated basins transition towards rain-dominated basins in winter (*Wagner et al.*, 2021). Thus, changes in snowpack likely explain some of the observed shifts in the flow duration curve. Flood event frequency and severity are expected to increase under future climate conditions due to further warming (*May et al.*, 2018), and an increase in precipitation volume and intensity from atmospheric river events

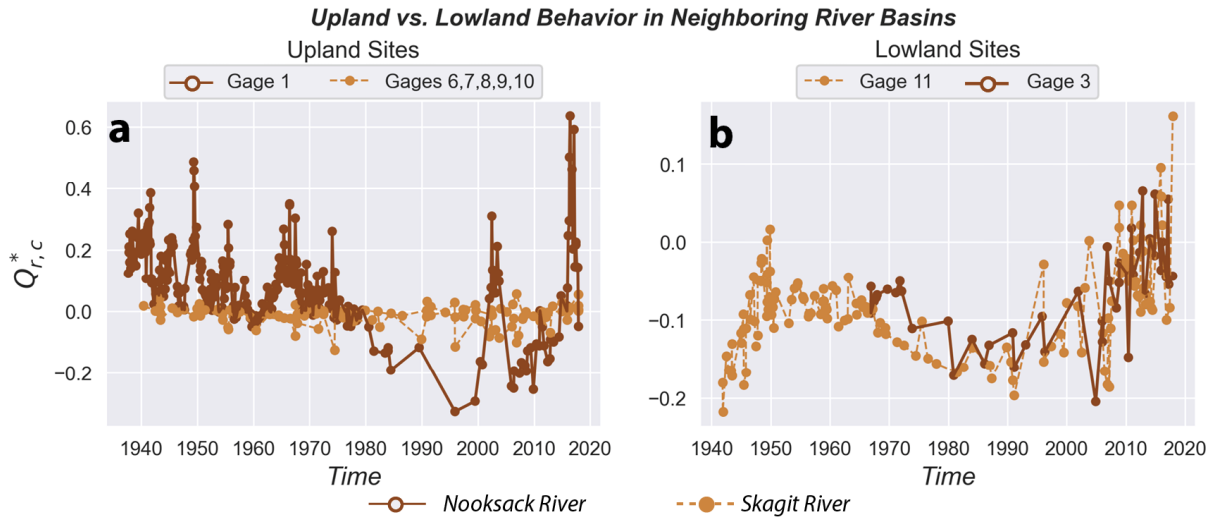

Figure 2.10: *Time series of normalized channel conveyance change Q^*_{rc} in (a) upland vs. (b) lowland sites in neighboring river basins demonstrate different along-profile morphodynamic behavior. In (b), lowland river gauging sites show remarkably similar temporal patterns of similar magnitude despite differing degrees of channel stability in upland gauging sites shown in (a). Q_{rc} are plotted with respect to 2015.*

(*Gershunov et al.*, 2019). It is thus probable that streamflow-driven flood hazards will continue to increase in unregulated western Washington basins. On aggregate, conveyance adjustments do not offset these changes to streamflow, but can locally increase or reduce flood hazard depending on the mode of response.

2.6.2 *Flood hazard drivers in regulated rivers*

In contrast to unregulated basins, flow regulation mutes or eliminates decadal increases in moderate flood streamflow (Fig 2.5 b). This is because dams increase flood storage (e.g., *Collier et al.*, 1996). Indeed, flow duration curves from regulated systems typically show a reduction in flow volume at the most infrequent floods (Fig 2.6 b) which can represent an increase in water storage (*Searcy*, 1959). It is likely that dams will continue to suppress the influence of changing climate and hydrology on regional streamflow; in a comparison of regulated and unregulated Columbia River Basin streamflow projections

over the next century, flow regulation dampens the shifts in timing and volume of cool season high-flows projected to occur in unregulated rivers (*Harrell*, 2021).

However, flow regulation does not necessarily reduce total flood hazard, because downstream channel conveyance losses can exceed reductions in flood flows. Regulated rivers on aggregate show a tendency for conveyance loss, although the upper envelope of the distribution also includes modest trends towards channel conveyance gain (Fig 2.5 b). While the aggregate decrease in conveyance capacity is only approximately 10% over 70 years and is much less than the variability between individual rivers, this trend is supported by other observations of channel adjustment in the region. Previous studies show that channels narrowed in four regulated rivers in the region (*Anderson and Jaeger*, 2020; *Collins et al.*, 2019; *Gendaszek et al.*, 2012; *Konrad et al.*, 2011), and shallowed in at least three rivers (*Anderson and Jaeger*, 2020; *Collins et al.*, 2019; *Gendaszek et al.*, 2012). Since dams can potentially cause conveyance loss or gain depending on how they influence the downstream flux of water or sediment (*Grant*, 2012), further studies comparing the natural and anthropogenic geomorphic drivers present in regulated basins are needed to understand how channel conveyance responds to the interactions of flow regulation and sediment supply in the region (e.g., *Anderson and Jaeger*, 2020; *Collins et al.*, 2019). Overall, it is critical to consider flood hazard change as a composite of conveyance change and streamflow variation in regulated rivers; assumptions of future flood hazard based solely on streamflow projections could under-predict hazards.

2.6.3 Modes of channel conveyance change and their relative importance for flood hazard

Our results show that conveyance variability can be more or less important for flood hazard depending on the ways in which cyclic, episodic or gradual changes to conveyance capacity augment or reduce changes to streamflow (Fig 2.7 e-h). However, can we predict when and where different modes of conveyance change will occur? Basin statistics don't correlate with certain conveyance modes, except for the seven cases of channel response to

extreme sediment supply events which tended to occur in steeper, lower-order basins (Fig 2.9 b). While the sample size of basins included in this study is small, this observation is consistent with *Slater and Singer* (2013), who also find that basin statistics including mean watershed slope, elevation and drainage density do not predict trends in alluvial river bed elevation or river bed variability across the United States. As discussed in Section 2.6.2, channels downstream of dams may be susceptible to conveyance changes influenced by dam operation and flow regulation. However, monotonic change and multi-decadal oscillations, (Fig 2.7 a and b) are common across a range of watersheds and lack correlation with basin slope, drainage area, or mean basin elevation (Fig 2.9 b).

In a region where unregulated rivers show an increase in moderate flood magnitude (Fig 2.5 a), it is interesting that monotonic conveyance changes show nearly equal occurrence of steady decreases and increases (Fig 2.7 a). Flow magnitudes around the bankfull return period (typically 1-3 yrs, (*Castro and Jackson*, 2001)) are generally considered important for establishing cross-sectional channel form for low- and moderate-gradient alluvial channels in temperate regions (*Leopold et al.*, 1964; *Wolman and Miller*, 1960). While many studies have explored the concept of defining a channel-forming discharge (e.g., *Blom et al.*, 2017; *Castro and Jackson*, 2001), channel adjustments in response to gradual changes in discharge are more complex because adjustments in alluvial channel gradient and bed-elevation require some relaxation time in response to a change in inputs (*Howard*, 1982). The response of gravel-bed rivers downstream of dams indicate that channels adjust their width and bed-elevation on the order of several decades after dam installation (*Grant*, 2012). Assuming no change to sediment supply, the cases where conveyance is steadily increasing are consistent with what theory suggests for river response to increasing discharge (*Lane*, 1955). However, the fact that steady conveyance gains appear to lag streamflow changes suggests that the rate of change to moderate flood discharge exceeds the response time scale for conveyance adjustment.

Steady conveyance decreases may be the result of changes to sediment supply, especially lateral sediment sources that are sensitive to fluvial processes. Puget Sound rivers

have high, coarse sediment supply from paraglacial terraces relatively low in the drainage basin (*Scott and Collins*, 2021). Nearly all terrace failures mapped in *Scott and Collins* (2021) deliver sediment directly to the adjacent river with lateral fluvial erosion being the dominant trigger of mass failure. Steady increases in moderate flood streamflow may thus activate unstable bluffs and increase the transport of paraglacial material to depositional zones. For example, the Skykomish River is an unregulated stream experiencing increasing moderate flood flows. Records from gage 13 (supporting information Fig S3) document a long-term, monotonic trend towards channel conveyance loss. This site is located on a bend downstream of a long-term outer bank failure that is documented to yield $\sim$ 8000 m^3/yr of sediment directly to the channel (*Scott and Collins*, 2021). Future investigation of sediment supplied by lateral terraces as a function of antecedent streamflow characteristics could illuminate how hydrologic changes feedback into sediment delivery from sources connected to rivers in the region.

Temporal oscillations in conveyance capacity can augment or reduce variations in streamflow, potentially amplifying total shifts in flood risk. Previous studies show that flood hazard can be non-stationary (e.g., *Read and Vogel*, 1969; *Slater et al.*, 2015; *Vogel et al.*, 2011) but often neglect the complexities of incorporating short-term behavior that can shift the direction of flood hazard trends. Periods of fluctuation (between 30 and 70 years) are of similar scale to cycles of wet/dry climate associated with the El-Nino/Southern Oscillation and the Pacific Decadal oscillation. However, conveyance fluctuations did not correlate with regional precipitation anomalies and there is little correlation in the phase of higher and lower conveyance between basins. This suggests that variations in sediment supply are a significant driver of conveyance fluctuations; while variations in sediment supply are presumably influenced by climate (e.g., *Anderson and Konrad*, 2019; *Leggat et al.*, 2015; *Menounos*, 2006; *Menounos and Clague*, 2008), the particulars of erosion in a given river basin may dominate over any regionally consistent climate-driven trends, resulting in a lack of regional synchronization in conveyance oscillations.

2.6.4 *Flood Hazard Predictions Involving Conveyance Variability*

Operational assessments of flood hazard predominantly rely on metrics such as inundation area and overbank flow velocity obtained from numerical simulations or observations that rely on hydrologic data alone (e.g., *Yang et al.*, 2006; *FEMA*, 2012). However, in this study, we show that variability in channel conveyance is also an important metric for exacerbating or alleviating flood hazard through channel adjustments (Fig 2.1b). While the four modes of conveyance change we present have different magnitudes and styles of variability (Fig 2.7), the potential for conveyance variability to modify flood inundation area will depend on the surrounding floodplain topography, which we did not explicitly consider in this study. Since slight adjustments to river geometry could propagate into large changes in inundation across low-gradient regions, moderate channel conveyance variability in reaches with low-gradient surrounding topography (e.g. the Puget Lowland) is likely to be of greater significance for flood inundation than high conveyance variability in reaches confined by valley walls. Thus, the information about historic conveyance variability presented in this study could be combined with topographic data surrounding USGS gages to identify at-risk areas, targeting inundation assessments in regions with both moderate or high conveyance variability and low-gradient surrounding floodplains.

Changes in flood inundation as a result of conveyance variability would be particularly valuable for assessing residential hazards. During the January 2009 White River flood event where extensive flooding was attributed to channel conveyance losses (e.g., *Czuba et al.*, 2010; *Green*, 2009), residents of surrounding towns relied on outdated flood maps for purchasing flood insurance (*Cornwall*, 2009). Incorporating inundation variability due to conveyance changes as an uncertainty buffer in flood maps could additionally help communicate risk more transparently to residents and stakeholder groups.

2.7 Conclusions

Channel conveyance variability is an important contributor to temporal variability in flood hazard in western Washington state. While the median regional variability in moderate flood streamflow is approximately twice that of median conveyance variability, conveyance variability contributed to flood hazard shifts in almost all systems considered. Moderate flood streamflow is consistently increasing in unregulated rivers, but conveyance change is not regionally consistent. Channel conveyance changes can be linear, oscillating, dominated by singular sediment supply events or influenced by flow regulation, and the relative importance of conveyance variability vs streamflow variability on flood hazard varies with the mode of channel adjustment. The influence of conveyance variability on flood hazard was more important than streamflow variability following unusually large storm or sediment supply events and can also be higher in regulated rivers, counteracting the effects of flow regulation on flood-risk. Short-term conveyance adjustments are more common and of higher magnitude than steady trends, indicating that it is necessary to quantify short-term channel behavior to accurately predict total changes in flood hazard. The time series of conveyance variability could be added to streamflow projections at USGS gages to improve predictions of flood hazard. Furthering our understanding of the mechanisms and controls on the different patterns of temporal variability in channel conveyance would aid in modeling and mapping future flood hazards.

Part II

Chapter 3

FLOODPLAIN-CHANNEL FLOW EXCHANGE EXPLAINS MAIN-CHANNEL BED ELEVATION CHANGE WITHIN AND BETWEEN PEAK FLOW EVENTS IN AN ENGINEERED RIVER

Abstract

River peak flows can substantially alter channel bed morphology over event timescales. However, morphodynamic changes can go undetected because measurements of pre- and post-peak flow bathymetry are often unavailable. This study investigates whether bed elevation changes during and between peak flows can be explained by spatial variation in river floodplain geometry and its corresponding effect on streamwise gradients in flow velocity. We analyze river bed elevation changes for different flow conditions across three ten-kilometer sections of the Waal River, the Netherlands, using bi-weekly bathymetry data obtained over the last 20 years. We compare relative bed elevation change during high vs low flows to streamwise changes in along-channel and transverse flow velocities extracted from hydrodynamic model output for high and low flows. We show that in a fixed, relatively constant-width main channel, cyclic, along-channel variations in bed elevation between low- and high-flow conditions, can arise from spatial gradients in flood flow velocity caused by floodplain geometry and floodplain-channel flow exchange. During peak flows, erosion occurs in regions where the floodplain narrows, forcing the flow to constrict and accelerate in the main channel, or where there is a spatial mismatch between floodplain and main-channel flow routing, resulting in floodplain flow entering or crossing the main channel. Transverse velocities perpendicular to the main-channel indicate where floodplain flow enters and exits the channel; these locations are strongly related with locations where the bed scours and deposits respectively during floods. This

study suggests that changes in main-channel bed elevation within and between flood events can be explained by the degree to which floodplain geometry and topography affect spatial hydraulic gradients during peak-flow conditions.

3.1 Introduction

River channel morphodynamics are sensitive to floods; peak flow events can cause abrupt changes to channel geometry (*Erskine*, 2011; *Magilligan et al.*, 2015) from which the channel morphology can either recover to its pre-flood state or be persistently modified (*Sofia and Nikolopoulos*, 2020). Flood variability is important for setting channel geometry and stability (*Davidson and Eaton*, 2018) variations in bed texture (*Lisle and Hilton*, 1999) and maintaining certain morphological patterns such as pool-riffle sequences (*De Almeida and Rodríguez*, 2011) and braiding or meandering (*Brewer and Lewin*, 1998; *Erskine*, 2011).

Morphodynamic changes occurring during a flood can affect flow conveyance capacity for future floods. Main channel deposition and narrowing can reduce flow conveyance and increase flood frequency (*Slater et al.*, 2015; *Slater*, 2016; *Stover and Montgomery*, 2001). Conversely, scour during peak flows can increase the conveyance capacity for flood flows (*Guan et al.*, 2016). Recent work shows morphodynamic changes can contribute to flood hazard nonstationarity (*Ahrendt et al.*, 2022; *Slater et al.*, 2015) and impresses the necessity of including geomorphic changes in frameworks for flood prediction (*Sofia and Nikolopoulos*, 2020). Thus, understanding morphodynamic change during floods is also important for predicting future flood hazards.

However, predicting intra-flood morphodynamic response for a given event is difficult due to temporal and spatial variation in patterns of erosion and deposition. Geomorphic response can be poorly related to peak flow duration and intensity (*Dury*, 1973). Temporally, the magnitude and ordering of previous flows can affect bed stability. A long period of low flows can re-organize the bed matrix to increase particle interlocking, increasing the threshold for incipient motion during subsequent high discharge events, while high flows can disrupt bed surface texture leading to high bed mobility post-flood

(*Masteller et al.*, 2019; *Milhous*, 1973; *Ockelford et al.*, 2019; *Reid et al.*, 1985). The particulars of sediment supply and climate in a given basin also affects channel response: higher sediment supply is related to higher bed mobility (*Lisle et al.*, 2000; *Pfeiffer and Finnegan*, 2018); in rivers where sediment production may periodically vary with climate (e.g., *Anderson and Konrad*, 2019), channel response may not consistently vary with discharge.

Despite the variability of channel response to peak flows, streamwise variations in lateral channel confinement have been shown to drive reach-scale gradients in stream power and channel response during peak flows (*Arkesteijn et al.*, 2021; *Nanson and Croke*, 1992; *Sholtes et al.*, 2018). Most previous studies have focused on geomorphic response in relation to river confinement as it pertains to total valley widths (e.g., *Sholtes et al.*, 2018; *Underwood et al.*, 2021; *Yochum et al.*, 2017), since in natural channels with a freely adjusting planform, the 'confining' river boundary usually occurs on distal valley geometry or non-erodible terraces. However, in engineered channels, the main-channel and/or floodplain boundaries are often fixed via levees and revetments, thus shifting the effects of confinement proximal to the main-channel. Here, we extend research on river response to confinement in a compound, meandering channel with a fixed main channel and leveed floodplain in order to understand the relationships between confining geometry and morphodynamic response during peak flows.

Compound river channels consisting of a main channel and a floodplain add complexity to flood hydrodynamics. Floodplains often have higher roughness than the main-channel due to vegetation, which can decrease total flow velocity when both the main channel and floodplain are active during peak flows (*Thomas and Nisbet*, 2007) and enhance lateral turbulence at points where flood flow is exchanged between the main channel and floodplain (*Liu et al.*, 2016). Generally, locations of flow exchange can cause energy loss due to vigorous secondary currents (*Sellin et al.*, 1995), which can change compound channel and floodplain flow conveyance depending on cross-sectional channel geometry, sinuosity, and roughness (*Ervine et al.*, 1993). Overbank flow across a fixed, meandering channel can also alter the location of peak flow velocities from the outer to

inner bend (*Toebes and Sooky*, 1967). The substantial shift in flow dynamics with water stage in compound channels may thus be expected to propagate into channel response, although the morphodynamic response of compound channels to floods is not well understood.

This work aims to assess whether spatial variation in floodplain planform geometry and topography can explain bed elevation response to floods and inter-flood recovery in the Waal River, a heavily-engineered, compound channel with a fixed planform. Since planform channel characteristics and floodplain topography are often readily available via remote sensing methods (e.g. satellite imagery and LiDAR-derived DTMs, *Piégay et al.* (2020)), this work is relevant for understanding regions prone to morphodynamic adjustments during floods in areas that lack sufficient bathymetry and sediment-transport measurements. We select the Waal River since previous work suggests that river channel bed elevation change during and between floods is dictated by spatial changes in local river geometry (*Van Denderen*, 2014). The Waal additionally has a rich monitoring dataset of high spatial and temporal resolution bathymetry data from which to analyze typical bed responses to both flood- and low-flow conditions (*Van Denderen et al.*, 2022b).

Specifically, we ask, 1) How does floodplain geometry and topography affect main-channel and floodplain flow exchange as water stage increases? 2) How does main-channel and floodplain flow exchange modify spatial gradients in flow velocity? And 3) How do corresponding spatial gradients in floodplain- & main-channel flow velocity feedback into bed elevation change within and between flood events? Since bed response during a flood is relatively difficult to measure, our goal is to provide context for how well geometric and topographic analyses of a river channel and floodplain indicate locations of bed response during peak flows and recovery between events. We also aim to understand generally how the hydrodynamics of overbank, compound flow can influence bed elevation change during floods and inter-flood recovery.

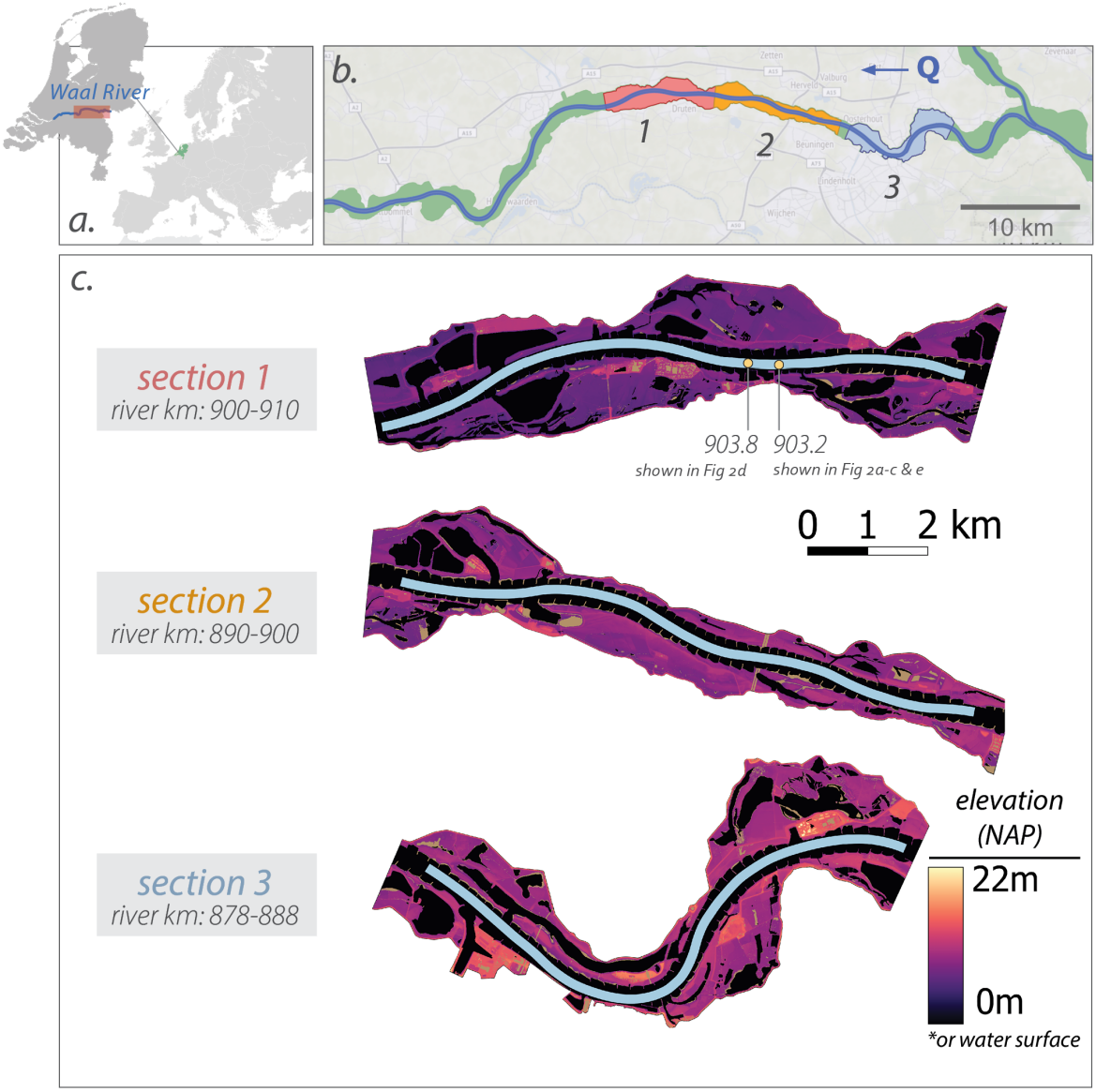

Figure 3.1: *Site map for three 10 kilometer study sections with varying floodplain width and sinuosity.* ***(a)*** *inset showing Waal River location in the Netherlands* ***b*** *study sections in the upstream Waal River;* ***(c)*** *topographic elevation (source data: Nederland (2021)), stitched and trimmed to the floodplain boundaries. Bed elevation data (compiled in Van Denderen et al. (2022a)) are obtained in the navigational channel of the main channel as highlighted in blue.*

3.2 *Site Information & Background*

We analyze relationships between floodplain topography, geometry, flow velocity, and channel response between peak- and low-flows across three 10km sections in the upper 40 km of the Waal River, the Netherlands, a west-flowing distributary of the Lower Rhine River discharging into the Atlantic Ocean. The three sections (Fig 3.1) extend from river kilometer 900-910 (section 1), 890-900 (section 2), and 878-888 (section 3). The sections begin 11 km downstream of the Pannerdense Kop, a major bifurcation in the Lower Rhine River 10 km downstream of the Dutch-German border where the river splits into the Pannerden Canal (the northern branch) and the Waal (the southern branch) (Fig 3.1 b). The bifurcation is a dynamic region that affects the upstream portion of the Waal River; recent work shows the Waal branch receiving an increasing fraction of discharge and experiencing higher erosion rates after a rapid succession of peakflow events in the 90s lead to abrupt sedimentation downstream of the bifurcation region (*Chowdhury et al.*, 2023). Peak flow events continue to initiate downstream migrating erosion waves in the Waal from the Pannerdense Kop (*Chowdhury et al.*, 2023).

Waal River hydrology is driven by snowmelt and rainfall. Snow is stored in alpine regions in the upper Rhine catchment during winter months while winter floods in the lower catchment typically occur from low-pressure system rainfall (*Te Linde et al.*, 2010). The mean annual maximum in daily discharge at Lobith, a gaging station just upstream of the Pannerdense Kop (Fig 3.1), is 6,650 m^3/s, and the mean discharge during the summer months (July-September) is 1,880 m^3/s according to mean daily streamflow data from the last century. The Waal River discharge is also affected by the Driel weir in the Nederrijn Lek downstream of the Pannerden Canal; during low flows the weir is closed and the Waal recieves a higher fraction of discharge than at high flows when the weir is open (*Chowdhury et al.*, 2023).

The Waal river channel is heavily engineered with historic interventions that include manual channel narrowing, groyne construction, dam installation, and side-channel con-

struction (*Ylla Arbós et al.*, 2021). A byproduct of engineering is a fixed river planform with spatial variation in floodplain width but a relatively constant main-channel width across the study sections (Fig 3.1). Since the planform is fixed, morphodynamic adjustments are limited to bed texture and elevation; the latter of which is the focus of this study. We select three sections of the Waal River with variation in floodplain width and sinuosity in order to consider streamwise shifts in floodplain geometry that may force different types of floodplain-channel flow interaction during floods: Section 1 has both channel meandering and floodplain width variation, Section 2 has a straighter main channel with a varying width floodplain, and Section 3 has a highly meandering channel and floodplain (Fig 3.1). Section 3 additionally has a 'fixed bed layer' consisting of an erosion-resistant rockfill installed in the downstream meander — the 'Nijmegen bend' — in 1985 to improve navigation around the sharp bend by adjusting the secondary flow such that the flow depth on the inner bend becomes deeper (*Havinga*, 2020).

During floods, overbank flows are subject to geometric and topographic routing on the floodplain which can cause spatial gradients in velocity in the main-channel that are unique to peak flow conditions since they do not occur when flows are confined to the main-channel. These gradients can result in a morphodynamic response; where flows spatially accelerate erosion will occur, and where flows spatially decelerate deposition will occur. Because the main-channel has a relatively constant width across the 30km analyzed in this study, gradients in velocity due to floodplain flow expansion and contraction of the floodplain are not present at low flows. Instead, the low flows becomes slightly non-uniform due to morphodynamic changes during peak flows resulting in in-filling and scour of the peak flow erosion and deposition respectively.

Here, we consider two ways floodplain geometry and topography can affect the streamwise accelerations and decelerations of flow during overbank flood conditions: 1) streamwise changes in floodplain width, and 2) topographic routing of floodplain flows that causes flows to plunge into and out-of the main-channel during floods. Roughness is also known to modify floodplain-channel flow exchange in compound channels, but it

is not explicitly considered in this study due to the complexity of quantifying its effects (e.g., *Ervine et al.*, 1993).

3.3 *Methods*

3.3.1 Bed elevation analysis

River bed adjustments can be characterized into two categories based upon the time-scale of response: a quasi-static component (adjustment to controls operating on slow time-scales) and a dynamic component (adjustment to controls varying over short time scales, e.g. those associated with a hydrograph) (*Arkesteijn et al.*, 2019). This work addresses the dynamic component by analyzing relatively short-term changes in the channel bed due to temporally variable discharge.

To analyze bed elevation changes, we use high-resolution bathymetry measurements from the Waal River in the Netherlands collected at bi-weekly intervals in the navigational channel over the last 20 years (e.g. Fig 3.2). The measurements are processed to raster tiles and averaged cross-sectionally across the 150m-wide navigational channel at every five meters longitudinally to obtain a streamwise average profile (*Van Denderen et al.*, 2022b). These longitudinal profiles span 16 years (2/14/2005-2/8/2021) with a median time between profiles of 14 days. Data are compiled in a remarkably accessible 'river atlas' (*Van Denderen et al.*, 2022a) with the capacity to rapidly interact with the data within a Graphical User Interface or to download it from the underlying database.

To analyze the dynamic component of bed adjustment, or relative bed elevation changes during high and low flow events, we leverage the wavelet analysis developed in *Van Denderen et al.* (2022b) to isolate river bed variation at length-scales of change typically associated with discharge fluctuations. The benefit of a wavelet analyses vs. other spectral analyses (i.e. Fourier) is that it can identify energy at a signal that may vary in space; this is important for rivers, because different length scales of change may be more or less important at different longitudinal locations on the river (*Van Denderen*

et al., 2022b). The wavelet analysis isolates length scales of change ranging from 300m to 4000m– these length scales are longer than the Waal River groyne spacing ($\sim$ 200m) to filter out bed changes that may occur locally as a result of groynes and are shorter than longer, equilibrium adjustments in the river. Previous work suggests these length scales are also typically most affected by discharge variations (*Van Denderen et al.*, 2022b). An example of cross-sectionally averaged bed elevations and the wavelet-processed signal is presented for two example locations in Fig 3.2 b-e.

Average river bed variation is computed for eight discharge categories to identify the typical morphodynamic response to different flow conditions. Discharge categories are based upon a median, riparian, and two- to five-year high water elevation in the Waal River (*Van Denderen and Van Hoek*, 2022). Here, we note the discharge ranges for each category based upon discharge measured at Lobith as:

$\overline{Q}_0$	<1,200 m^3/s
$\overline{Q}_1$	1,200 m^3/s - 1,600 m^3/s
$\overline{Q}_2$	1,600 m^3/s - 2,200 m^3/s (median flow)
$\overline{Q}_3$	2,200 m^3/s - 2,800 m^3/s
$\overline{Q}_4$	2,800 m^3/s - 3,700 m^3/s
$\overline{Q}_5$	3,700 m^3/s - 5,000 m^3/s (bankfull flow)
$\overline{Q}_6$	5,000 m^3/s - 6,800 m^3/s (2-year flow)
$\overline{Q}_7$	>6,800 m^3/s (5-year flow)

We aim to isolate regions that show the highest bed elevation response to and recovery between peak-flow events. We thus characterize the degree of difference in bed elevation changes between high and low flows using a linear fit (Fig 3.2 g & h). We calculate the total range of bed level change across all discharge conditions, $\Delta\eta$, from the slope of this fit multiplied by the total discharge range (Q_0- Q_7) (Fig 3.2 h). A high absolute value of $\Delta\eta$ highlights a large river response between low and high flows while the sign of $\Delta\eta$ indicates in which direction the response typically occurs; positive values of $\Delta\eta$ means peak flows tend to deposit while low flows erode (e.g. Fig 3.2 g), and negative values of

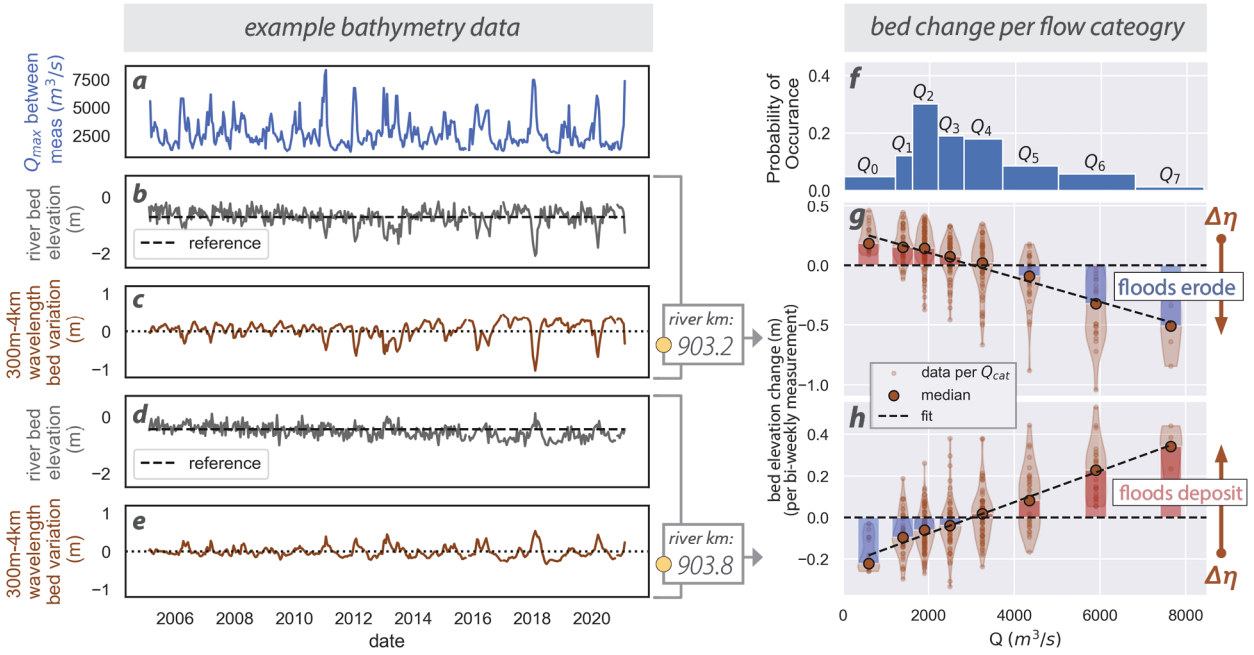

Figure 3.2: *Bathymetry data at two example locations (section 1) with opposite peak-flow bed response and low-flow recovery, along with average bed response per discharge (Q) category;* ***(a)*** *maximum antecedent discharge measured at Lobith for each biweekly bed measurement;* ***(b)*** *&* ***(d)*** *cross-sectionaly averaged bathymetry data (i.e. bed elevation) for 2005-2021 study period at river kilometer 903.2 & 903.8 respectively* ***(c)*** *&* ***(e)*** *bed elevation variation data around a reference mean after processing with a wavelet filter (λ=300m - 4km, Section 3.3.1);* ***(f)*** *fractional probability of observing a flow for eight discretized discharge categories;* ***(g)*** *&* ***(h)*** *wavelet-processed bed elevation changes grouped by discharge category representing antecedent discharge for each measurement, brown points and bars show the mean change per Q category-bars are colored by tendencies towards erosion (blue) and deposition (red), Δη is calculated from the slope of the dashed line (a linear fit to the mean biweekly bed elevation changes) multiplied by the discharge range*

$\Delta\eta$ mean peak flows tend to erode while low flows deposit (e.g. Fig 3.2 h). This single $\Delta\eta$ value that represents the degree of response across discharge categories allows us to examine correlations between bed response and gradients in floodplain width.

3.3.2 *Characterizing floodplain topography and geometry*

We characterize spatial changes in floodplain geometry and topography to understand how this affects flood routing into and out of the main channel and whether this corre-

sponds to strong differences between high- and low-flow bed elevation variations. We analyze both floodplain width along with topographic inundation for the same eight flow categories in Section 3.3.1.

To quantify floodplain width, we rely on the 'Baseline dataset' provided by the Dutch water ministry, Rijkswaterstaat, which contains schematized boundaries of the main-channel and floodplain (*Scholten and Stout*, 2013). We generate a centerline of the Waal main channel using the python centerline package (*Todić*, 2014) and measure floodplain width at transects perpendicular to this line every five meters along the study sections. The difference in bed level variation between high and low flows ($\Delta\eta$) is compared to streamwise changes in floodplain width to identify whether the degree of difference between high and low low bed elevation changes are explainable by spatial gradients in floodplain width.

Since flood flows may not always inundate the entire floodplain, we also consider relatively higher elevation floodplain structures as potentially important for routing floodplain flow into and out of the main channel. To quantify this, we topographically 'inundate' a 0.5m resolution digital terrain model (DTM) of the floodplain: DTM tiles are compiled from the AHN4 dataset (*Nederland*, 2021) and clipped to the Baseline floodplain boundaries (Fig 3.1 c). This topographic inundation is based upon a water surface in the main-channel at each flow category extracted from WAQUA model output (discussed in Section 3.3.3). For the same cross sections used to measure floodplain width, we extend the water surface in the main-channel across the floodplain and identify regions below this elevation. This method is similar to cross-sectionally derived relative elevation models used to cartographically visualize floodplain topography (e.g., *Coe*, 2016) and define channel migration zones (e.g., *Olson et al.*, 2014). We then use the inundated cross sections to visualize channel-floodplain connectivity at different discharges. We additionally compute a total inundated width for the highest flow category.

3.3.3 *Hydrodynamic conditions between low- and high-flows*

We analyze hydrodynamic model output to discern whether floodplain geometry and topography are representative of spatial gradients in flow velocity during flood conditions, and to identify regions of floodplain and main-channel flow exchange in relation to bed elevation changes between peak and low flows. We rely on the Waal subdomain (*Zagonjolli*, 2015) of the Dutch WAQUA (WAter movement and water QUAlity modeling) model that simulates shallow water hydraulics on a two-dimensional curvilinear grid (*Rijkswaterstaat*, 2015). WAQUA is developed and maintained by Rijkswaterstaat and is used to design standard flood protection measures. The model has additionally been leveraged by numerous research investigations in the Rhine River branches including the influence of bed roughness on water level (*Warmink et al.*, 2013) as well as discharge partitioning between branches (*Schielen et al.*, 2007).

We analyze model output for flow conditions within the lowest and highest discharge categories for which we analyze bed response, 1020 m^3/s and 8000 m^3/s respectively. For our analyses, we aim to isolate flow velocities indicating flow exchange between the main-channel and floodplain to understand how overbank flooding drives streamwise gradients in sediment transport capacity. We compute a projection of the (x,y) velocity output at each transect perpendicular to the main channel (Section 3.3.2) in directions normal and parallel to the transect which gives us velocity components in the streamwise (flow directed along the main-channel) and transverse (flow directed perpendicular to the main-channel) directions. Spatial changes in streamwise velocity indicate accelerations and decelerations of flow in the direction of the main channel while spatial changes in transverse vectors indicate changes in flow velocity perpendicular to the main channel; in the case of flood flows, this can indicate where flows accelerate into or out of the main channel. Velocity projections are extracted every 1m along each transect. Since bed elevation change is driven by spatial changes in flow velocity, we compute cross-sectional averages of both streamwise and transverse components to identify spatial patterns in

velocity and how this is modified by main-channel and overbank flow exchange.

3.4 *Results*

3.4.1 *The role of floodplain geometry and topography in routing flood flows*

The DTM-derived floodplain inundation between Waal river km 878 and 910 reveals regions of connectivity between the Waal River channel and floodplain, and gives intuition for how the floodplain topography will route flow as water stage increases (Fig 3.3). Notably, the floodplain does not steadily 'fill-up' originating from the main-channel; distal portions of the floodplain in sections 1-3 are topographically low, and even at the lowest flow category ($\overline{Q}_0$) there are regions that are at an elevation equal to or lower than the main-channel water surface (Fig 3.3). Due to higher floodplain topography blocking connectivity to the main-chanel (Fig 3.1), these ponds or low-lying regions are not actively flowing at low water stages.

As the water stage increases, floodplain flow initiates through distinct breaks in channel-adjacent topography causing flow in these regions (Figs 3.3, &3.4). We term these locations *critical topographic flood nodes*: channel-adjacent locations which are topographically higher than the distal floodplain blocking the initiation of velocity in side channels, but which are topographically lower than the main-channel banks in the streamwise direction, providing an inlet/outlet of main-channel and floodplain exchange. These are marked in Fig 3.3. Notably, these are also the locations where the highest average bed response and recovery takes place during flood and inter-floods (Fig 3.4 c.1-c.3; Appendix Figs 3.7 - 3.9).

3.4.2 *Flood and inter-flood bed response and recovery*

The Waal River bed between river km 878 and 910 shows a spatially variable response to both high and low flows (Fig 3.4 c.1-c.3). Peak flows (Q>6,800 m^3/s) have a tendency to systematically erode some regions and deposit in others with a mean of up to 0.5m

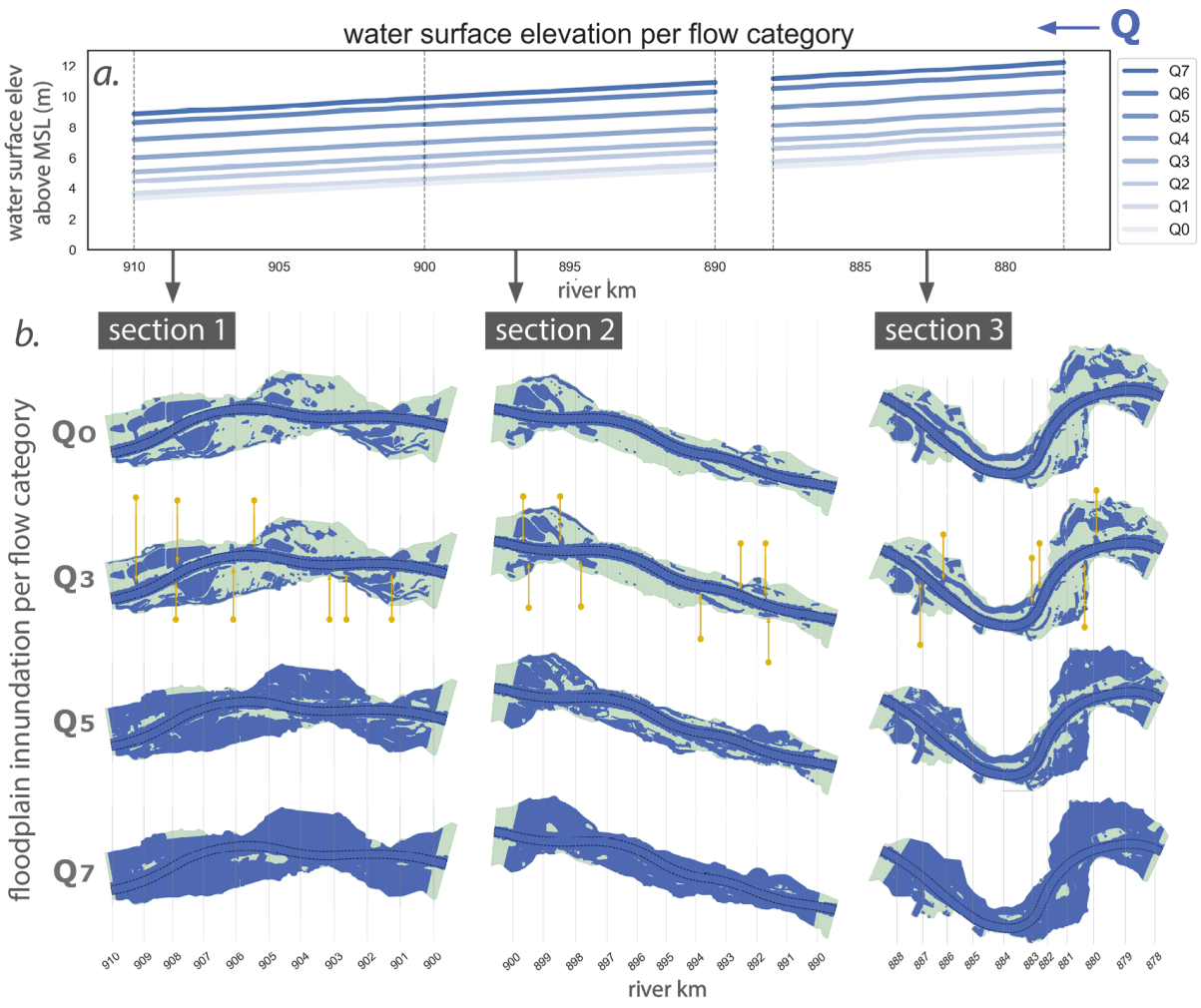

Figure 3.3: *Topographically-derived floodplain inundation at a subset of discharge categories; (a) shows the mean water surface elevation in the main channel with river km across the study sections (data derived from WAQUA model output, provided by Rijkswaterstaat (2015)); (b) planform maps of regions on the floodplain at or below the main-channel water surface (shown in blue), the location critical nodes connecting the floodplain to the channel are marked in yellow for the Q_3 discharge map*

of erosion and 0.4m of deposition between bi-weekly measurements (Fig 3.4 c.1-c.3). Low flows (Q<1,200 m^3/s) also showed a tendency to systematically erode and deposit at different locations with a median of up to 0.3m of erosion and 0.25m of deposition between bi-weekly measurements. The highest low flow bed responses tend to 'mirror' peak flow bed change with an opposing morphodynamic recovery; this mirroring effect is most prominent in Section 1 river km 901-901.7, 903-904.7, 905.8-906.9, & 908.8-909.4 (Fig 3.4 c.1 & Fig 3.7); Section 2 river km 891-892.5, 893-984.5, & 898.2-898.8 (Fig 3.4 c.2 & Fig 3.8,); and very modestly in Section 3 river km 886.4-887 (Fig 3.4 c.3 & Fig 3.9).

We explain the bed response and recovery in locations with mirrored morphodynamic response as a result of floodplain geometry and topography that forces flood flows to enter or exit the main-channel resulting in streamwise gradients in flow velocity that are different than those present at low flows. This is suggested by both the average bed elevation response across discharge categories and topographic inundation. Between $\overline{Q}_3$ and $\overline{Q}_5$, the direction of mean bed elevation variation changes sign (Fig 3.2 g & h). While the degree of low flow recovery at locations of high peak flow change varies (Fig 3.4 c.1-c.3), this change in sign is consistent across sections (Appendix Figs 3.7-3.9). This is also the discharge range where the floodplain begins to become notably connected to main-channel flow in the topographic inundation analysis (Fig 3.3 $\overline{Q}_3$-$\overline{Q}_5$). The observed coherence between floodplain flow activity (Fig 3.4 a.1-b.3) and a change in the direction of bed response (Appendix Figs 3.7-3.9) suggests that overbank flooding is affecting streamwise patterns of sediment transport and bed response.

As the floodplain becomes active, flow momentum is exchanged between the main-channel and floodplain through critical topographic flood nodes (Fig 3.3) modifying transverse (3.4 b.1-b.3) and streamwise velocity gradients (Fig 3.4 a.1-a.3). Locations of floodplain-channel flow exchange and direction are evident where where velocity vectors (Fig 3.4 a.1-a.3) and streamlines (Fig 3.4 b.1-b.3) show flow entering or leaving the main channel, resulting in downstream acceleration or deceleration of downstream flow, and a non-zero transverse flow velocity in the main channel. Prominent flow-exchange regions

include:

- **Section 1** (Fig 3.4 a.1&b.1 & Appendix Fig 3.7) river kms:
  - 901-901.4 (flow entering main-channel from river-right, exiting river-left)
  - 902.2-903.1 (flow entering main-channel from river-left, exiting river-right)
  - 903.6-904 (flow exiting river-left)
  - 904.4 (flow entering river-left, exiting river right)
  - 905.1-906.5 (broad region of flow entering river-right, exiting river-left)
  - 906.7-907.3 (flow exiting river right)
  - 908 (flow entering river-right)
- **Section 2** (Fig 3.4 a.2 & b.2 & Appendix Fig 3.8):
  - 890.5 (flow exiting river-right)
  - 893.5-894.5 (flow entering river-left, exiting both river-left and river-right)
  - 895.4 (flow exiting river-left)
  - 897.3 (flow exiting river-right)
  - 898 (flow entering river-left)
  - 898.7-899.5 (flow exiting river-left and river-right)
- **Section 3** (Fig 3.4 a.3 & b.3 & Appendix Fig 3.9):
  - 879.5 (flow entering river-right)
  - 879.8-880.3 (flow entering river-left, exiting river-right)
  - 881.5 (flow entering river-left, exiting river-right)
  - 882-882.8 (flow exiting river-left)
  - 886.9-888 (flow entering river-left, exiting river-right)

Since water depth at these locations is low at the onset of flooding, floodplain velocities entering and leaving the channel here are typically high (Appendix Figs 3.10 - 3.12). Where floodplain flows enter the main-channel and exit on the opposing side, prominent bed elevation response to peak flows is also typically observed, although the degree of recovery during low flows varies between sections (Fig 3.4 c.1-c.3; Appendix Figs 3.7 - 3.9).

3.4.3 *The influence of floodplain geometry on flood event bed change and recovery*

Morphodynamic response and recovery between high and low flows is associated with streamwise changes in floodplain geometry or topography that forces flows to enter and exit the main-channel at high water stages. We highlight two features that explain the strongest dynamic flood/inter-flood response across the study sections: 1) floodplain- to main-channel flow-crossing (Fig 3.5) and 2) gradients in floodplain and total inundated width (Fig 3.6). The difference between these two factors is their streamwise symmetry in the way they force flood flows to enter and exit the main-channel: floodplain width gradients result in a bilateral, symmetric streamwise flow expansion or contraction (Fig 3.6a & b) whereas floodplain meandering imparts a direction to floodplain-channel flow exchange resulting in non-zero transverse velocities. We describe the relative occurrence and role of these two factors as follows.

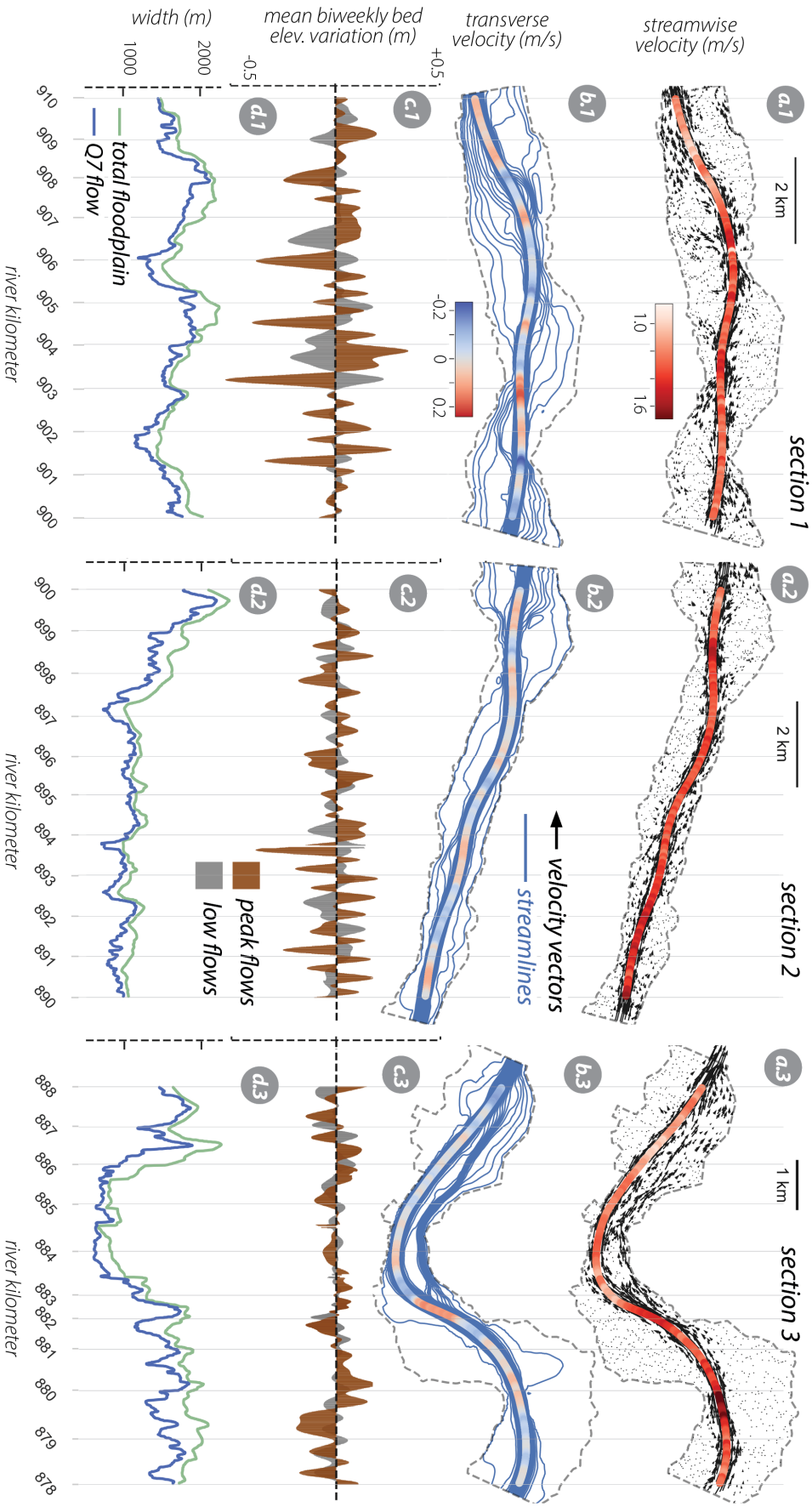

Figure 3.4: *see next page*

Figure 3.4: *Streamwise patterns in hydraulic model output (a.1-b.3) bed elevation changes (c.1-c.3) and floodplain width (d.1-d.3).* ***(a.1-a.3):*** *red center line shows cross-sectionally averaged, main-channel flow velocity in the streamwise direction computed from WAQUA model output for a discharge in the highest, $\overline{Q}_7$ flow category, ($Q = 8000m^3/s$ at Lobith). Black vectors indicate flow direction and relative magnitude of modeled flow velocity;* ***(b.1-b.3):*** *red and blue center line shows cross-sectionally averaged, main-channel flow velocity in the transverse direction: positive values (red) indicate transverse flow towards the river-right direction (typically up), negative values (blue) indicate transverse flow towards the river-left direction (typically down), flow streamlines are plotted in blue for $Q = 8000m^3/s$ model output.* ***(c.1-c.3):*** *average bed elevation change during for the highest flow category (brown) and the lowest flow category (grey);* ***(d.1-d.3):*** *floodplain width (green) measured from transects perpendicular to the main-channel, transect width inundated at the highest flow category shown in blue as computed from $\overline{Q}_7$ topographic inundation maps (Fig 3.3).* ***Note****: Spatial maps of all streamwise and transverse model output are available in Appendix Figs 3.10 - 3.12; bed elevation responses for all flow categories are available in Appendix Figs 3.7 - 3.9)*

3.4.3.1 Floodplain flow crossing

Floodplain flow crossing modifies both the streamwise and transverse velocities in the main-channel, and is strongly related to locations where the bed scours during floods and deposits during low flows. As floodplain flow is asymmetrically routed into and out of the main channel, this imparts a nonzero mean transverse flow in the main channel resulting in a cyclic streamwise variation in transverse velocity with the sign corresponding to the dominant direction of floodplain inflow and/or outflow (Fig 3.4 b.1-b.3). This variation in transverse flow affects the streamwise component of velocity in the main-channel (Fig 3.4 a.1-a.3) due to misalignment of floodplain and main-channel flow direction. This results in an along-channel gradient in sediment transport unique to overbank flow conditions. We describe the sequential feedbacks between main-channel and floodplain flow velocity in relation to bed response for an example of prominent floodplain flow crossing from river left to river right (Fig 3.5):

1. On the upstream end of the crossing, positive transverse velocities (Fig 3.5 b-1) reflect flow entering the channel, with a peak in transverse velocity (0.6 m/s) at the location where flow plunges from the left floodplain into the main-channel (Fig 3.5

e-1). This abrupt velocity decrease in the transverse direction, is consistent with the concept of flow 'refraction' that occurs at the main-channel/floodplain interface where floodplain flow takes on the direction of higher velocity main-channel flow (*Bijker*, 1980; *Blom*, 1997) At the same location, streamwise velocities show river-left floodplain flow with a relatively lower main-channel mean velocity (1.1m/s). Morphodynamic change is minimal at both peak and low-flows (Fig 3.5 d).

2. At the midpoint of the crossing, flow vectors are most aligned with the main-channel (Fig 3.5 b-2 & e-2), accelerating flow in the streamwise direction (Fig 3.5 c-2, f-2). The average streamwise velocity in the main channel increases (Fig 3.5 c-2, f-2). Peak erosion occurs (Fig 3.5 d) at the location of greatest streamwise acceleration in peak flows (Fig 3.5 c) while deposition occurs at low flows.

3. As flow leaves the channel, transverse velocities peak on the opposing right bank (Fig 3.5 e-3) and streamwise velocity, while still relatively high, begins to decrease along-channel as the river right floodplain shows non-zero floodplain flow (Fig 3.5, c-3, f-3).

4. On the downstream end of the crossing, streamwise velocities decrease (Fig 3.5 c-4, f-4) as transverse velocities reflect flow exiting both sides of the main-channel (Fig 3.5 e-4). Peak deposition occurs (Fig 3.5 d) at the location of greatest streamwise decrease in peak flow velocity (Fig 3.5 c).

3.4.3.2 *Gradients in floodplain and flow width*

While flow crossings can explain nearly all the prominent locations of morphodynamic response during peak flows (Fig 3.4 c.1-c.3), floodplain width variation also affects floodplain flows; since the main channel width is relatively uniform, changes to floodplain width can cause expansions and contractions of the flow unique to flood conditions. A conceptual expectation for this process is shown in Fig 3.6 a & b:

- **(a)**: During flood events, spatial floodplain widening allows flows to expand laterally, which results in a streamwise decrease in flow velocity and sediment transport capacity, depositing sediment during peak flows (Fig 3.6 a, upstream). Where the floodplain spatially narrows, flow width is re-confined towards the main channel, resutling in a streamwise increase in flow velocity & sediment-transport capacity, which erodes the bed during peak flows (Fig 3.6 a, downstream).

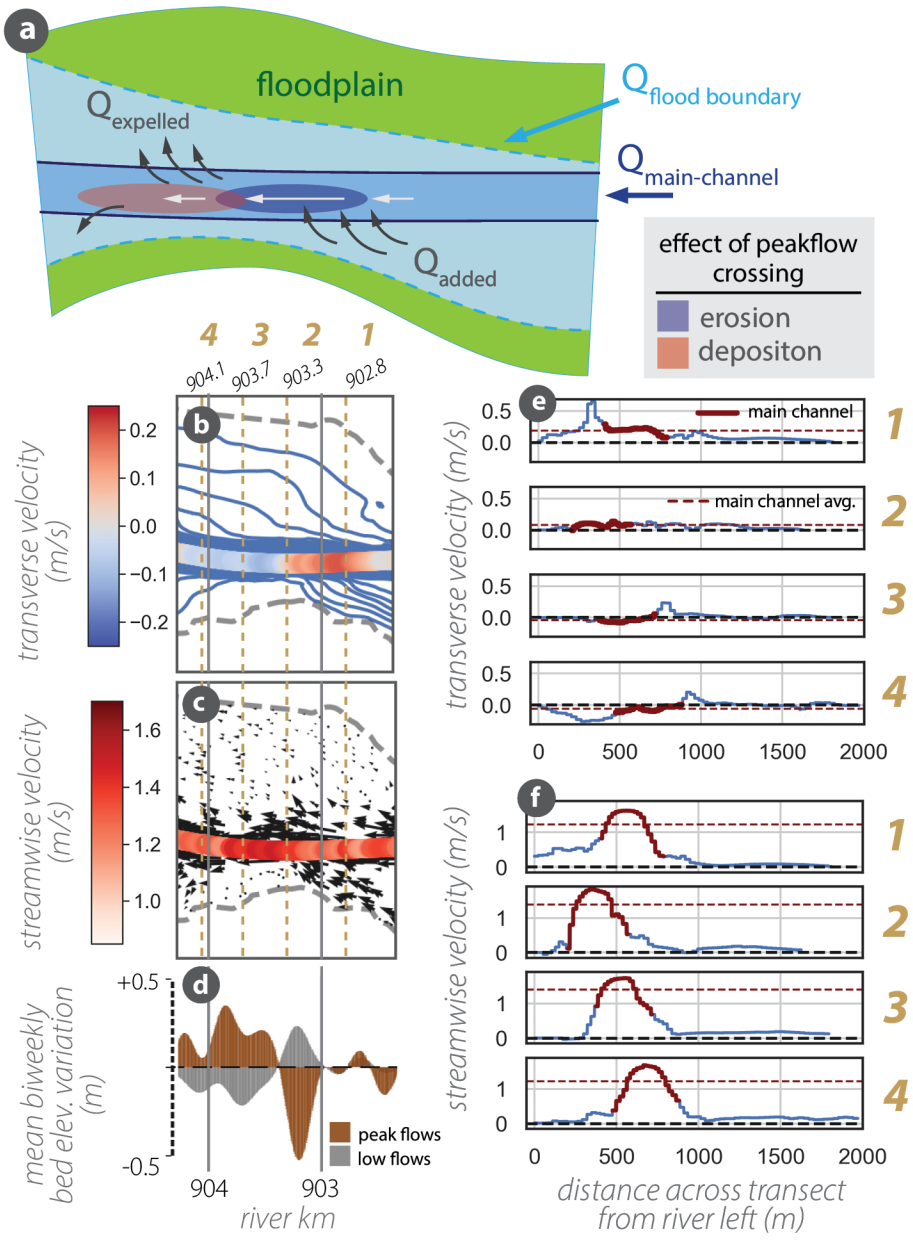

Figure 3.5: ***(a)****: conceptual schematic of flow crossing shown in the data below, with related regions of erosion and deposition;* ***(b-d)****: subset of streamwise changes in velocity and bed elevation response shown in Fig 3.4 for river km 902.3-904.2 including–* ***(b)*** *main-channel averaged transverse velocity and streamlines,* ***(c)*** *main-channel averaged streamwise velocity and floodplain flow vectors, &* ***(d)*** *average peak- and low-flow bed elevation response.* ***(e & f):*** *2km transects of the (e) transverse, and (f) streamwise velocity shown for four example locations: 1) upstream of flow crossing, 2) point of aligment of transverse and streamise velocity components, 3) downstream of flow-crossing, flow exiting on river-right, 4) downstream of flow-crossing, flow exiting on both sides of main-channel*

- **(b)**: During relatively low flow conditions (Fig 3.6 b) where the flow is limited to the main channel with a constant width but is still high enough to transport sediment and rework the channel bed, main-channel flow is no longer affected by spatial gradients in lateral confinement. Instead, the river responds to the morphodynamic changes that took place during previous floods. The velocity gradients resulting from the deposition mound (Fig 3.6 b, upstream) and erosion pit (Fig 3.6 b, downstream) cause the mound and pit to translate and disperse primarily downstream with mild spreading upstream due to backwater effects. Thus, under low flows we expect the intra-flood morphodynamic disturbances to disperse and diffuse.

We thus consider gradients in total floodplain width as an additional explanation of bed elevation change during and between flood events. Floodplain width varies between 500m and 2500m for river km 878-910, showing broad spatial patterns of widening and narrowing across all study sections (Fig 3.4 d.1-d.3), some of which co-occur with the conceptually expected channel bed response during peak flows (Fig 3.6 a & b). This includes the river kilometers:

- **902.8-903.1 (Section 1)** floodplain narrowing, peak-flow incision, low-flow deposition
- **903.3-903.8 (Section 1)** floodplain widening, peak-flow deposition, low-flow incision
- **905.5-906 (Section 1)** floodplain narrowing, peak flow incision, low flow deposition
- **906.5-907 (Section 1)** floodplain widening, peak flow deposition, low flow incision
- **893.5-893.8 (Section 2)** floodplain narrowing, peak flow erosion, low flow deposition
- **893.8-894.5 (Section 2)** floodplain widening, peak flow deposition, low flow erosion
- **886.4-887 (Section 3)** floodplain narrowing, peak flow erosion, low flow deposition

The total width of the innundated floodplain for the highest flow category typically tracks total floodplain width (Fig 3.4 d.1-d.3), although this metric does not capture the influence of topographic routing, and thus neglects the fact that while the floodplain elevation is lower than the water surface, it may not be actively flowing nor contributing to spatial gradients in main-channel velocity. However, where floodplain flow vectors abut the distal floodplain levee boundary, varying floodplain width may cause spatial

flow acceleration and deceleration in the main-channel. We thus test the influence of spatial gradients in floodplain width on flood and inter-flood bed elevation response in select subareas of Section 1 (river km 902.5-904, Fig 3.6 c) and Section 2 (river km 893.3 - 894.5, Fig 3.6 d), where velocity vectors show flow being guided by the floodplain boundary (Fig 3.4 a.1-a.3) and where transverse flow velocities reflect flow leaving the channel on both the left and right banks (Appendix Figs 3.10 a, 3.12 a).

For a simple, straight channel (e.g. Fig 3.6 a & b), we expect $\Delta\eta$ to correlate with streamwise gradients in floodplain width ($\Delta W/\Delta x$), where greater floodplain constrictions and expansions result in more pronounced differences in bed elevation changes between high and low flows. Fig 3.6 shows $\Delta\eta$ plotted against ΔW for a subarea of section 1 (river km 902.5 – 904, Fig 3.6 c) and a subarea of section 2 (river km: 893.3 - 894.5, Fig 3.6 c) where the floodplain narrows and subsequently widens. A 1:1 relationship is plotted between $\Delta\eta$ and $\Delta W/\Delta X$ as a first scaling estimate for a simple straight channel. While the data in Fig 3.6 c & d often overlap, or parallel this relationship suggesting that distal floodplain widths are indeed influencing bed elevation response and recovery to floods, the trend is not consistent along the channel due to the influence of flow-crossing. For example, at the upstream end of subarea 1 (Fig 3.6 c, dark purple points), despite spatial floodplain widening, there is relatively minimal bed elevaton variation between high and low flows (near-zero $\Delta\eta$). This may be explained by the erosional influence of floodplain flow crossing (Fig 3.5 a) which co-occurs with this location.

3.5 *Discussion*

The primary goal of this study is to analyze the role of geometric and topographic floodplain routing in driving bed elevation response between peak- and low-flows due to its role in modifying streamwise and transverse flow velocities in the main-channel during floods. Our topographic analysis of successive floodplain inundation illuminates critical topographic flood nodes (Fig 3.3) that connect low elevation, occasionally channelized distal floodplain topography and typically become active at water stages between Q_3 and

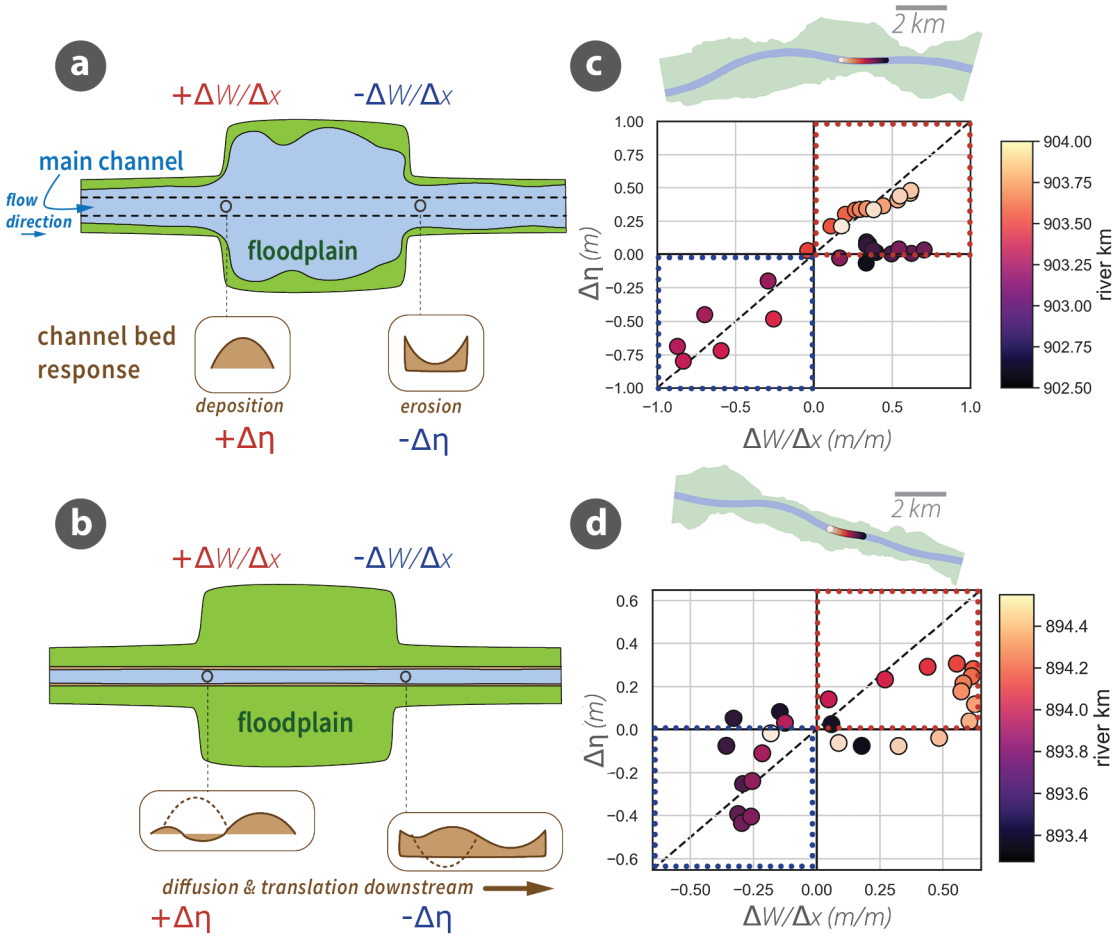

Figure 3.6: ***(a & b)****: conceptual expectation for influence of floodplain width change on bed elevation response during* ***(a)*** *floods and* ***(b)*** *low flows in a constant-width main-channel.* $\Delta W/\Delta X$ *notes the change in width* (ΔW) *with streamwise river distance* (Δx) ***(c & d):*** *tests the influence of streamwise width gradients* ($\Delta W/\Delta X$) *against bed elevation response and recovery during peak flows quantified by* $\Delta\eta$ *(computation demonstrated in Fig 3.2 g & h).* $+\Delta\eta$ *indicates deposition (erosion) during peak (low) flows, while* $-\Delta\eta$ *indicates erosion (deposition) during peak (low) flows (see (a & b) panels for concept). Data points are colored by river km, dashed line shows 1:1 relationship between* $\Delta\eta$ *&* $\Delta W/\Delta X$*. Points in the lower-left quadrant correspond to floodplain narrowing regions (see a & b), points in the upper-right quadrant correspond to floodplain widening regions (see a & b)*

Q_5 discharge categories; these locations are important for routing floodplain flow in- and out of the main-channel (Fig 3.4 a.1-a.3; b.1-b.3). Analysis of flow hydraulics at these locations confirms that flow acceleration into, across, and out of the main-channel results in a sequence of systematic erosion and deposition during floods where flows enter and exit the channel respectively; inter-flood bed recovery opposes this change (Fig 3.5).

Since floodplain topography is complex, flood flows rarely expand or contract unilaterally, but rather escape or re-enter the main-channel through critical topographic flood nodes. Thus, while total floodplain width changes can partially explain the morphodynamic change within and between flood events (Fig 3.4 d.1-d.3, Fig 3.6), floodplain flow crossing the main channel at topographic flood nodes mainly explains the locations of marked morphodynamic response and recovery between high and low flows (Fig 3.5). The locations of flow crossing also have the capacity to suppress the expected response due to floodplain width change alone (Fig 3.6 c).

Spatial variation in erosion and deposition in response to discharge fluctuations was previously reported in *Van Denderen* (2014) and *Van Denderen et al.* (2022b), and posited to likely be in relation to variation in floodplain width as a potential modifier of longitudinal gradients in flow velocity. The idea that lateral flow exchange can affect main-channel morphodynamics is not new to Waal River management strategies: these dynamics have been leveraged in constructing longitudinal training dams to laterally divert flow at high water stages mitigate main-channel erosion (*Czapiga et al.*, 2022). However, here we show that the flow re-entering at locations of lateral exchange can maintain enough momentum in the transverse direction to result in flow-crossing, which causes a streamwise pattern of local scour and downstream deposition in response to peak flows (Fig 3.5). Generally, the floodplain topography dictating compound flooding across all the upper Waal River study sections promotes flow-crossing rather than unilateral expansions and contractions, causing a morphodynamic response where water enters and exits the main-channel. Computing changes in total inundation width from geometric or topographic methods does not always capture bed response and recovery to peak flows, because it neglects the

directionality of floodplain flow.

It should be noted that flow crossing consistently occurs with spatial gradients in floodplain width, making it difficult to independently decompose the effects of each. We identify the effects of crossing as causing a non-zero, mean transverse velocity which is indicative of flow that is actively crossing the channel; if flow was strictly accelerating or decelerating as a result of changes to flow width, this would not affect transverse velocities but predominantly manifest as an acceleration and deceleration of velocity in the streamwise direction. While flow crossing appears to be important for bed elevation response within and between flood events, further work is needed to fully partition this effect from spatial gradients in flood width. This could be done, for example, by using an idealized model where channel meandering and floodplain width gradients can be co-varied.

Here, we analyze bed response and recovery in an engineered channel with fixed width, however a common response to floods in natural rivers or those that are free to adjust in planform is channel widening (e.g., *East et al.*, 2017; *Nardi and Rinaldi*, 2015). Indeed, river widening is posited to be a preferential mechanism for channel adjustment because it requires a smaller volume of sediment than deepening for a given response (*Wohl*, 2014). Thus, it is unclear to what degree the drivers of bed elevation response and recovery to peakflows observed here would apply to channels with a freely adjusting planform.

Additionally, the conventional understanding of 'floodplain' and 'channel' in natural channels may not be true for an engineered channel. A floodplain typically forms over a period of time, with the distal parts reflecting an antecedent flow regime (*Nanson and Croke*, 1992). This engineered channel has seen substantial main-channel narrowing and straightening (*Ylla Arbós et al.*, 2021), thus potentially distancing it from the typical physical and geometric relationship between floodplains and natural compound channels. Indeed, a floodplain meander pattern that *opposes* the main-channel meanders such as in Section 1, would be highly unusual for natural channels, and potentially amplifies

flow-crossing and bed response during overbank flows.

Our findings suggest that engineering projects designed for maintaining morphodynamic equilibrium in the main channel should additionally consider spatial gradients in floodplain width and sinuosity. Most engineering projects tend towards channel straightening, especially in the Lower Rhine (*Ylla Arbós et al.*, 2021, 2023; *Chowdhury et al.*, 2023). We show that straightening a main-channel without considering a co-meandering floodplain can augment flow crossing and morphodynamic response during flood stages; in the simplest planform terms, channels where the floodplain centerline crosses the main channel centerline at a high angle of difference will be particularly prone to flood- and inter-flood bed elevation response in the main channel as a result of how this geometry changes spatial velocity gradients during peak flows.

3.6 Conclusions

We analyze spatial patterns in average bed response and recovery between peak- and low-flows as they relate to spatial gradients in floodplain geometry and topography in the highly engineered Waal River. We find that low elevation channel-adjacent topography that routes floodplain flows into and across the main-channel predominantly explains a spatial sequence of erosion and deposition where flows enter and exit the channel respectively; these regions recover with opposing bed change during low flows. Spatial changes in total floodplain width explain bed elevation response and recovery to peak flows where the flow spans the entirety of at least one side of the floodplain, although this occurs infrequently; the upper Waal River floodplain topography typically imposes directionality to peak flows which accelerate into the main-channel from the floodplain with enough momentum to cross to the main-channel. This causes important local transfer between transverse (along-channel perpindicular) and streamwise (along-channel parallel) flow velocity components, which contributes to bed response during floods. These results enhance our understanding of spatial patterns in bed elevation response to floods in compound channels; large responses will occur where topography forces floodplain flows

to cross the channel and/or the floodplain expands and contracts. These findings may apply towards predicting changes in post-flood channel navigability and flood hazard due to inter-flood morphodynamic changes.

3.7 *Appendix*

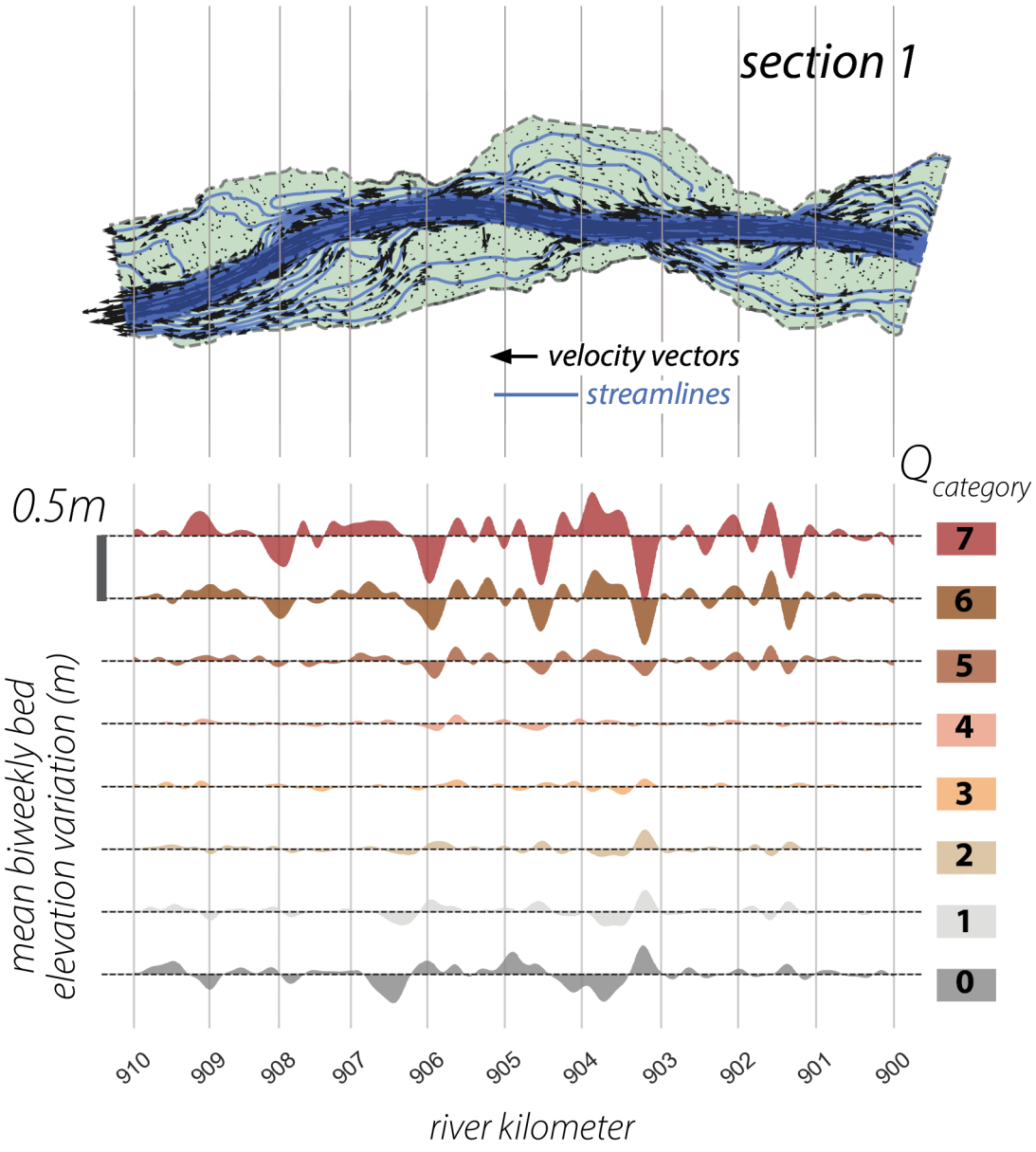

Figure 3.7: *Section 1: mean bi-weekly bed elevation variation plotted for all discharge categories; upper map shows streamlines and flow vectors for in* Q=8000m^3/s *(Q_7 category) WAQUA model output*

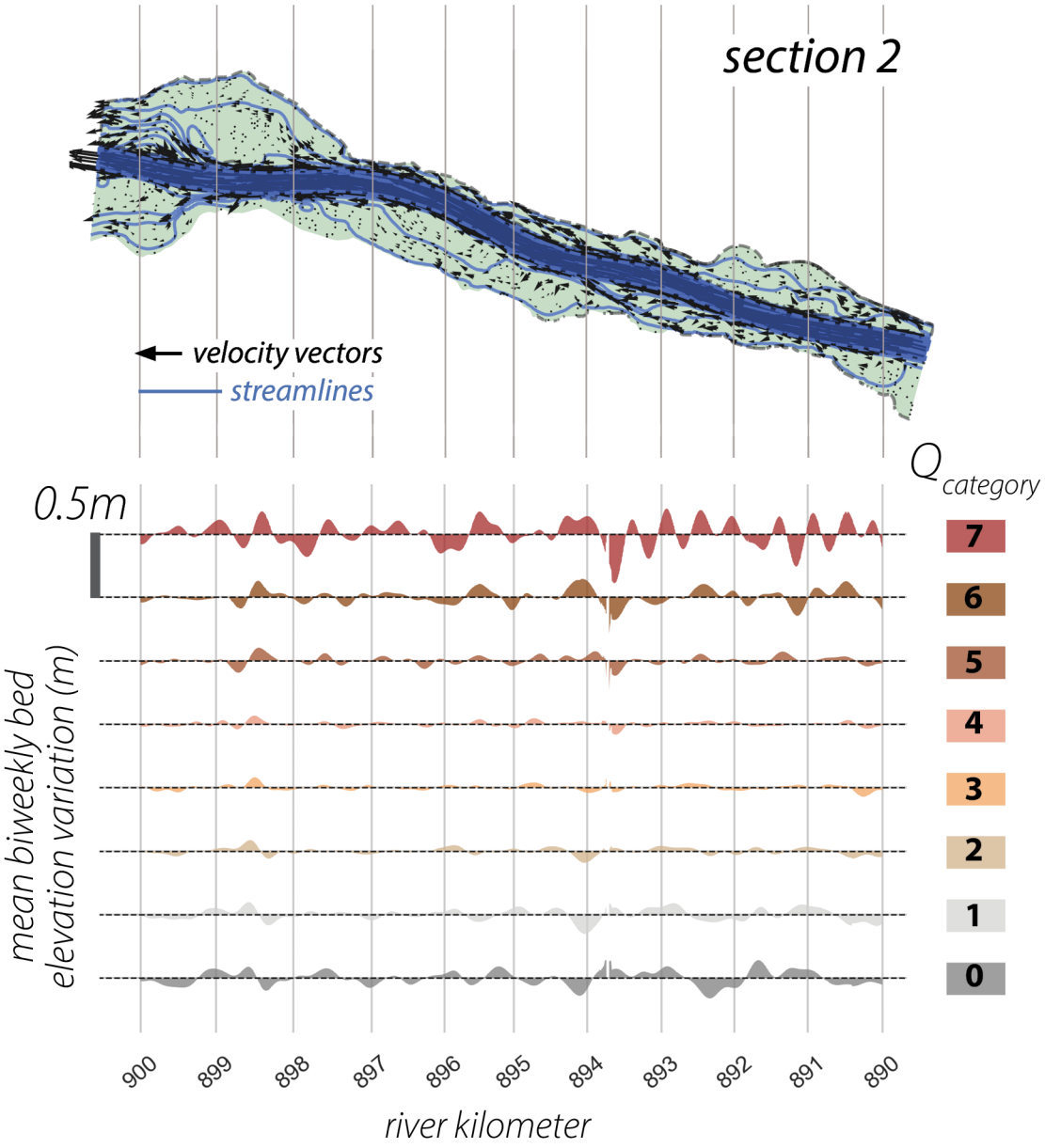

Figure 3.8: *Section 2: mean bi-weekly bed elevation variation plotted for all discharge categories; upper map shows streamlines and flow vectors for in* Q=8000m^3/s *(Q_7 category) WAQUA model output*

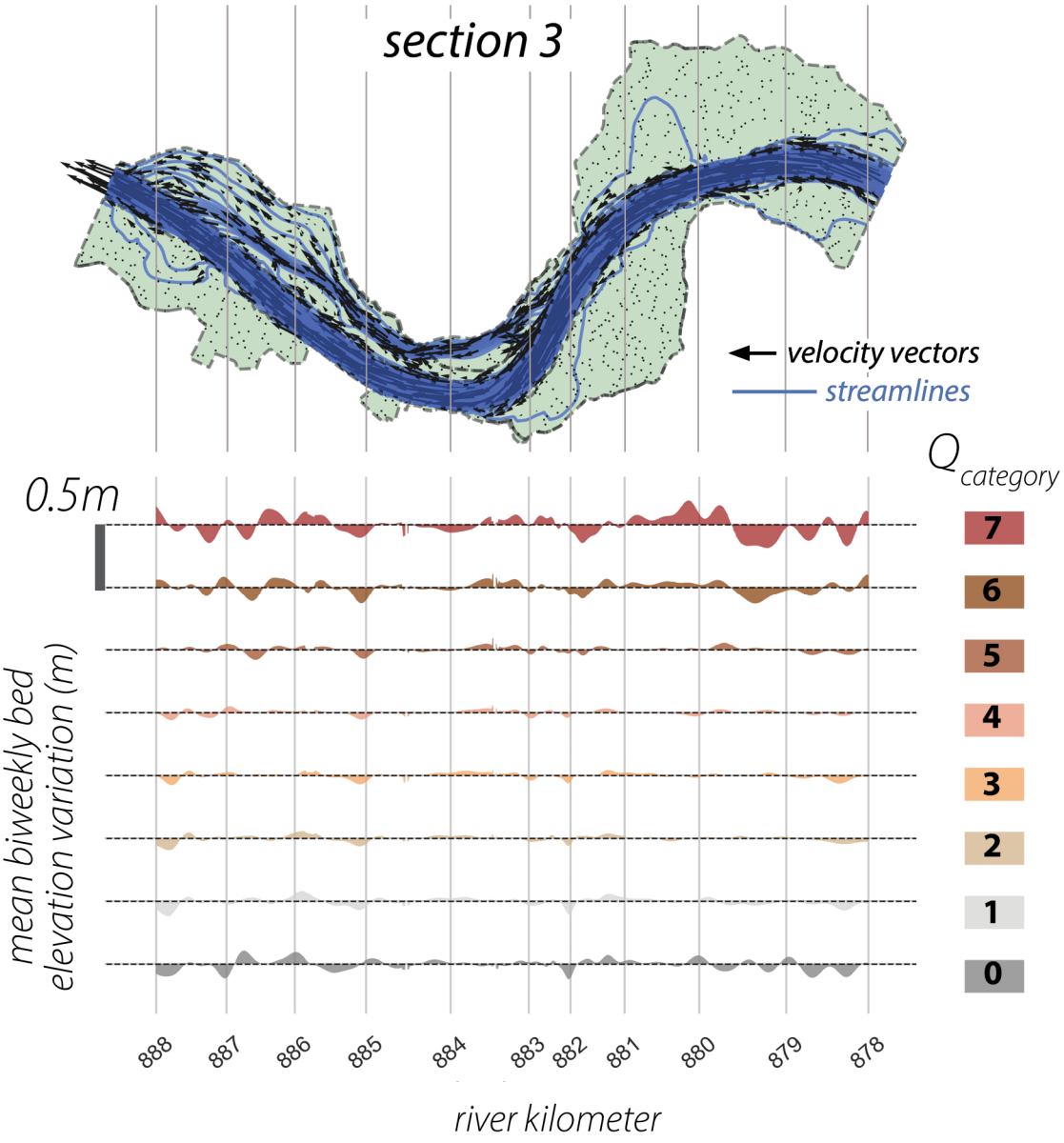

Figure 3.9: *Section 3: mean bi-weekly bed elevation variation plotted for all discharge categories; upper map shows streamlines and flow vectors for* Q=8000m^3/s *(*Q_7 *category) WAQUA model output*

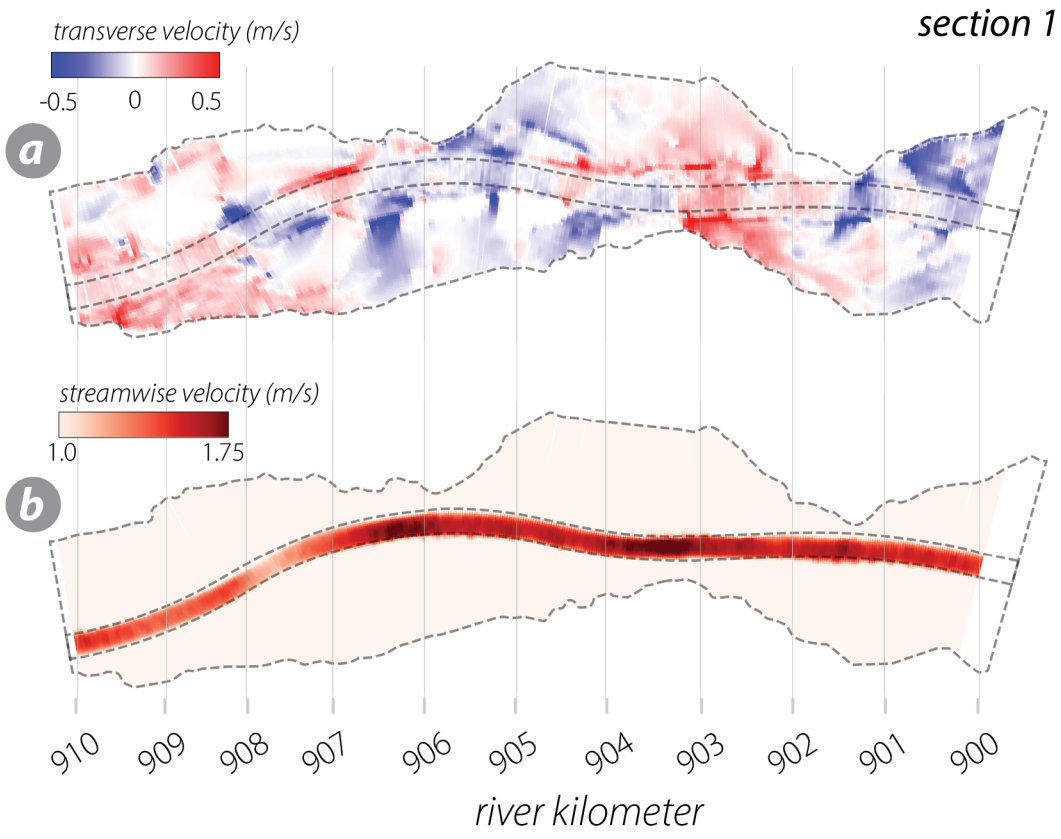

Figure 3.10: *Section 1: Map of (a) transverse and (b) streamwise velocities for* Q=8000m^3/s *(Q_7 category) WAQUA model output. In (a) positive transverse velocities (red) indicate flow towards the right bank, negative transverse velocities (blue) indicate flow towards the left bank.*

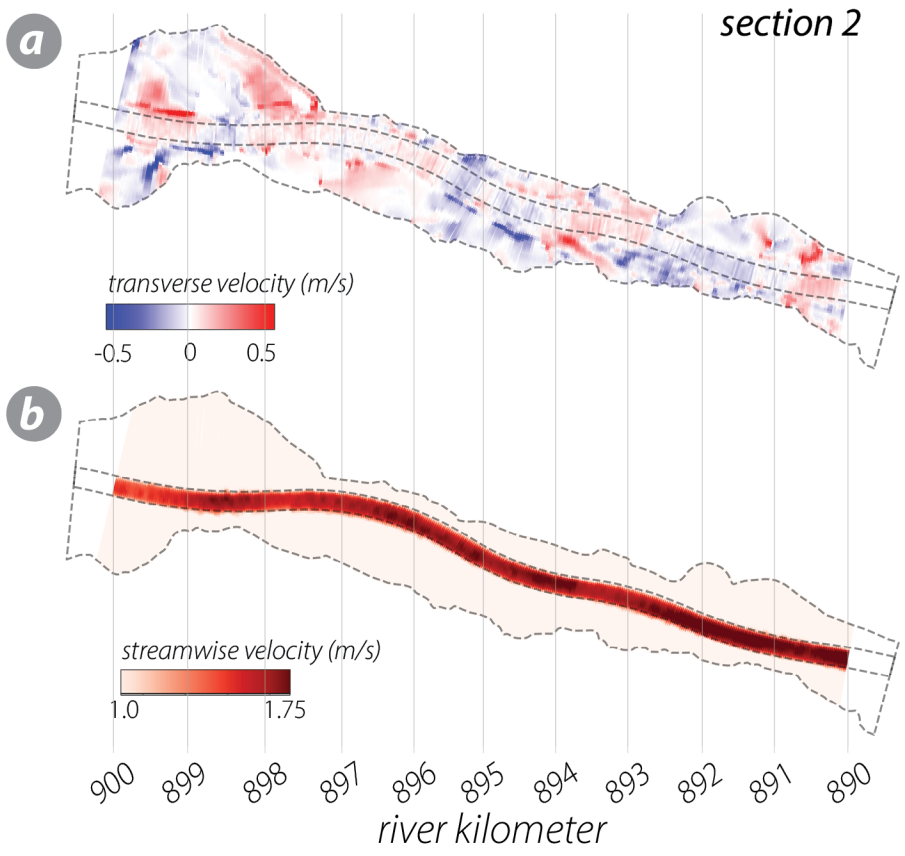

Figure 3.11: *Section 2: Map of (a) transverse and (b) streamwise velocities for Q=8000m^3/s (Q_7 category) WAQUA model output. In (a) positive transverse velocities (red) indicate flow towards the right bank, negative transverse velocities (blue) indicate flow towards the left bank.*

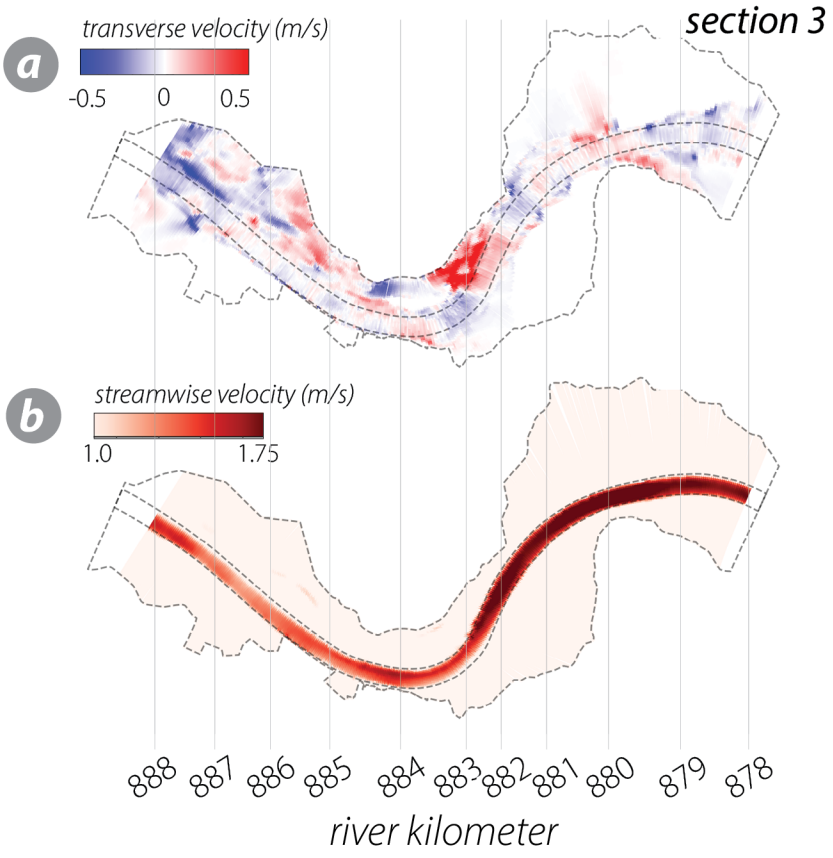

Figure 3.12: *Section 3: Map of (a) transverse and (b) streamwise velocities for Q=8000m^3/s (Q_7 category) WAQUA model output. In (a) positive transverse velocities (red) indicate flow towards the right bank, negative transverse velocities (blue) indicate flow towards the left bank.*

Part III

Chapter 4

RIVER MORPHODYNAMICS AND FLOODING ON THE NOOKSACK RIVER ALLUVIAL FAN APEX: AN INVESTIGATION OF DRIVERS AND FEEDBACKS

Abstract

Understanding the complex interplay between floods and river morphodynamics is crucial for effective river management, as it has implications for predicting and mitigating overbank flooding events. However, limited research exists on how river morphodynamics and overbank flooding co-evolve, particularly during extreme floods. In this study, we use a Delft3D numerical simulation to investigate flood hydraulics and river morphodynamics in the November 2021 flood event in the Nooksack River, western Washington State. This flood caused severe damage to river-adjacent communities along the Lower Nooksack, and flood waters overtopped the levees near Everson, WA, traveling over 25 km north towards the Fraser River and causing extensive and costly damages across the U.S.-Canada border. Our analysis focuses on the feedbacks between river morphodynamics and floods, examining streamwise changes in flood hydraulics (flow velocity and inundation width) and morphodynamics (bed elevation change). We find that within the Everson overflow region, bed elevation changes in the main channel are commonly located where flow spatially accelerates or decelerates during flood peaks; in particular, flow deceleration is observed at locations of overbank flooding. At the Everson overflow location, bed deposition co-occurs with a sudden along-channel velocity decrease and temporal onset of overbank flow, suggesting that the hydraulics of overbank flooding can contribute to local morphodynamic adjustment. We also investigate how channel adjustments during the first November 2021 flood peak affect flooding during a secondary flood peak occurring

two weeks later. Our findings provide insights for Nooksack River floodplain managers who are actively seeking to understand and mitigate flow overtopping.

4.1 Introduction

Floods are important for modulating the morphology of river channels; they can disrupt grain-scale armouring of the channel (*Masteller et al.*, 2019; *Milhous*, 1973; *Ockelford et al.*, 2019; *Reid et al.*, 1985); correspond to the growth and decay of bedforms in both sand- and gravel-bedded rivers (*Dinehart*, 1992; *Julien and Klaassen*, 1995); and cause in-channel scour or deposition (*Guan et al.*, 2016). Local scour or deposition is often dependent on spatial changes in channel and floodplain geometry (Chapter 3) or temporal period during the flood hydrograph (i.e. rising vs. falling limb) (*Miall*, 1977). These morphodynamic adjustments can affect flood hazard in subsequent events; an increase in bed roughness can exacerbate the rise in water surface with discharge (e.g., *Paarlberg et al.*, 2010), and a reduction in conveyance capacity through in-channel deposition or narrowing can increase overbank flow frequency (e.g., *Slater et al.*, 2015; *Stover and Montgomery*, 2001) and extent (*Ahrendt et al.*, 2022).

Floods cause morphodynamic change because they simultaneously deliver high shear stress, as well as potentially alter the spatial gradients in hydrodynamics. For example, when overbank flow occurs, floodplain geometry begins to control the spatial gradients in hydraulics including flow velocity, shear stress, and sediment transport capacity (Chapter 3). These gradients may differ from low-flow conditions, resulting in spatial flow accelerations/decelerations in the main channel that are unique to flood conditions. This can result in a morphodynamic response in a channel bed that has adjusted to in-bank flow.

River bed response can be thought of as comprised of a 'quasi-static' (long-term shift towards equilibrium) and 'dynamic' (short term variation in response to flows) response (*Arkesteijn et al.*, 2019, 2021). In this framework, peak flows or flood events function as a perturbation to a long-term state, which, over time, are balanced by the morphodynamic

changes caused by intermediate and low flows. This can happen with modest high flows from which the channel is often able to almost entirely recover between events (Chapter 3), as well as in response to more intense storms. For example, in Puerto Rico *Li et al.* (2020) show that long-term channel conveyance trends are comprised of punctuated resonses to tropical cyclones with modest recovery between events.

However, previous investigations show floods can sometimes cause a threshold shift in the subsequent morphodynamics of both natural and engineered alluvial systems. For example, floods are often a trigger of river avulsions or bifurcations (*Kleinhans et al.*, 2013). In an existing bifurcation on the Lower Rhine River, *Chowdhury et al.* (2023) show that back-to-back peak flows caused rapid sedimentation in one branch downstream of the bifurcation and initiated a change in flow partitioning between downstream channels.

The occurrence of both temporary and persistent shifts in river dynamics underscores an uncertainty in the longevity of channel response to floods. The difficulty of conducting rapid field measurements of river geometry during peak flows has limited existing research on channel adjustment and recovery during a flood hydrograph. While long term sediment storage trends may be assessed by creating Digital Elevation Models of difference (DoDs) across the same location over time (e.g. *Anderson et al.*, 2019), there are insufficient data surrounding floods to definitively assess whether long-term trends are mostly steady or composed of discrete responses to floods. Whether a river will recover from a given peak flow or if the peak flow will cause lasting change to the system is uncertain and may be inconsistent between flood events.

Alluvial fans are particularly vulnerable to abrupt and persistent changes during peakflows, namely, due to the propensity for avulsions at their apex (*Schumm*, 1977; *Slingerland and Smith*, 2004). Alluvial fans form where rivers transition from a confined to unconfined region with a lower gradient causing deposition of a substantial fraction of sediment load (*Kleinhans et al.*, 2013). Over time, this deposition super-elevates the channel above the surrounding floodplain making it more energetically favorable for the river to avulse to a new course (*Bryant et al.*, 1995). Avulsions often initiate due to a

'trigger' event such as a flood (*Aslan et al.*, 2005; *Slingerland and Smith*, 2004).

Here, we investigate the role of an extreme flood event in altering channel morphology on the Nooksack River, Washington State, specifically where it exits a mountain valley and flows out onto an alluvial fan. This location has historically experienced flooding (*Boyd et al.*, 2019) associated with severe and costly damages (*Vanderklippe*, 2021). We focus on feedbacks between the hydrodynamics of overbank flooding and morphodynamic change that occurs during the event. We contextualize this process with the long-term record of geomorphic change, and consider how this region poses unique management challenges due to the interaction between hydrodynamics, morphodynamics, and river interventions.

4.2 Background

4.2.1 Nooksack River Geomorphology

The Nooksack River heads in the North Cascades, draining three forks; the North Fork, Middle Fork, and South Fork (Fig 4.1). The larger North and Middle Forks drain the respective north and southwest slopes of Mt. Baker, a glaciated stratavolcano of the Cascadia forearc (*Coombs*, 1939), while the South Fork drains minor tributaries originating in alpine regions of the Twin Sisters Mountain. Retreating glaciers on Mt. Baker have left unstable proglacial valleys that deliver sediment to the Nooksack headwaters; climate-driven fluctuations in coarse sediment-supply from these regions have been linked to decadal-scale channel-bed disturbances propogating downstream (*Anderson and Konrad*, 2019). Relatively coarse sediment is also supplied laterally to all three forks through bank erosion and landsliding in channel-bounding paraglacial terraces (*Scott and Collins*, 2021).

The three Nooksack forks converge into the Lower Nooksack River just upstream of Deming, Washington where the North Cascades mountain front transitions into the Fraser Lowland; a triangular depression bounding the border of northwestern Washington and British Columbia filled by proglacial outwash during the last continental glaciation

(*Kovanen and Slaymaker*, 2015; *Kovanen et al.*, 2020). Just downstream of where the river exits the valley, it encounters an E-W trending relict glacial outwash channel (Fig 4.2) including narrow, subparallel grooves of $\sim 8m$ depth scoured during Late Pleistocene outburst floods (*Kovanen et al.*, 2020) just north of Everson (Fig 4.2). The Nooksack River has created a 'v-shaped' alluvial fan bounded within the glacial outwash channel and outburst flood features. Alluvial deposits are present in both the west and east arms of this fan reflecting fluvial deposition from present and historic river courses respectively.

Prior to the late Holocene, the Nooksack River flowed through the northeast channel shown in Fig 4.2, discharging into the Fraser River via the Sumas Valley (Fig 4.1). There is historical evidence of a significant Nooksack River avulsion between several hundred and 5,000 years ago that redirected the river to its current course terminating in the Puget Sound (*Maudlin and Stark*, 2007; *Pittman*, 2019; *Pittman et al.*, 2003). Before this event, the majority of sediment carried by Nooksack ended up in the Sumas Valley rather than the present Nooksack floodplain; Sumas Valley sediment cores show the progradation of Nooksack fan sediments into the southern half of the Valley with decreasing fluvial competence after the retreat of the continental ice sheet (*Cameron*, 1989). Relict meander scars of similar size and radius as the Nooksack along with Native American legends suggest that the Nooksack River avulsed south to its current course in the Late Holocene (*Pittman et al.*, 2003). The estimated avulsion location occurs in a broad transition region from a relatively confined valley to unconfined lowland, areas that are typically prone to mountain-front (*Gearon and Edmonds*, 2022) or fan (*Brooke et al.*, 2022) avulsions. However, the Nooksack fan shape and growth appears to be uniquely dominated by glacial outwash topography inhibiting its formation of a typical cone-shaped deposit with convex cross-fan profiles (*Bull*, 1968). The present-day drainage divide between the Nooksack and Fraser Rivers bounds the river-right bank of the present day Nooksack channel (Fig 4.2) and the drainage divide at the apex of the Nooksack fan remains precariously low.

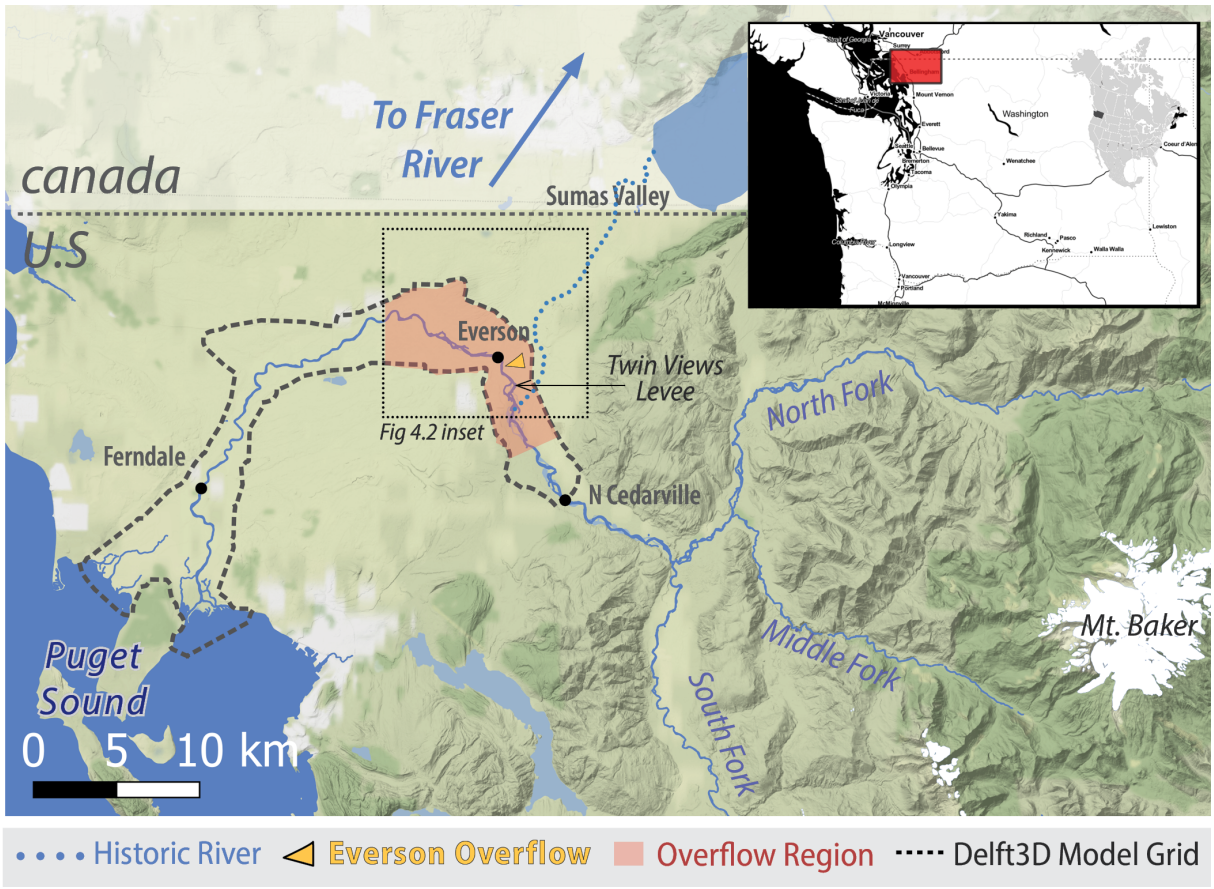

Figure 4.1: *Map of the Nooksack River system including the Lower Nooksack Delft3D Model domain; the overflow region analyzed in this study is highlighted with the Everson Overflow marked. Location of historic river course leading to Sumas Lake is marked in the location of the present-day Sumas Valley. USGS River gages are marked at North Cedarville, Everson, and Ferndale. Levee confinement begins at the Twin Views Levee. Fig 4.2 shows topographic inset of the Nooksack alluvial fan.*

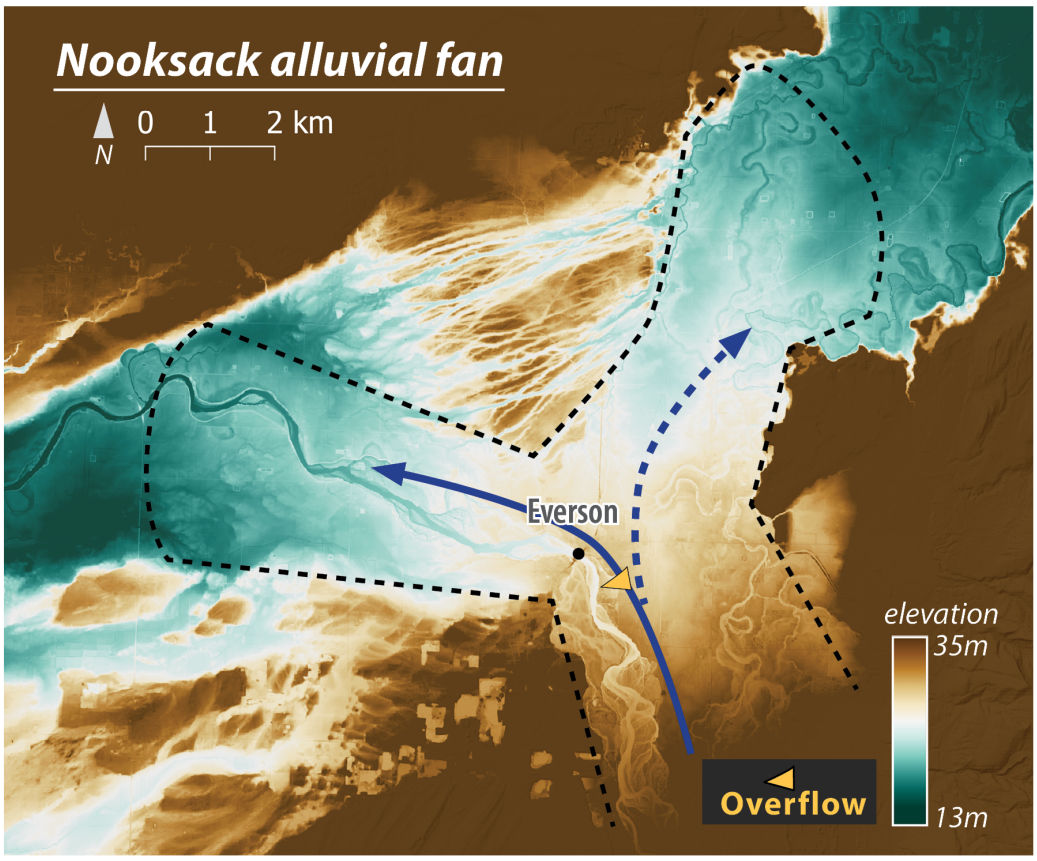

Figure 4.2: *Modern Nooksack alluvial fan is outlined by a dashed, black line on a Digital Terrain Model (DTM) around the Everson Overflow region (inset location shown in Fig 4.1); colors are stretched to show local elevation differences. Nooksack fan occupies a larger E-W trending glacial outwash channel and fan growth is obstructed by relict glacial features creating a 'v' shape; fan extent is noted by higher elevation alluvial deposits (whiter colors) present in both the west and east arms. The Everson Overflow is situated at the apex of this v-shaped fan. Solid, blue arrow shows present day Nooksack River course and dashed, blue arrow shows pre-avulsion course. (DTM data is from the North Puget 2006 USGS LiDAR campaign accessed via WA-DNR (2023))*

4.2.2 *The Everson-Overflow Reach*

Perhaps unsurprisingly, the low drainage divide near the town of Everson, WA has resulted in substantial overbank flooding. During peak flows, the river spills overbank near the appex of the Nooksack fan (Fig 4.2) and reoccupies its historic floodplain in the Sumas Valley region. This location of overtopping has been coined by local floodplain managers as the 'Everson Overflow' (Fig 4.1). The ∼20km bounding the Everson Overflow, has been highlighted as the most complicated reach in the Lower Nooksack river as a result of the interplay between hydrology, hydraulics, geomorphology and management (*Boyd et al.*, 2019). This location is complicated by its coincidence with 1) a natural streamwise transition from confined valley to unconfined fan; 2) a transition from an established, older channel to a relatively young channel per the historic avulsion; and 3) the streamwise onset of channel leveeing, which begins to substantially confine the main-channel ∼2 km upstream of the Everson Overflow (Fig 4.1).

There is additionally evidence of recent channel aggradation near the Everson Overflow; *Anderson et al.* (2019) report temporal differences between digital elevation models spanning the Lower Nooksack River indicating 0.7m of channel aggradation in the Everson Overflow, between 2005-2016. This aggradation combined with persistent overflow has driven local floodplain managers to focus on the role of morphodynamics and sediment-routing through the Lower Nooksack, with particular focus on flood hazard in the Everson Overflow (e.g., *Boyd et al.*, 2019).

4.2.3 *The November 2021 Flood*

On November 14, 2021, an atmospheric river delivered significant precipitation to the Nooksack River region resulting in extensive flooding (*Gillett et al.*, 2022; *Patel et al.*, 2021). Atmospheric river events are long, narrow strips of warm tropical water vapor, that can cause considerable amounts of rainfall when forced to rise by terrestrial mountain rangs (*Ralph et al.*, 2018). Historically, atmospheric rivers have been responsible for nearly all of

the peak annual streamflows in northwestern Washington State (*Neiman et al.*, 2011).

Two days after the storm, substantial inundation was still present in the Lower Nooksack River including overflow towards Canada in its relict channel course (Fig 4.3). This overflow from the Nooksack River caused extensive flooding in the Sumas Prairie (*Patel et al.*, 2021) and prompted international debate over whether the U.S. should be financially responsible for Canadian flood damages (*Vanderklippe*, 2021). Discussions have continued regarding morphodynamic interventions on the Nooksack; some Canadian government officials argue for further leveeing around Everson, while Nooksack floodplain managers protest that this will push flood hazard downstream (*Hoekstra*, 2022). The Nooksack River and management of flooding at the Everson Overflow reach is pitted in an interesting discussion of trans-boundary flood management; this underscores a pressing need to understand dynamics contributing to overflow at this location.

4.2.4 Overbank flow hypothesis

In the context of historic deposition at the Everson Overflow (*Anderson et al.*, 2019; *Boyd et al.*, 2019) as well as abrupt in-channel deposition observed during the November 2021 event (Fig 4.3), we present the following hypothesis regarding feedbacks between overbank flow and channel aggradation (Fig 4.4). As downstream flow is diverted laterally, this results in a fractional loss in flow ($Q_{overbank}$) and reduction in streamwise sediment transport. This may lead to aggradation concurrent with channel overflow. We aim to investigate both channel aggradation and overbank flooding using the Delft3D model described in the subsequent section.

4.3 Methods

4.3.1 Delft3D Hydromorphodynamic Model

We use a Delft3D-Flexible Mesh hydrodynamic model (*Morgan et al.*, in prep.) to simulate hydraulic and morphodynamic conditions during the November 2021 flood. This model

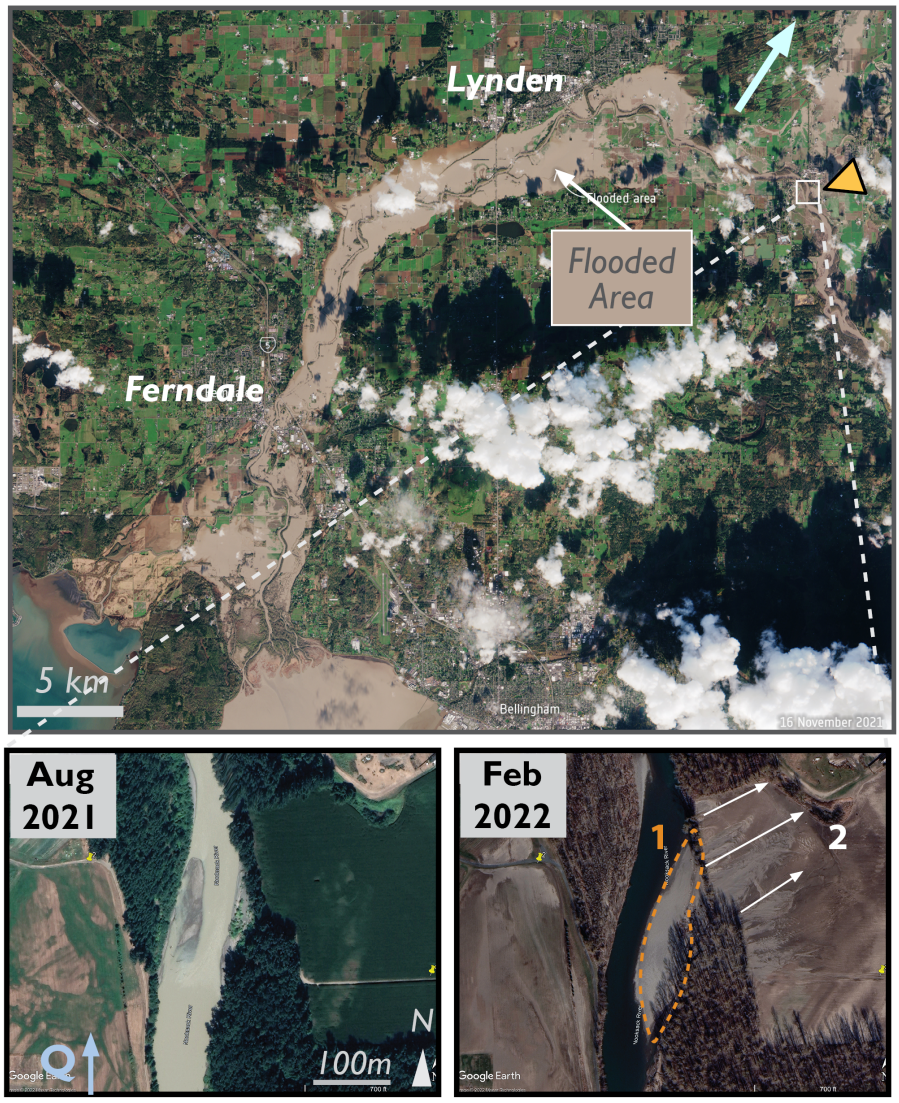

Figure 4.3: TOP: *Satellite imagery on November 16 showing mud-colored flooded regions on the lower Nooksack and overflow north to Canada (imagery modified from Hansen et al. (2021)).* **BOTTOM**: *Nooksack channel at overflow site 3 months before (left) and after (right) November 2021 flood. Morphodynamic change occurred in the channel during the 2021 flood including deposition of (1) a river-right bar and (2) floodplain deposits reflecting the route of overbank flow. (Imagery from Google (2021): Maxar Technologies & Google (2022))*

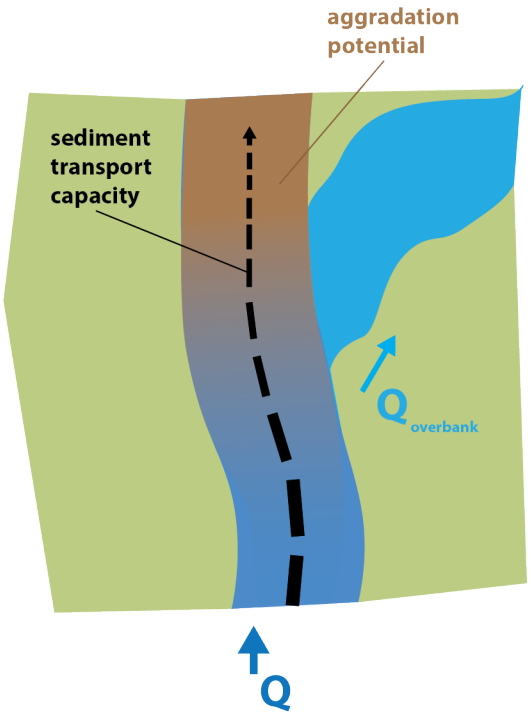

Figure 4.4: *Hypothesized feedbacks between overbank flow ($Q_{overbank}$) and bed elevation change at the Everson Overflow: overbank flooding causes a streamwise decrease in sediment transport capacity resulting in aggradation*

is described in full in *Morgan et al.* (in prep.), which we briefly summarize here. The model domain spans the entire Lower Nooksack River, extending from the river gage at North Cedarville (USGS gage #: 12210700) to the Puget Sound (Fig 4.1). The model mesh consists of a curvilinear grid centered on the active channel, and an unstructured, triangular grid on the floodplain. Bathymetry data is based upon a 2015 topo-bathy dataset that synthesizes airborn LiDAR measurements with channel cross-sections. Sediment transport is modeled using the Wilcock & Crowe sediment transport formulation (*Wilcock and Kenworthy*, 2002). The Delft3D model is applied in a 'depth-averaged' fashion, meaning it does not resolve velocity with vertical depth within the water column.

Model grain-size and hydraulic roughness (mannings-n) are calibrated using hydrographs from 2006 and 2015 Nooksack flood events. Grain-size is based upon D_{16}, D_{50}, & D_{84} field measurements from *Morgan et al.* (2020). Initial D_{50} grain size for each model cell is set in *Morgan et al.* (in prep.) by simulating bed shear stresses (τ) for several arbitrary bankfull flow events and using the Shields equation (4.1) with a reference Shields parameter ($\tau_{*r} = 0.037$) that minimizes differences between average bankfull τ from simulations and existing D_{50} data. This τ_{*r} value is then used to initialize D_{50} grain size to all cells. A grain-size distribution is created at each cell by fitting distributions to the measured D_{16}, D_{50}, & D_{84} and mapping this distribution to all cells based upon the D_{50} value applied using the τ_{*r} (*Morgan et al.*, in prep.).

$$D_{50} = \frac{\tau}{\rho g (s-1) \tau_{*r}} \tag{4.1}$$

The model is additionally initialized with a single floodplain grainsize distribution based upon average values of borehole data (*Morgan et al.*, in prep.).

The simulation of the 2021 flood event spans approximately one month from November 1 - December 8, 2021. Hydrologic boundary conditions for this event are supplied using streamflow data from the North Cedarville gage (Fig 4.1, *USGS-NWIS*). Sediment-supply is provided as a flow-dependent equilibrium condition at the upstream boundary.

4.3.2 *Analyzing Streamwise Hydrogeomorphic Patterns*

Our analyses aim to capture streamwise patterns in channel hydraulics and morphodynamics associated with the overbank flooding process. Since it is often difficult to discern broad streamwise patterns exclusively from spatial maps, we distill the model results into a cross-sectionally averaged longitudinal profile. To do this, we compute average morphodynamic and hydraulic parameters at 2km transects (e.g. Fig 4.5 d-f) perpendicular to an active channel centerline. We use a centerline previously used in *Anderson et al.* (2019) and *Boyd et al.* (2019) to compute bed elevation change from long term differences in digital elevation models. This enables us to compare modeled bed elevation changes that occur during the flood event to existing data (e.g., *Anderson et al.*, 2019) documenting long-term changes in landscape surface.

For each transect we compute bed elevation, channel velocity and flow conveyance, in the main-channel (Fig 4.5 d & e). We define the main-channel (shown in Fig 4.5 c) based upon the modeled 'wet-channel' with a depth greater than 1.5m at bankfull flow; bankfull flow is estimated as 700 m^3/s based upon the two-year recurrence flow for the Ferndale gage (USGS gage #: 12213100, Fig 4.1). Ferndale is used as it has the longest flow record of river gages in the domain. The simulated hydrograph passes through Q=700 m^3/s four times during the simulation (Fig 4.5 b). Since the river channel is a braided, relatively dynamic channel upstream of the Everson Overflow (<8 km from the upstream boundary, Fig 4.5 a), we compute the main-channel as the average 'wetted channel' for all occurrences of bankfull flow. Downstream of the Everson Overflow (>8 km from the upstream model boundary, Fig 4.5 a) we set the active width using the 'wet-channel' criteria based solely upon the first rising limb; we do this, 1) because the channel is confined by levees and is thus relatively static, and 2) because water left on the floodplain after the flood-peak creates deep ponds that skew the main-channel estimate (see spikes in active width for $>$ 8 km downstream, Fig 4.5 a).

We use the average bed level change, flow velocity, and conveyance (Fig 4.5 d & e) to

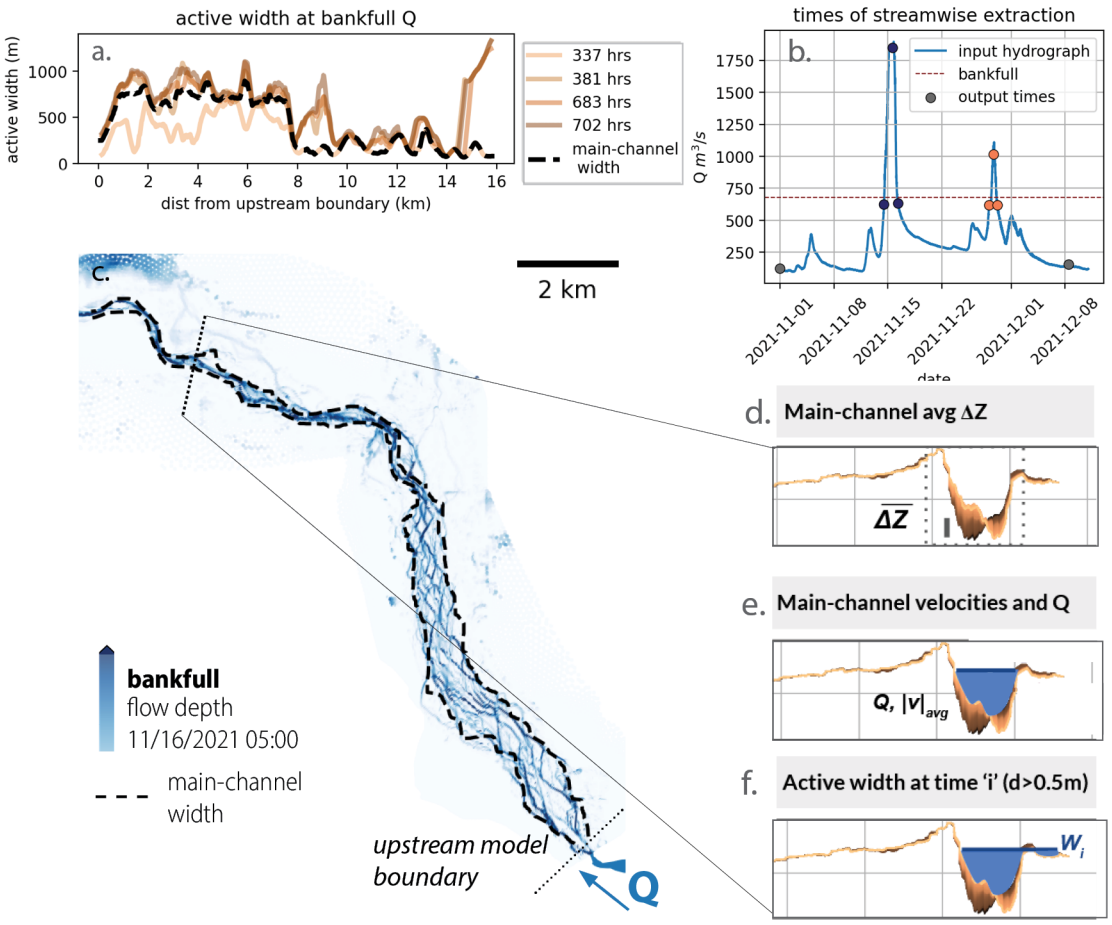

Figure 4.5: *Methods for defining active channel width and computing streamwise cross-sectional averages from Delft3D model output.* ***(a):*** *active bankfull width vs. distance downstream from model boundary for four occurrences of bankfull flow;* ***(b):*** *input model hydrograph at North Cedarville, 700 m^3/s bankfull flow is noted with a dashed red line, dots represent output times for which model results are extracted at transects and cross-sectionally averaged.* ***(c):*** *map of flow depth at the Everson Overflow region extracted for bankfull flow on the falling limb of the first flood peak (11/16/2021, 05:00 or model time=381) hours. The location of example transect shown in (d-f) is marked* ***(d-f):*** *conceptual diagrams of parameters computed at an example channel transect including* ***(d)*** *average bed level change,* ***(e)*** *average velocity magnitude $|V|_{avg}$ and flow conveyance* ***(Q)*** *in the main channel, and* ***(f)*** *active flood width across the entire 2km transect*

understand how streamwise patterns in morphodynamics and hydraulics are co-evolving in the main-channel. We use active width (Fig 4.5 f) to estimate streamwise changes in the degree of overbank flooding. Data is extracted from the Delft3D model at an evenly-spaced 4m resolution along transects with a streamwise spacing of 15m. Because we are interested in the relationship between morphodynamic changes and *overbank* flooding, we select to analyze output immediately below bankfull on rising and falling limbs of the hydrograph, along with each flood peak (Fig 4.5 b). This allows us to quantify and compare changes that occur before, during, and after overbank flow conditions on both the rising and falling limb. This also allows us to quantify bed response and/or recovery that occurs between flood peaks.

4.4 Model Validation

4.4.1 Comparison with Field Data

Data for validating the accuracy of morphodynamic changes during the November 2021 flood are sparse; however, four USGS transects were measured during and immediately following the simulation period (Fig 4.6 b) at the Everson gaging location (Fig 4.1). We compare the model behavior at the cross-sectional transect nearest the Everson gage for overlapping model times (Fig 4.6 e) to consider whether the model is capturing cross-sectional dynamics near the Everson Overflow. These transects are shown trimmed to the main channel in Fig 4.6 a, with the USGS transects centered at the main-channel mid-point (Fig 4.6 b). Note, that there is a slight vertical offset in absolute elevation between the measured and modeled datasets potentially due to a slight spatial difference in measurement/extraction location. To understand if the model transects capture similar morphodynamic patterns, we compute a mean bed elevation of each transect along with an area below the water surface of 25m, since we are most interested in central channel dynamics. We compare these two computations in Fig 4.6 c & d. A dashed line representing a 1:1 slope with a vertical offset is plotted for reference: due to the linear

datum difference between transects, the computed numbers for bed elevation and area do not exactly correspond; most important, is that the relative trend between modeled and measured transect bed elevation and area is similar.

Aside from the first model transect (black line Fig 4.6 a) the model shows the evolution of a central river bar consistent with the data (Fig 4.6 b). Since the initial model state reflects 2015 bathymetry, we don't necessarily expect the early-time simulaton to reflect the observed bathymetry in 2021. We thus neglect this first transect in our quantitative comparison of bed elevation (Fig 4.6 c) and cross-sectional area (Fig 4.6 d). These computed metrics suggest that the model is capturing cross-sectional dynamics at the Everson gage: a deeper channel with greater cross-sectional area is observed on the falling limb of the first flood peak, with relatively higher bed elevation and reduced cross-sectional area for the second flood peak and end of simulation.

4.4.2 Comparison with Satellite Observations

The satellite imagery from before and after the November 2021 flood shows the development of a river-right bar at the Everson Overflow (Fig 4.3). As a visual check for whether the model is capturing similar reach-scale dynamics in this region, we plot cross-sectional transects overlapping the Everson Overflow location: Fig 4.7 shows these transects spanning a 75m streamwise reach, beginning 8.745 km downstream of the model boundary.

Transects show the development of a river-right bar relatively early in the simulation time; we show later on that this bar initiates during the first flood peak (Fig 4.11). Additionally, the transects show overbank flood deposits on the right bank similar to that observed in the post-flood imagery (Fig 4.3). There is some persistant channel scarring in the right floodplain in this region (Fig 4.3, lower-left subpanel), suggesting overbank floods have historically had energy to erode the floodplain in this location, however, the meter-scale channel erosion observed on the modeled floodplain likely

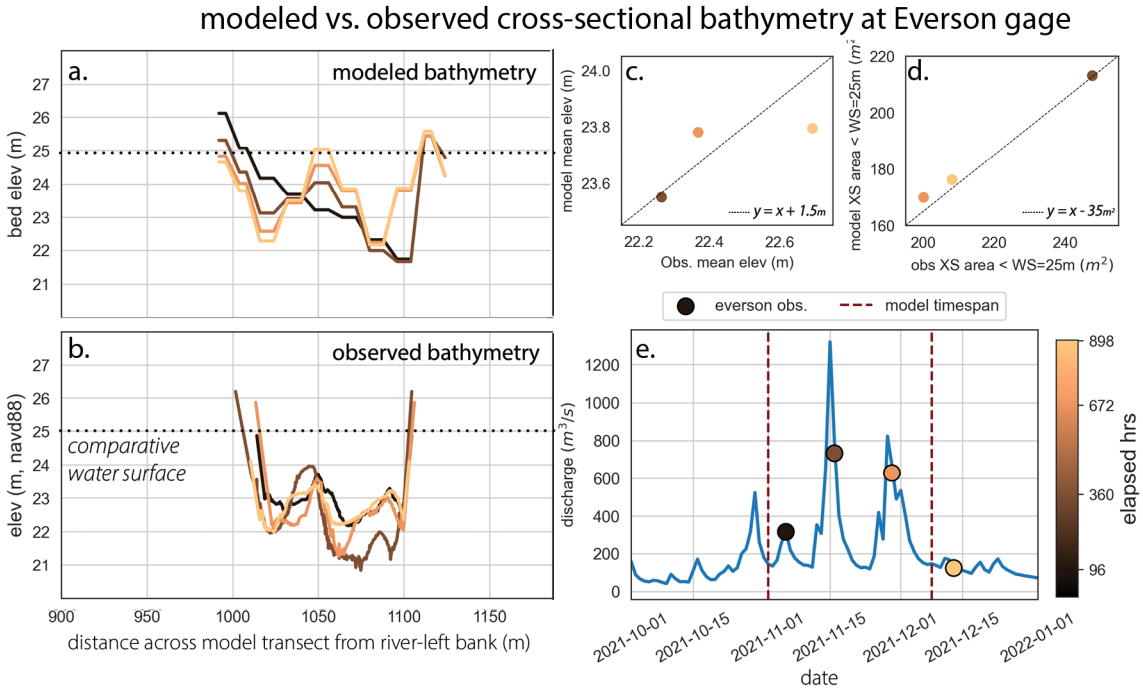

Figure 4.6: *Comparison of modeled vs. observed cross-sectional bathymetry for observations overlapping model simulation time at the Everson river gage.* ***(a):*** *modeled transects, colors correspond to times shown in (e), (b): observed bathymetry, colors correspond to times shown in (e),* ***(c)****: relationship between modeled vs. observed mean bed elevation at transects,* ***(d):*** *relationship between modeled vs. observed cross-setional area below the comparative water surface of 25m,* ***(e):*** *North Cedarville hydrograph showing observation times and model simulation span*

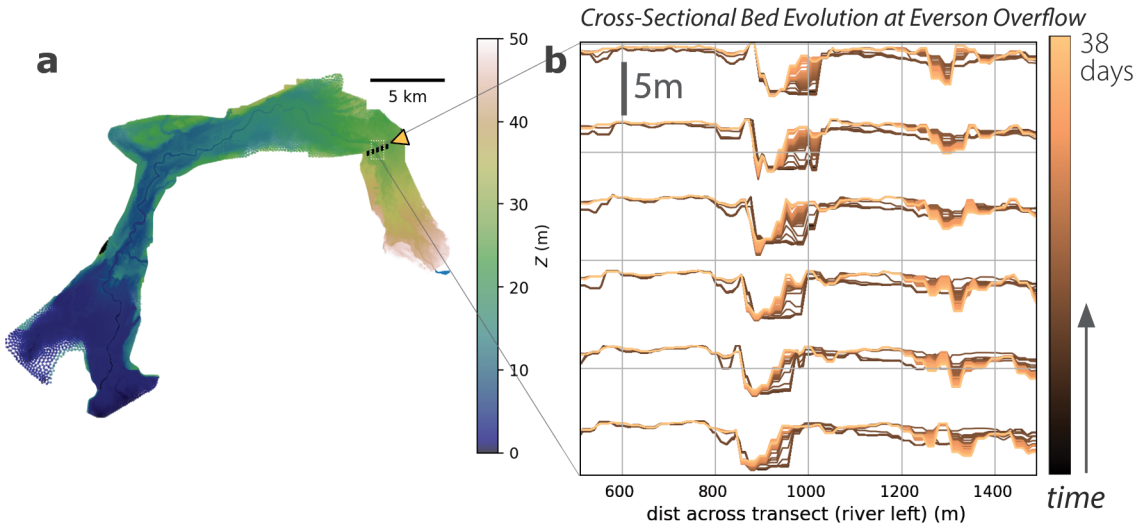

Figure 4.7: *Cross-sectional evolution at Everson overflow.* ***(a):*** *shows model domain where a 75m streamwise reach of transects are extracted at the Everson overflow (represented as orange arrow). A small white box shows the inset location of Fig 4.11,* ***(b):*** *shows elevation at cross-sectional transects stacked from upstream (at the bottom) to downtream (at the top); transects begin at 8.745 km downstream from model boundary and are spaced 15 m streamwise. Transect colors show relative model simulation time; browner colors represent earlier times, yellower colors represent later times*

overestimates typical overbank elevation change. Nevertheless, the consistency between modeled channel bar formation and floodplain deposition with that observed in satellite imagery suggests that the model is capturing morphodynamic processs at this critical location of overbank flow.

A question unanswerable from the satellite imagery was whether the river-left region concurrently deepened with bar formation; this transect data shows that minimal river-left deepening occurred on the upstream and downstream ends of the bar, with very modest deepening at the location of the bar. We discuss how bar formation with a lack of river-left deepening modifies channel conveyance in the subsequent section.

4.5 *Results*

The Delft3D hydro-morphodynamic model shows complex changes in Lower Nooksack channel morphology during the November 2021 event; the highest changes in bed elevation across the model domain occur around and upstream of the Everson Overflow (Appendix Fig 4.14) which is the region we focus on in these results (Fig 4.8). Channel adjustment styles range from braiding, lateral widening/narrowing, and erosion/deposition depending on location within the domain. While morphodynamic adjusments on the floodplain are typically modest in comparison to the main-channel, overbank flows around the Everson Overflow show a substantial erosion capacity, including the development of an erosional channel near the Twin Views Levee that does not occur in reality (Appendix Fig 4.15). Since we are primarily interested in streamwise changes in bed level and flood extent, the following results do not focus on this section, but we acknowledge that there are known regions misrepresented by the model (further commentary in Section 4.6.4).

4.5.1 *Spatial patterns in bed level adjustment and flood depth*

Cross-sectionally averaged streamwise results through the Overflow Region (Fig 4.8) show meter-scale adjustments to bed level during the November 2021 flood. The upper four kilometers of the domain show high magnitude deposition, but this may be due to the position of the model boundary on a transition reach where the river rapidly widens, resulting in an abrupt drop in peakflow velocity and deposition; this is discussed further in Section 4.6.4. We thus consider dynamics mostly between four to 16 kilometers downstream of the model boundary (Fig 4.8 c.1-c.7).

Cumulative deposition is observed at the Everson Overflow location, 8.75 km downstream of the model boundary (Fig 4.8 c.1-c.7) that initiates after the flow exceeds bankfull on the rising limb and peaks during the first flood (Fig 4.8 b.1-b.2, c.1-c.2 and 4.10 c). Deposition here manifests as river-right bar, as discussed in Section 4.4.2. The 1km reach

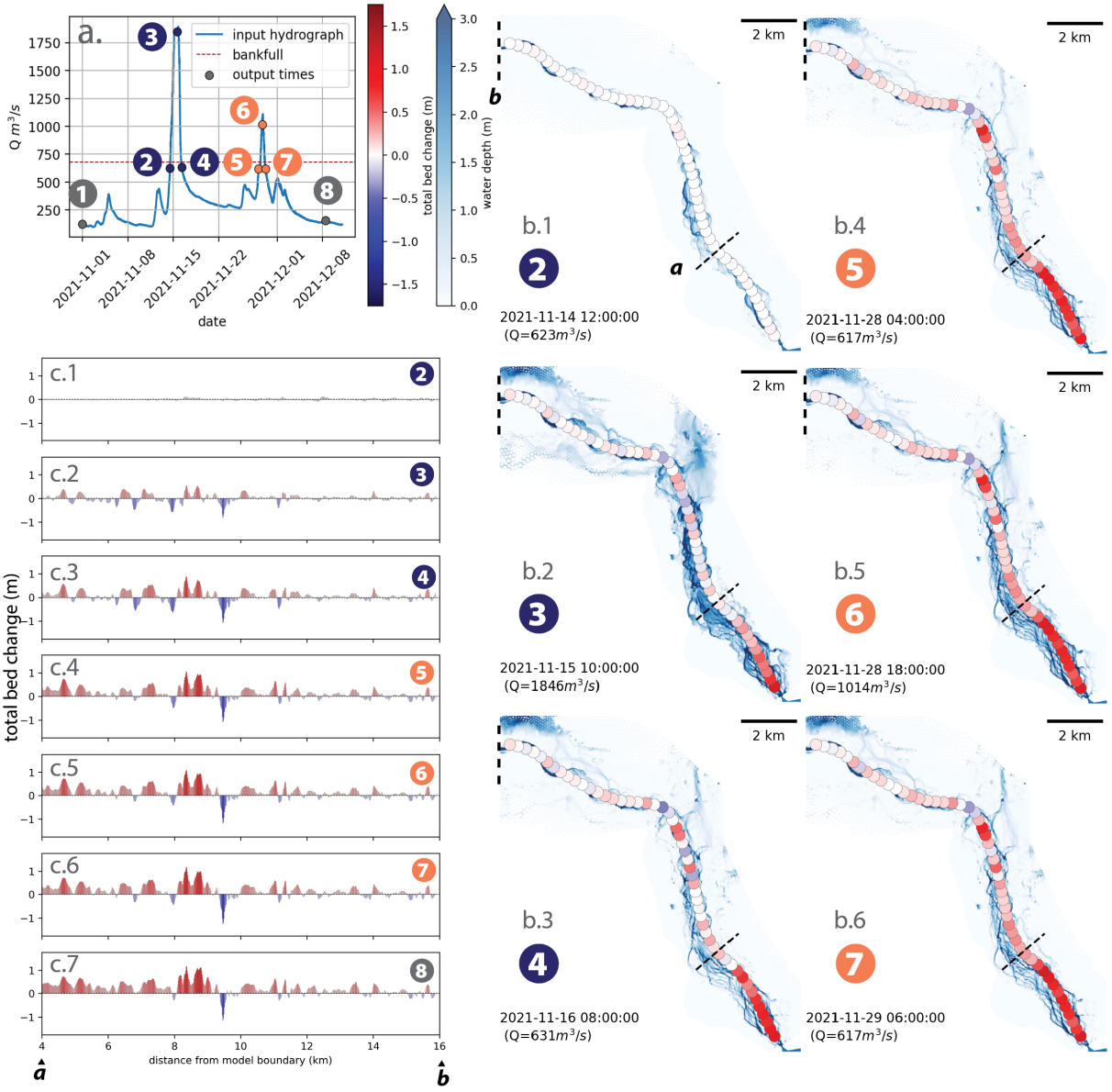

Figure 4.8: ***(a):*** *North Cedarville flood hydrograph with times of plotted output, #s 2-3 are associated with the first flood peak, #s 5-7 are associated with the second flood peak.****(b.1-b.6):*** *Spatial maps of flow depth and cross-sectionally-averaged bed change for the output times labeled in (a); (c.1-c.7): bed elevation changes from 4-16km downstream from the model boundary, the Everson Overflow is at 8.73 km, the Everson Bridge is ∼ 100 m downstream of here*

around the Overflow (8-9km) has notably the highest magnitude response observed in the ten kilometers bracketing this region (Fig 4.8). Persistent incision is also present at the Everson bridge 9.3km downstream of the model boundary, with regions of modest incision present during the rising limb of the first flood peak (Fig 4.8 b.2-b.3; c.2-c.3), which mostly transition to net aggradational by the end of the simulation (Fig 4.8 c.7).

Water depth maps show flow that occupies a multi-threaded region in the upper eight kilometers of the model domain, which then transitions to a confined single channel (Fig 4.8 b.1-b.6). At this transition, substantial river-right overflow is observed during the flood peak beginning at the streamwise onset of channel confinement and peaking at the Everson Overflow location (Fig 4.8 b.2). For the subsequent model duration, water occupies a mild, north-flowing channel scar evolved during the peak flood (Fig 4.8 b.3-b.6). Downstream of the Overflow, both the left and right floodplains are active during the first flood peak (Fig 4.8 b.2) and predominantly the right floodplain for the second flood peak (Fig 4.8 c.2). We discuss how this overbank flow is related to flood hydraulics and bed response in the following section.

4.5.2 Streamwise and temporal patterns in flood hydraulics and bed response

Streamwise patterns in inundation width, bed level adjustment, and flow velocity and conveyance (Fig 4.9) can be partitioned into four response reaches: (1) an upstream model boundary region ($\sim$ 0-2 km downstream), (2) an unconfined transport region ($\sim$ 2-8 km), (3) the Overflow section ($\sim$ 8-9.5km) and (4) a confined downstream channel ($\sim$ 9.5-16 km).

Upstream model-boundary reach: In the upstream model-boundary region ($\sim$ 0-2 km), the river transitions from a narrow, confined channel to a broad, multi-threaded channel as it exits the mountain front (Fig 4.1), corresponding to an abrupt increase in bankfull width (Fig 4.5 a). During the flood, inundated width spatially increases over the upper 1 km (Fig 4.9 a.1-a.7); this corresponds to an abrupt spatial decrease in flow

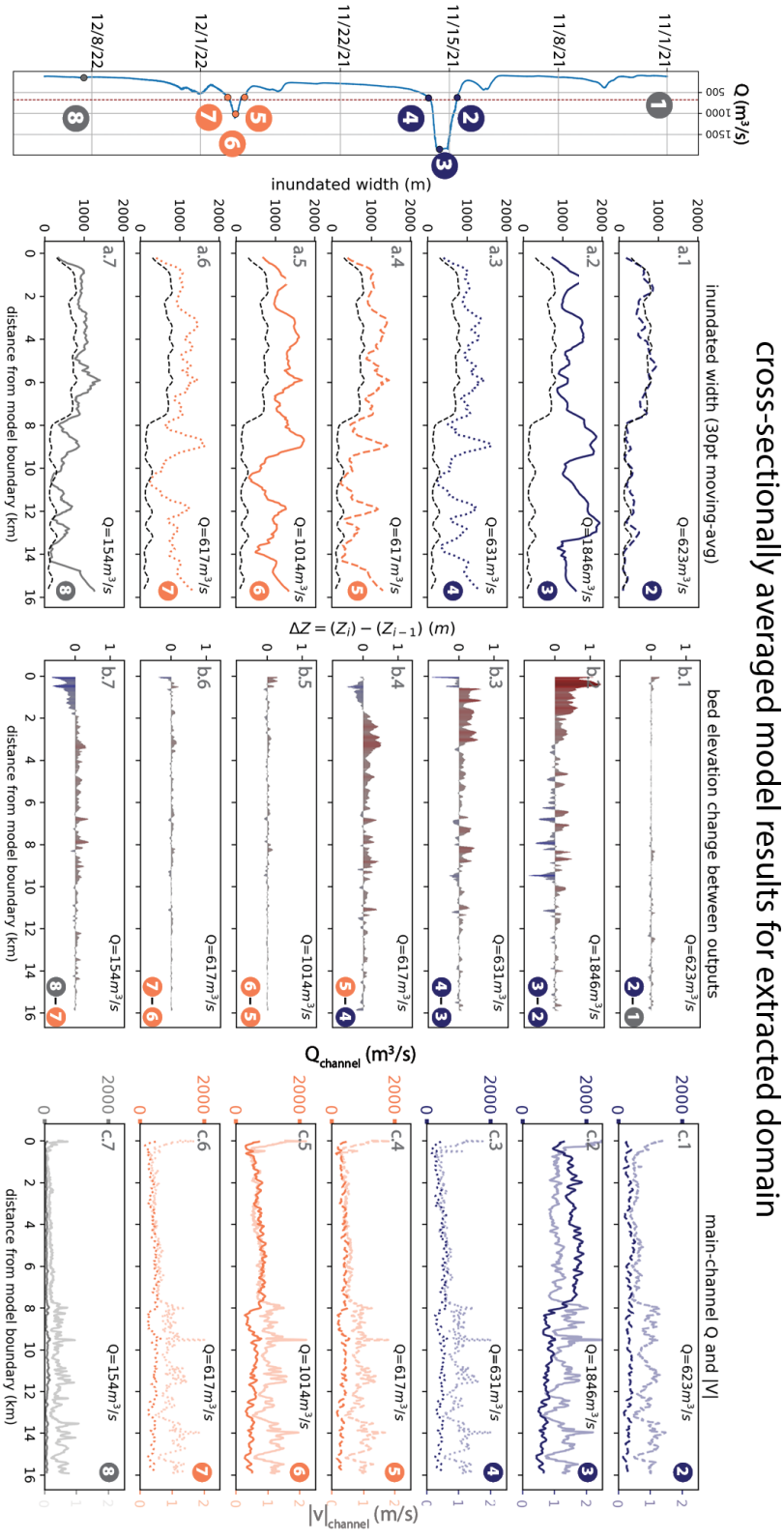

Figure 4.9: *see next page*

Figure 4.9: *Streamwise plots of cross-sectionally averaged model results for seven output times vs. distance from upstream model boundary,* ***(a.1-a.7)****: active innundated width, black dashed line represents bankfull channel width computed in Fig 4.5,* ***(b.1-b.7)****: bed elevation change between current and previous output,* ***(c.1-c.)****: flow conveyance computed as the discharge passing through the main-channel is plotted in a darker shade; mean, main-channel velocity is plotted in a lighter shade*

velocity (Fig 4.9 c.1-c.7), with little spatial trend in main-channel flow conveyance. The bed responds to the sudden spatial decrease in velocity with deposition during the rising limb of the first flood-peak with decreasing magnitude through the upper two kilometers (Fig 4.9 b.2). This depositional mound is partially eroded and transported downstream during the falling limb of the first flood peak and inter-flood period (Fig 4.9 b.3-b.4). Lower magnitude deposition occurs here during the second flood peak (Fig 4.9 b.5); notably, this area shows erosional recovery during inter-flood periods (Fig 4.9 b.4, b.7).

Unconfined transport reach: In the unconfined transport region ($\sim$ 2-8 km), bankfull width averages around a relatively constant 750m (Fig 4.5 a). Average main-channel flow velocity and conveyance are also spatially consistent through this region (Fig 4.9 c.1-c.7). The bed elevation dynamics through this section reflect propagation and diffusion of the deposition mound at the upstream boundary during both above- and below-bankfull conditions (Fig 4.9 b.3-b.7).

Overflow reach: At the onset of confinement ($\sim$ 8km) there is an abrupt spatial decrease in bankfull width (Fig 4.5 a), corresponding to an abrupt spatial increase in flow velocity (Fig 4.9 c.1-c.7). On the rising limb of the first flood peak, abrupt narrowing and flow acceleration at the onset of confinement ($\sim$8km) corresponds to mean bed erosion (Fig 4.9 b.2). A peak in velocity at the Everson bridge (9.3km) also results in local erosion (Fig 4.9 b.2). Additionally, there is an abrupt 50% drop in flow conveyed by the main-channel during the flood peak between the kilometer upstream of the Overflow (mean conveyance between 8-9km, $\overline{Q}_{upstream}$=1550 m^3/s) and the kilometer spanning the Overflow region

(mean conveyance between 7-8km, $\overline{Q}_{overflow}$=800 m^3/s) (Figs 4.9 c.2, 4.10 a & b).

The Overflow reach shows an important temporal changes in streamwise flow conveyed by the main-channel; before the flow reaches bankfull, flow conveyance in the main-channel is relatively consistent in space (Fig 4.9 c.2) and similar within the main-channel at the overflow vs. the upstream kilometer (Fig 4.10 a). However, after flows exceed bankfull during the first flood peak, the river bed begins to aggrade in the Overflow section (Fig 4.10 c), with a main-channel flow conveyance that is consistently lower than the upstream kilometer for the rest of the simulation (Fig 4.10 a & b). This persistant decrease in conveyance at the Overflow results in a 40% streamwise 'dip' in flow conveyance through this section during the falling limb of the first flood (Figs 4.9 c.3 and 4.10 a & b; $\overline{Q}_{upstream}$=530 m^3/s to $\overline{Q}_{overflow}$=360 m^3/s). Conveyance remains lower in the Overflow section through the second flood peak (Figs 4.10 a & b and 4.9 c.4-c.6), and there is subsequent a 50% streamwise decrease at main-channel conveyance the overflow during the second peak (Figs 4.9 c.5 and 4.10 a & b; $\overline{Q}_{upstream}$=790 m^3/s to $\overline{Q}_{overflow}$=410 m^3/s.

Overbank flooding at the Everson Overflow is related to a combination of both pre-existing channel geometry that abruptly narrows in space at this location as well as potential changes to conveyance that occur during the event. It is notable that the temporal onset of overbank flooding, identifiable by where ($\overline{Q}_{overflow}/\ \overline{Q}_{upstream}$) < 1 in Fig 4.10 b, co-occurs with bed aggradation in the Overflow section suggesting a relationship between flooding and bed elevation change (Fig 4.10 c). The Overflow section subsequently conveys less flow than the upstream kilometer even after flows return to in-bank conditions between events, suggesting persistent changes to channel conveyance during the first peak that can affect main-channel conveyance capacity for the second event.

Confined, downstream reach: In the downstream section ($\sim$ 8-16 km), flow velocity remains generally high, with spatial flow acceleration and deceleration related to streamwise changes in local channel geometry. This section shows spatially varying patterns of

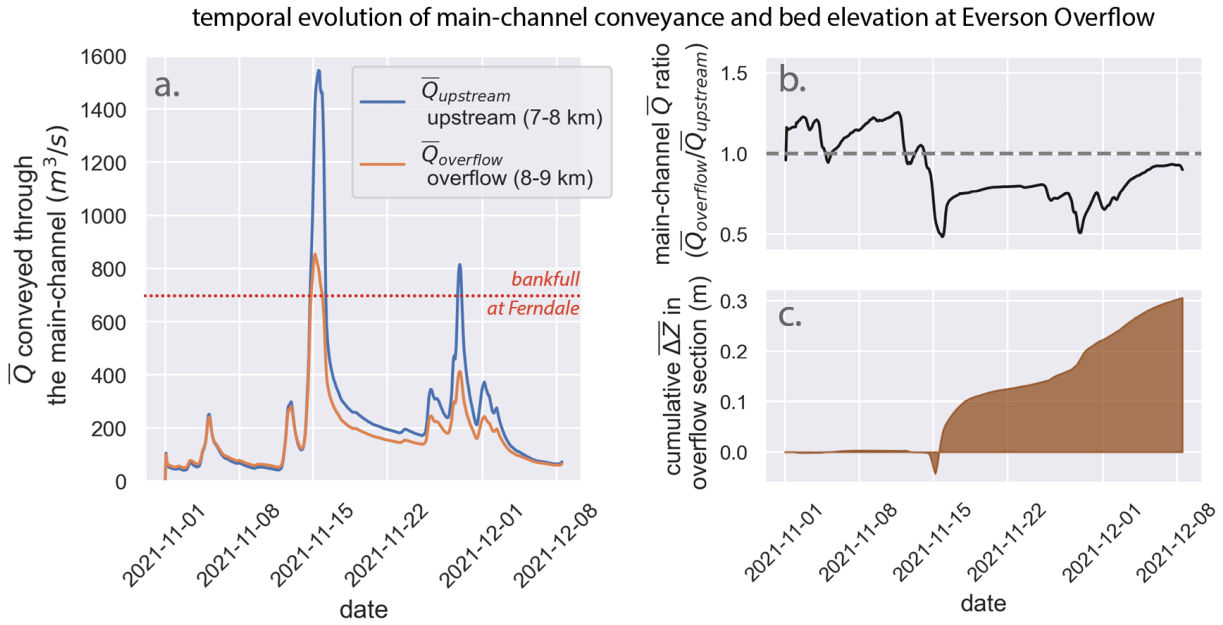

Figure 4.10: *(a) temporal changes to average flow ($\overline{Q}$) conveyed in the main-channel for 1km around the Everson Overflow ($\overline{Q}_{overflow}$: averaged 8-9km downstream from the model) boundary vs. the upstream 1km, ($\overline{Q}_{upstream}$: averaged 7-8km downstream from the model boundary); (b) temporal ratio of $\overline{Q}_{overflow}$ to $\overline{Q}_{upstream}$, values below one indicate that the main-channel at the Everson Overflow is conveying less flow than the 1km upstream; (c) cumulative average bed elevation change (ΔZ) at the Everson Overflow (7-8km).*

erosion and deposition that changes between above- and below-bankfull conditions (Fig 4.8 b.1-b.7), resulting in minimal cumulative changes in comparison to upstream (Fig 4.8 c.7).

4.5.3 *The Dynamics of Overbank Flooding At Everson*

At the Everson Overflow location, the river-right alluvial ridge slope is nearly twice as steep as the the streamwise main-channel slope. The initial topography on the river-left shown in Fig 4.7 b has an average slope of 0.006 between 1000-1250 m distance across the transect; the average slope in the main-channel at this location is 0.0034. Thus, when flows exceed bankfull, it becomes energetically favorable for flow to exit the channel laterally.

Due to the propensity of aggradation and reduced main-channel conveyance at

this location during the first flood peak (Fig 4.9), we investigate the two-dimensional hydraulics and morphodynamics at the Overflow location to understand whether this is driven by overbank flow. In Figure 4.11, we present spatial maps of flow depth (a-c) flow velocity (d-f) and bed elevation (g-i) for a 750m along-channel distance spanning the Everson Overflow. We compare these to cross-sectionally averaged parameters plotted with the same y-location to understand how main-channel calculations of flow velocity and acceleration along with bed change are manifesting two-dimensionally (Fig 4.11).

Minimal bed elevation changes occur prior to bankfull flow on the rising-limb of the first flood peak (Fig 4.11 g). Velocity vectors are primarily oriented down the main channel (Fig 4.11 d) with modest flow acceleration and deceleration related to channel depth and meandering (Fig 4.11 a).

Between the time of bankfull flow occurrence on the rising-limb and the first flood peak, aggradation initiates at y=200m in the Overflow section shown in Fig 4.11 h. This co-occurs with an abrupt decrease in flow velocity due to bilateral overbank flow; overflow is visualized most prominently by spatial velocity vectors exiting the main-channel at y=425m, but causes the highest deceleration in flow at y=280m, just downstream of the bar formation. Flow re-entering the floodplain is responsible for local velocity acceleration at y=200m and y=450m. The concurrence of aggradation with a streamwise decrease in velocity due to overbank flow suggests a relationship between morphodynamics and overbank flow.

The development of a river-right bar is evident at the time of falling-limb bankfull-flow (Fig 4.11 i). Aggradation shifts slightly downstream between the flood peak and falling-limb bankfull creating a net region of aggradation during the first flood peak from y=200-400m (Fig 4.11 h & i). Flow velocity spatially accelerates at y=225m (Fig 4.11 f), as the bar confines channel flow width. Spatial patterns in flow-depth (Fig 4.11 f), and velocity gradients are altered post-flood (Fig 4.11 f).

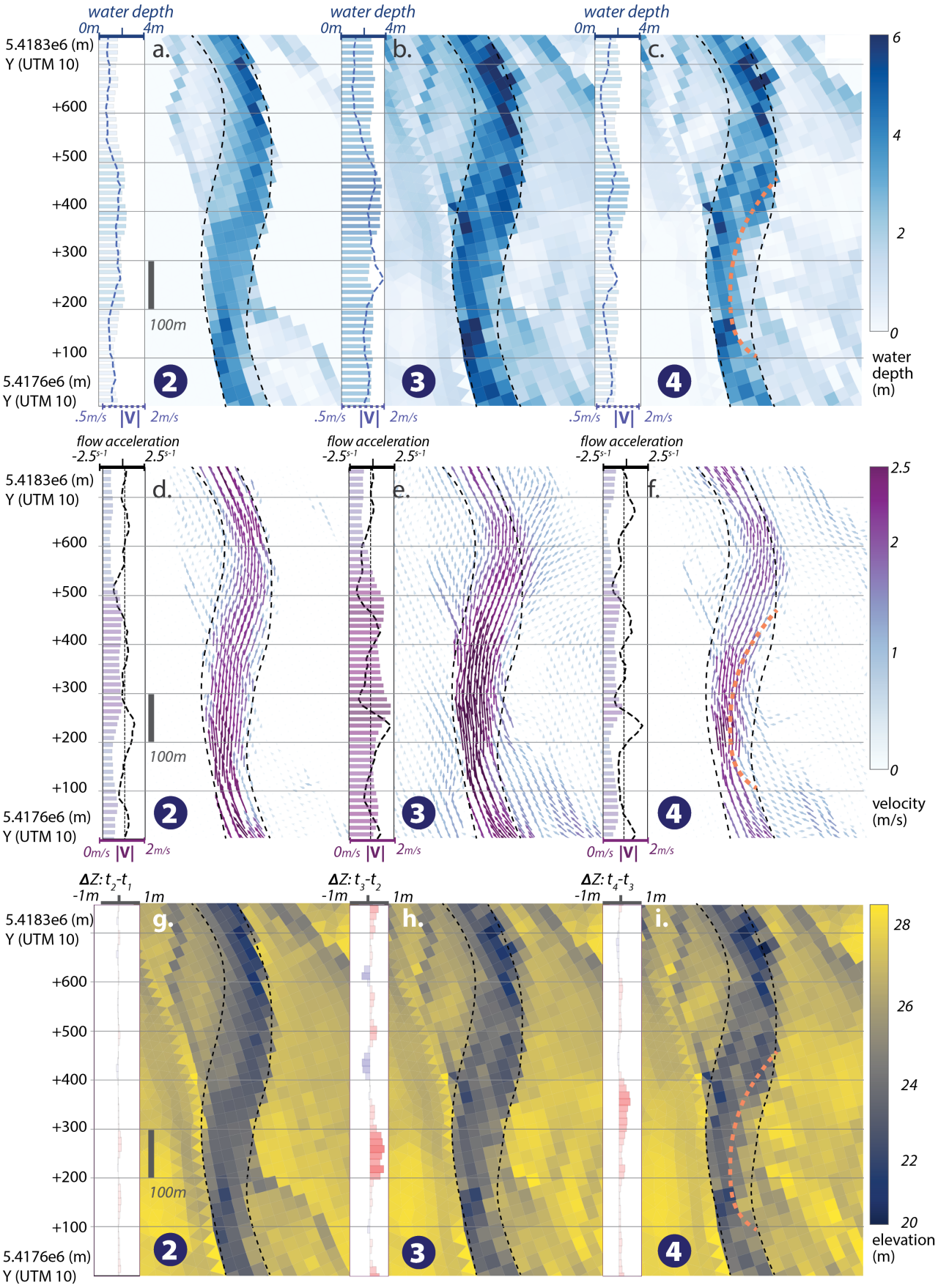

Figure 4.11: *see next page*

Figure 4.10: *Maps of hydrodynamic and morphodynamc model output at the Everson Overflow, side panels show associated transect averages plotted on the same y-axes as the maps across the 800m section. Bold blue numbers correspond to the hydrograph output time noted on Fig 4.8, & Fig 4.9. (a-c): spatial maps of water depth, side panels shows water depth as blue bars and mean channel velocity as a dashed blue line. (d-f): flow velocity vectors colored by velocity magnitude, side panels show flow velocity as purple bars and flow acceleration as a dashed, black line. (g-i): maps of bed elevation, side panels show bed elevation change between model output times*

4.5.4 Comparison of Event-Scale Bed Level Change with Long-Term Trends

Streamwise-averaged bed elevation changes show little consistency with local patterns in long-term bed level trends estimated from digital elevation models of difference (DoDs) (data provided by Scott W. Anderson, *Anderson et al.* (2019)). This provides little indication that long-term trends in channel elevation are composed of discrete responses to extreme floods (Fig 4.12). Similar erosion at the Everson bridge (9.7km downstream) and upstream of the overflow (8km downstream) is observed between the model and the 2022-2016 DoD, but the model predicts much less downstream deposition. The model predicts most aggradation at the Everson Overflow (8.7km downstream), between 4-16 km downstream; the DoDs also typically show bed level increase in this location but to a varying, sometimes small degree.

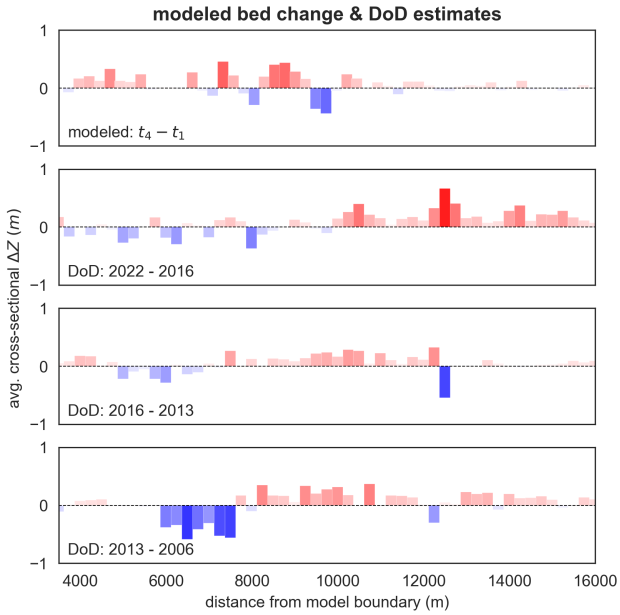

Figure 4.12: *Streamwise bed elevation results predicted by the Delft3D model vs. Digital elevation models of difference (DoDs). Delft3D modeled differences show cumulative bed elevation changes through the entire simulation, with t_4 and t_1 referring to times marked in the hydrograph in Fig 4.8a. DoD Data provided by Scott W. Anderson.*

4.6 Discussion

We analyze a Delft3D hydro-morphodynamic model to understand connections between overbank flooding and morphodynamic response through the Everson Overflow region in the Nooksack River, Washington State. We find meter-scale bed elevation that varies in magnitude within different sections of the domain; an upstream model-boundary region, an unconfined transport region, the Everson Overflow, and confined downstream channel. Streamwise patterns in hydraulics and morphodynamics show that main-channel conveyance was reduced at the Everson Overflow in combination with overbank flooding.

4.6.1 Feedbacks between flood hydraulics and morphodynamics

The onset of aggradation is coincident with overbank flows during the November 2021 flood event at the Everson Overflow. An abrupt streamwise increase in inundated width (Fig 4.9 a.2), local streamwise reduction in velocity coincident with overbank flow (Fig 4.11 e), and concurrent aggradation (Fig 4.11 h, i, and 4.10 c) suggests the importance of overbank flooding in local morphodynamic response.

Flow exchange between the main-channel and floodplain is largely responsible for changing the streamwise gradients in velocity in the Everson Overflow (Fig 4.11 e). Flow converges into the main-channel upstream of the overflow over a vegetated, high-elevation, river-right bar as the channel meanders northward (bottom-right location in Fig 4.11 g, vegetation shown in Fig 4.3). This flow is subsequently expelled bilaterally at the overflow location (Fig 4.11 e y=450m). This overflow appears to affect the velocity predominantly in the 100m immediately upstream. This region of rapid deceleration is also where the river-right bar forms (Fig 4.11 h,i), although the location is not precisely concurrent with instantaneous velocities shown in Fig 4.11 e & f. This may be due to 1) a time-lag between hydraulics and morphodynamic response (*Mackin*, 1948), or 2) the dynamics of bar formation which are three-dimensional and can be self-reinforcing due to the way they locally modify water depth and velocity (*Redolfi*, 2021). Thus, while the

bed level response to overbank flooding appears to be mostly local, it may be shifted slightly up or downstream depending on where the influence of overbank flow affects velocity gradients, and complexities associated with the style of bed response.

Whether channel response to extreme flood events is reflected in long-term morphodynamic patterns in the Nooksack River is unclear. It is not obvious that the long-term trend in bed level is comprised of discrete flood responses. Comparison with DoD data (including *Anderson et al.* (2019)) showed few similarities (Fig 4.12). However, because the model simulates the 2021 flood event on 2015 bathymetry, this comparison is convoluted by the fact that the model may not be positioned to reproduce trends observed between these time periods.

4.6.2 *The effect of bed changes on post-flood channel conveyance*

This work builds on previous investigations suggesting that conveyance changes can affect flood hazard (*Ahrendt et al.*, 2022; *Buffin-Bélanger et al.*, 2017; *Guan et al.*, 2016; *Slater et al.*, 2015; *Sofia and Nikolopoulos*, 2020), by providing a direct example of morphodynamic changes during an initial, extreme flood peak which reduce main-channel flow conveyance for a secondary flood peak.

Bed aggradation at the Everson Overflow initiates with the temporal onset of flooding during the first flood peak (Fig 4.10 b & c) and results in a local streamwise reduction in flow conveyance that persists through the second flood peak (Fig 4.9 c.1-c.6). During and between both the first and second flood peaks, the Everson Overflow also conveys less flow than the upstream kilometer; even after flows have returned to in-bank conditions, the Overflow section conveys 25% less flow than the upstream section (Fig 4.10 b). Thus, the model suggests that the risk of overbank flooding at the Everson Overflow may compound between back-to-back flood events due to morphodynamic changes. It is important to note that overbank flooding at the Everson Overflow is related to a combination of both pre-existing channel geometry that abruptly narrows in space at this location as well as

potential changes to conveyance that occur during the event.

While some regions, particularly the upper model domain, show incisional recovery between flood peaks (Fig 4.9 b.4 & b.7) there is little to no bed recovery in the Overflow reach (Fig 4.10 c). Previous analyses of incisional channel recovery to extreme aggradation from floods suggests recovery time scales can range from immediately following the event to multiple years (*Lisle*, 1981). We do not simulate low-flow conditions in this study, but given a longer period of low flows, it is possible that the deposition at the Everson Overflow could diffuse and propogate downstream.

4.6.3 Spatially propogating vs. locally static bed response

Previous research has suggested that the decadal-scale aggradation trends at the Everson Overflow region are a result of climate-driven modulations to headwater sediment-supply propogating downstream (*Anderson and Konrad*, 2019; *Anderson et al.*, 2019). Under this expectation, bed level fluctuations may both increase but also alleviate flood risk on decadal time scales. The fact that overbank flooding appears to locally modify local river morphodynamics imparts a different expectation for flood risk in which there are persistent, local regions of aggradation or degradation. This has ramifications for flood hazard managers who may be planning for flood hazards on decadal timescales; whether aggradation at the Everson overflow is downstream-propagating or static in space may prompt different mitigation strategies.

4.6.4 Capabilities and shortcomings of the Lower Nooksack Delft3D Model

While we typically may not expect a depth-averaged, spatially explicit, morphodynamic model to accurately represent changes on the bar scale, this Lower Nooksack Delft3D Model captures cross-sectional evolution at the Everson gage (Fig 4.6) and observed river-right bar formation at the overflow (Fig 4.7) remarkably well. Two- and three-dimensional morphodynamic models are often considered to have low predictive qualities at a given

location due to their high sensitivity to local hydraulics and sediment-supply during floods combined with potential inconsistencies in model bathymetry (*Lauer et al.*, 2016). The model in this study also uses initial bathymetry from 2015 and is missing potential morphodynamic changes occurring during several high flows occurring in winter 2016 and 2020 (*USGS-NWIS*). While the cross-sectional bathymetry at Everson is initially rather poorly represented by the model (Fig 4.6 a vs. b), it rapidly adjusts during the event to replicate an observed river-center bar during the simulation.

However, the model does create a deeper north-flowing channel upstream of the Everson overflow that was not observed during the November 2021 event (Appendix Fig 4.15). This channel occurs at a transition just downstream of the Twin Views levee where the river-right topography abruptly decreases (Appendix Fig 4.15 a, b). Two other, north-flowing regions of scour are also observed further upstream/east, but to a lesser degree. Satellite imagery from immediately after the event shows standing water in these regions (Appendix Fig 4.15 c), suggesting that flow was indeed routed through these multiple paths north near the Overflow, however without the degree of scour shown in the model, particularly where flow leaves the channel. Satellite imagery shows these regions as a heavily vegetated (Appendix Fig 4.15 c), which may stabilize the landscape in ways not represented in the model. Additionally, numerous armouring projects have been conducted to protect the river-right bank (*Boyd et al.*, 2019) including some precisely where the scour channels are created. The inclination for the model to evolve north-flowing 'avulsion-like' channels at this region does present an interesting commentary on the sensitivity of the Nooksack/Fraser drainage divide: in a physically-based morphodynamic model, the flow dynamics upstream of the Overflow reach suggest a preference for northward flow which is capable of creating new channels.

Abrupt sediment deposition at the upstream model boundary during the November 2021 flood is likely a result of the position of the model boundary on a transition reach between a relatively confined section and a wide multi-threaded region. While the reach immediately upstream of the model boundary is shown to be a source of sediment for

regions in the upstream model domain (*Anderson et al.*, 2019), it is difficult to untangle informative morpohdynamic information from the upper 2km of the model domain due to boundary effects. The effects of abruptly deposited sediment may have a diffuse influence downstream, though the propogation of this deposition does not appear to reach the Everson Overflow during this one-month simulation. Re-positioning the upstream boundary to a different location, or creating a stable section with similar width and depth to the unconfined, transport section (2-7km downstream) would potentially mitigate high hydraulic gradients and bed response in the upstream model domain.

Local flood managers have expressed concerns related to morphodynamics and flooding that this model may contribute towards understanding. These concerns include quantifying a possible under-prediction of peakflow magnitude due to local intra-flood conveyance increases at gaging stations, along with understanding sediment-routing through the Everson Overflow reach. The application of this model towards assessing streamwise dynamics in hydraulics and morphodynamcis during floods points to its potential usefulness for Nooksack flood management. Addressing the abrupt hydraulic transition at the upstream boundary, and adding floodplain roughness to mitigate overbank incision may improve the interpretation of results across the domain for future applications.

4.6.5 *The effects of abrupt, streamwise lateral confinement on flood hydraulics and morphodynamics*

The onset of channel confinement near the Twin Views levee (Fig 4.1) demarcates a transition in model adjustment magnitude and style; the wider, braided channel upstream of the Twin Views Levee (e.g. Fig 4.5 c) shows both lateral and vertical restructuring during the November 2021 event, including channel widening, braiding, and areas of both shallowing an deepening. In contrast, morphodynamic changes downstream of the Twin Views levee are predominantly confined to restructuring of the main-channel with

some erosion and/or deposition on the floodplain. This location addtionally corresponds to an abrupt visual change in the degree of ponding on the floodplain (Fig 4.3). Upstream of levee confinement, there is little floodwater present outside the multi-threaded channel, while downstream of levee confinement extensive floodwater is present on the floodplain, albeit, potential shifts in floodplain infiltration may also contribute to this pattern.

Propensity for floodplain inundation is shown in the model as an abrupt streamwise decrease in flow conveyed through the main-channel at the onset of confinement (Fig 4.9 c.2). This drop in main-channel flow indicates that the reduction in bankfull width at this location is not sufficiently compensated by an increase in velocity. This imbalance, combined with the influence of overbank flow during extreme floods, is likely to cause persistent bed response at this transition location.

4.6.6 Is a future Nooksack River avulsion of concern?

Topographically, the Everson Overflow region is located at an avulsion-prone region: this river segment co-occurs with a transition between confined valley and alluvial fan, a typical location prone to mountain-front or fan avulsion (*Brooke et al.*, 2022; *Gearon and Edmonds*, 2022). The present channel topography at this region additionally promotes channel overflow during floods due to relatively steeper perpendicular levee slopes vs. main-channel slope. The hydro-morphodynamics of the November 2021 flood event suggest channel overflow is connected to local aggradation; were this cycle to perpetuate naturally, the system may tend towards an avulsion. This possibility is underscored by documentation of at least one historic avulsion in this region (*Pittman et al.*, 2003; *Pittman*, 2019; *Maudlin and Stark*, 2007) and a presently low Nooksack/Fraser drainage divide (*Boyd et al.*, 2019).

Pragmatically, a full avulsion is unlikely; human intervention will plausibly and perpetually seek to suppress a full change in river course. The numerous communities living in the channel-bounding regions of Everson, WA have been vocal in their demand

for flood protection, and the economic value of U.S. and Canadian farms populating the Sumas Valley in the Nooksack overflow course motivate river protection (*Hoekstra*, 2022). While avulsions are considered abrupt events on geomorphic timescales, they often happen in successive stages (*Kleinhans et al.*, 2013) especially in large systems where it takes substantial excavation to establish a new channel, for example, over several large floods. Interventions between floods such as sediment-removal and levee-reinforcement will likely prevent the river from building on consecutive events, thus mitigating full avulsion risk.

This region nevertheless poses a unique management challenge: feeder channels to alluvial fan apexes are known to be dynamic and unpredictable (*Parker et al.*, 1998) with abrupt aggradation during single flood events *Slingerland and Smith* (2004) or cyclic periods of aggradation/incision (*Schumm*, 1977). Here, we observe substantial aggradation in an avulsion reach during a single event; while other research in the Nooksack basin suggests disturbances are downstream-propogating from upland sediment supply (*Anderson et al.*, 2017), this work suggests the conceptual hypothesis proposed in Fig 4.4 also contributes to local bed response.

4.7 Conclusions

We analyze feedbacks between river morphodynamics and overbank flooding during the November 2021 flood using a Delft3D model of the Lower Nooksack River. The model suggests meter-scale bed elevation changes occurred during a month-long simulation with two subsequent flood peaks. We additionally find that bed level co-evolves with flooding; high bed changes occur where flow accelerates and decelerates during flood peaks commonly in relation to overbank flooding. This is particularly important in the Everson Overflow where aggradation occurs in the main-channel with overbank flooding which causes local flow deceleration. Aggradation near the Overflow contributes to a streamwise reduction in main-channel flow conveyance during a subsequent flood peak. These results provide insight to Nooksack River floodplain managers grappling with how

to manage a Nooksack River that persistently overtops and reoccupies a historic north-flowing course. This work additionally provides a broader example of morphodynamic response during flood events and its potential for modifying subsequent flood hazard.

4.8 Appendix

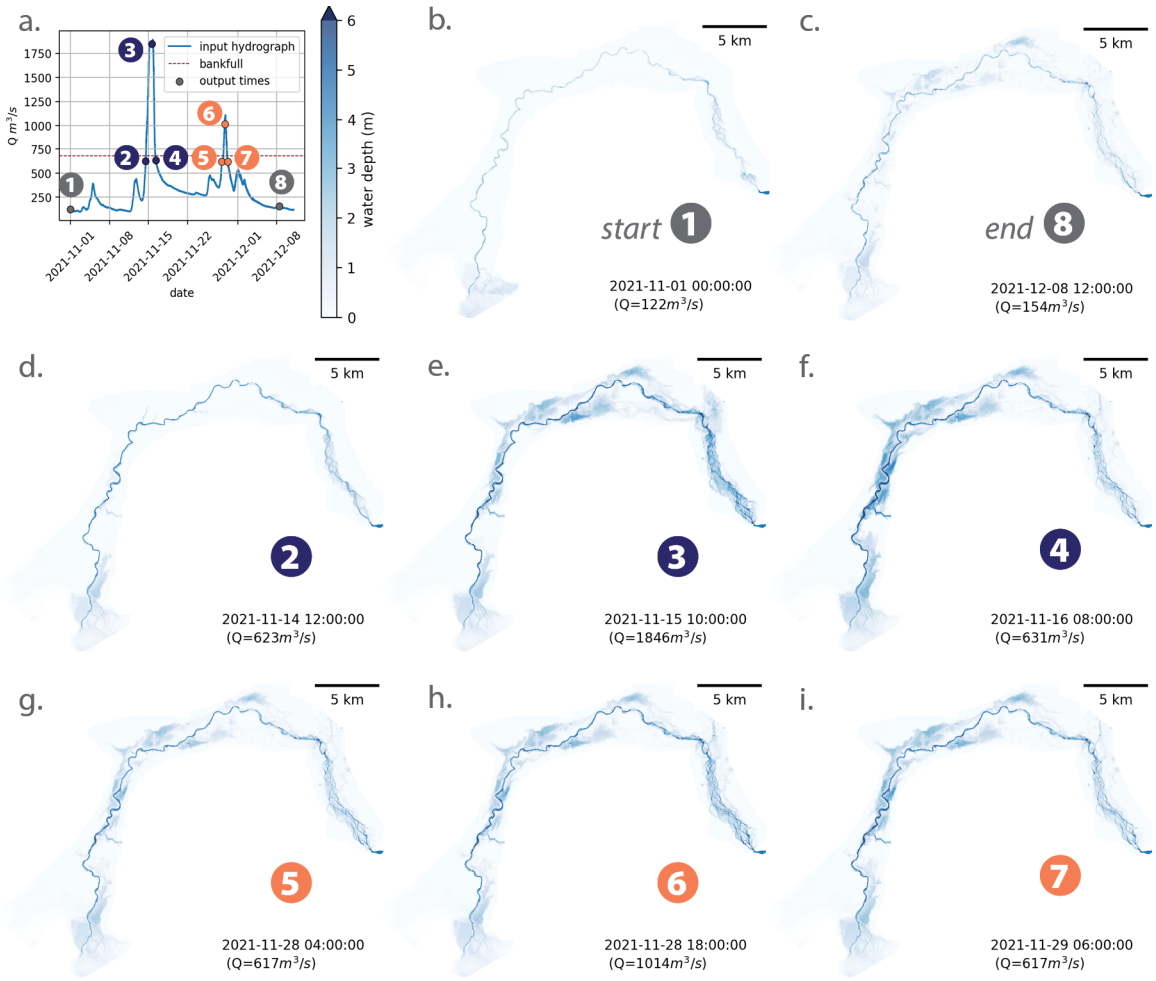

Figure 4.13: *(Appendix) Modeled flood depth for entire Nooksack domain, (a): input hydrograph at North Cedarville showing eight output times, (b) Initial water depth, (c-i) water depth at selected output times*

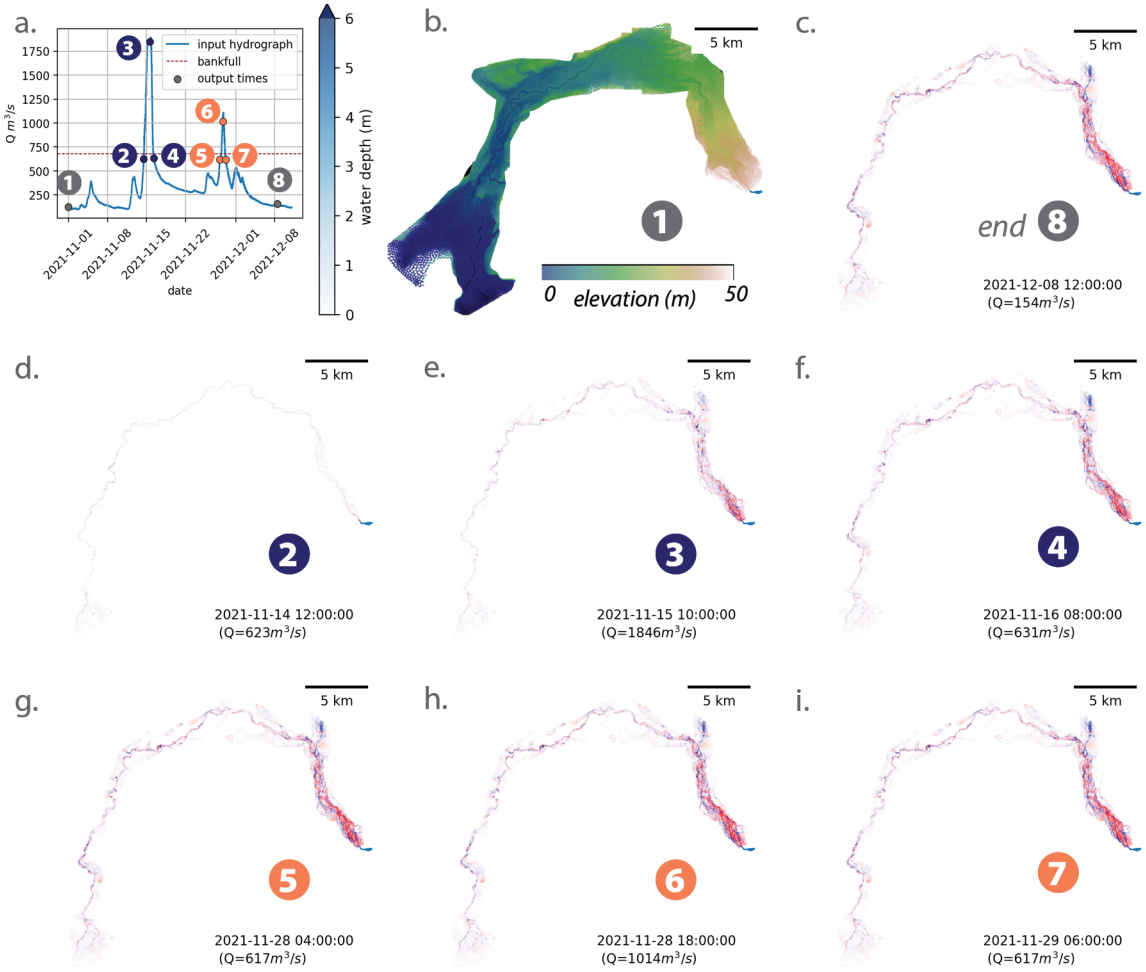

Figure 4.14: *(Appendix) Modeled bed elevation changes for entire Nooksack domain, (a): input hydrograph at North Cedarville showing eight output times, (b) Initial model elevation, (c-i) bed elevation changes with respect to the initial model elevation*

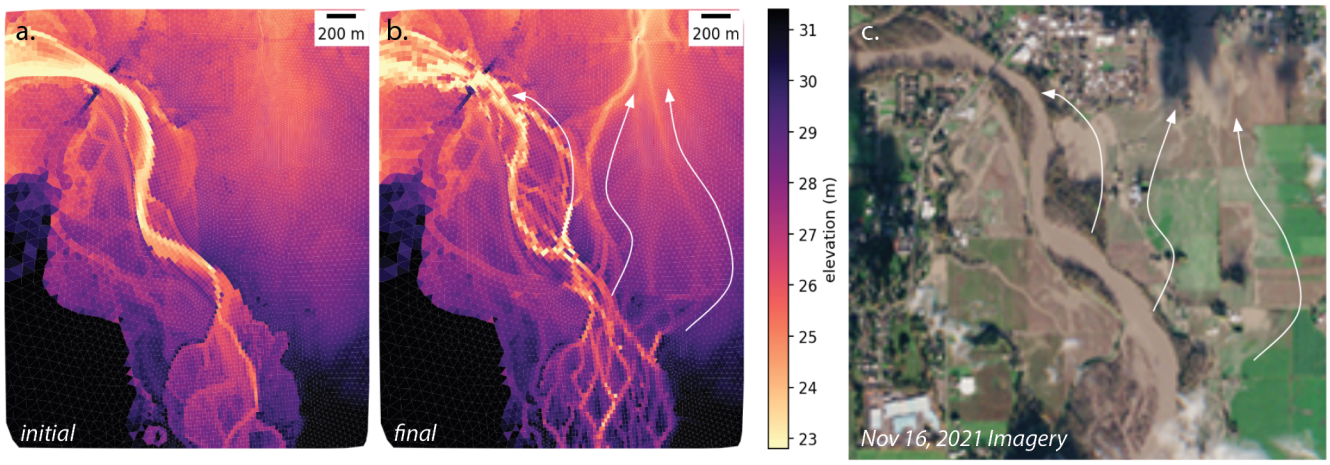

Figure 4.15: *Appendix: Northflowing Channels Created by Delft3D* ***(a)*** *initial model elevation,* ***(b)*** *final model elevation with white arrows noting flow directions and erosional channels,* ***(c)*** *November 16, 2021, post-flood satellite imagery shows flow occupying areas similar to the overflow channels in the model (shown in b)*

Chapter 5
CONCLUSIONS

This thesis investigates feedbacks between river morphodynamics and overbank flooding on engineering timescales in three parts:

- ***Part I*** quantifies the relative importance of historic variation in channel conveyance capacity vs. streamflow variation in Western Washington State where both hydrology and sediment-supply are affected by climate-change. This section points to conveyance unsteadiness as an important driver of flood hazard variability.

- ***Part II*** explains spatial variation in bed elevation response and recovery to peak flows through floodplain topography and geometry that affects floodplain-channel flow exchange. This section demonstrates that overbank flooding can affect spatial gradients in flow velocity that correspond to bed adjustments; additionally, in the absence of robust inter-flood bathymetry data, floodplain topography and geometry may aid in predicting regions prone to dynamic bed level response to peak flows.

- ***Part III*** examines the co-evolution of hydraulics and morphodynamics during an extreme flood in Northwestern Washington State and finds that overbank flooding can affect channel adjustments on the event-scale, underscoring the conclusions of Part II. Part III suggests that persistent, local aggradation may occur as a result of overbank flooding in a region of pressing management concern.

The subsequent section bullets key findings from Parts I-III along with references to prominent supporting figures. Overall, these findings expand understandings of the relationship between morphodynamics and floods with applications for flood hazard management and river channel maintenance.

5.1 *Summary of Key Findings*

5.1.1 *Part I*

- Conveyance is commonly unsteady at 50 Washington river gages and its variation can be equal to variability of moderate flood streamflow (Fig 2.4 & 2.7).

- Short-term changes in channel conveyance can have a greater influence on flood risk than long-term, steady adjustments (Fig 2.7).

- In rivers where flow regulations suppress moderate floods, channel conveyance losses can counteract reductions to streamflow (Fig 2.5 b & 2.7 d,h).

5.1.2 *Part II*

- Floodplain-channel flow exchange explains locations of bed elevation response and recovery to peakflows in the upstream Waal River (Fig 3.4)

- The onset of overbank flow occurs at distinct points of low-elevation channel-adjacent topography (Fig 3.3); which can accelerate flow into and across the main-channel (Fig 3.4)

- Floodplain flow crossing primarily explains bed elevaton response and recovery to peakflows (Fig 3.5); spatial gradients in floodplain width are a secondary control (Fig 3.6)

5.1.3 *Part III*

- The Lower Nooksack River Delft3D model suggests meter-scale bed changes occured during the Nov 2021 flood (Fig 4.8); consistent with the few available measurements (Fig 4.6) and anecdotal observations (e.g. Fig 4.3 vs. Fig 4.7)

- High bed changes occur where hydrodynamic gradients intensify during peak-flows (Figs 4.9 & 4.11).

- At the Everson Overflow, flow decelerates in relation to both overbank flooding and channel meandering (Fig 4.11); modeled bed aggradation occurs in the form of a river-right bar (Figs 4.7 & 4.11), reducing main-channel conveyance capacity (Fig 4.9)

- Morphodynamic change during the first Nov 2021 flood peak alters spatial patterns of flow acceleration (Fig 4.11) and conveyance at the Everson Overflow (Fig 4.9) for a second flood peak

5.2 *Open Questions & Future Work*

While this work addresses some of the dimensions characterizing feedbacks between morphodynamics and floods, morphodynamic responses, as introduced in Section 1.3 are complex and multi-modal. While detangling dynamics across the systems studied in this thesis, I have found myself questioning why a preferential morphodynamic response will arise (e.g. vertical bed changes vs. width adjustments), or whether there are feedbacks between river responses and fundamental morphodynamic controls (i.e. sediment-supply). Here, I highlight specific topics born of these questions that pose viable future research opportunities.

5.2.1 *River bed response to climate variability*

In Part I (Chapter 2), we observe that in two adjacent Western Washington basins (the Nooksack & Skagit River basins), downstream channel conveyance changes are remarkably consistent (Fig 2.10); both the lowland Skagit and Nooksack gages show similar channel conveyance changes both temporally and in relative magnitude. Meanwhile, upstream channel conveyance changes are distinct between the basins (Fig 2.10). *Ander-*

son and Konrad (2019) suggest that in the Nooksack River, this pattern observed at the lowland gage is due to a climate-driven perturbation in upstream sediment-supply that is propagating downstream as a non-diffusive series of river bed elevaton changes with celerity related to slope. Despite the two basins' proximity and shared headwaters in the North Cascades, upland sediment sources from these regions are disconnected from the lower Skagit river by the Upper Skagit and Baker Dams. If the bed elevation pattern at the lowest Nooksack gauge is indeed driven from coarse, upland sediment delivery it is striking that the pattern matches a different lowland basin so closely with minimally shared upland sediment-sources.

An alternative, explanation for the similar channel response in the lower Nooksack and Skagit is that fluctuations in sediment-supply and mean annual water level is driven more locally–this may still be connected to climate, which could explain why both basins show remarkable similarity in response. Puget Lowland river channels have access to ample lowland sediment deposited during the last continental glaciation (*Booth*, 1994), and have incised these deposits over time creating terraces that deliver coarse sediment relatively low in the river network (*Scott and Collins*, 2021). Thus there are known sources of lowland sediment supply, but an open question remains whether these sources are responsive to perturbations in climate.

Across the region, river conveyance oscillates on decadal- to multi-decadal timescales (*Ahrendt et al.*, 2022) commiserate with climate cycles such as the Pacific Decadal Oscillation (*Kahya and Dracup*, 1993). However, whether these are driven by headwater or more supply is unknown. This presents the following future research question:

Future Research Question 1: *In regards to climate variability which can modify both flood intensity and sediment supply, do rivers predominantly propagate these effects downstream or respond more locally?*

5.2.2 *Feedbacks between floods, sediment supply, and channel response*

A subsidary question to Future Research Question 1 probes the possibility that there could be feedbacks between floods and lateral, mid- to low-network sediment supply. *Scott and Collins* (2021) point to fluvial erosion as a likely contributor of mass failure in river-adjacent terraces. Thus, it may follow that fluctuations in river water level and discharge can affect the rate and magnitude of sediment-delivery. Indeed, *Liang et al.* (2015) find that river river level fluctuations are a dominant driver of bank collapse in the Lower River Murray in Southern Australia. On unstable hillslopes, landslides in direct contact with rivers have been shown to mobilize more frequently than non-connected landslides (*Šilhán*, 2022), but whether the frequency and timing of this activation is related to antecedent streamflow has yet to be quantified.

The way this lateral sediment supply responds to changes in streamflow may affect channel response. In Part I (Chapter 2), we observe both steady channel conveyance increases and decreases in a region with increasing moderate flood streamflows in unregulated rivers. Chapter 2 postulates that steady increases in flood streamflow may activate lateral sediment delivery, affecting downstream river response, but this has yet to be fully investigated. This prompts the following research question:

Future Research Question 2: *Do feedbacks between floods and channel adjacent sediment supply propagate into local and downstream bed response?*

5.2.3 *The effects of compound channel structure on morphodynamic response to floods*

Part II (Chapter 3) investigates bed response in an engineered compound channel and finds that main-channel floodplain flow exchange is related to floodplain flow crossing the main-channel or expanding or contracting due to spatial gradients in width. However, flow crossing and spatial width gradients consistently co-occur making it difficult to attribute the relative contribution of each to hydraulics and bed response. Testing the

contribution of planform structure to spatial gradients in flow velocity and shear stress could be done using an idealized model.

Fig 5.1 presents a preliminary idealized model that may be used towards this end, built using the Landlab modeling infrastructure (*Barnhart et al.*, 2020; *Hobley et al.*, 2017). The scale and wavelength of meanders can be varied for both the main-channel and levee boundaries. A simulation of a steady, overbank flow using the Landlab Overland Flow component (*Adams et al.*, 2017) shows meander-scale spatial patterns in channel hydraulics (Fig 5.1 b-d, g) and channel-floodplain flow exchange (Fig 5.1 f) that may be compared between varying compound channel bathymetry. The code for this model is coming soon to the Landlab Github repository (folder location: `https://github.com/landlab/landlab/tree/master/notebooks/tutorials/overland_flow`). This model may be used to test the following question:

Future Research Question 3: *What are the effects of meandering channel structure on river bed response in compound floods?*

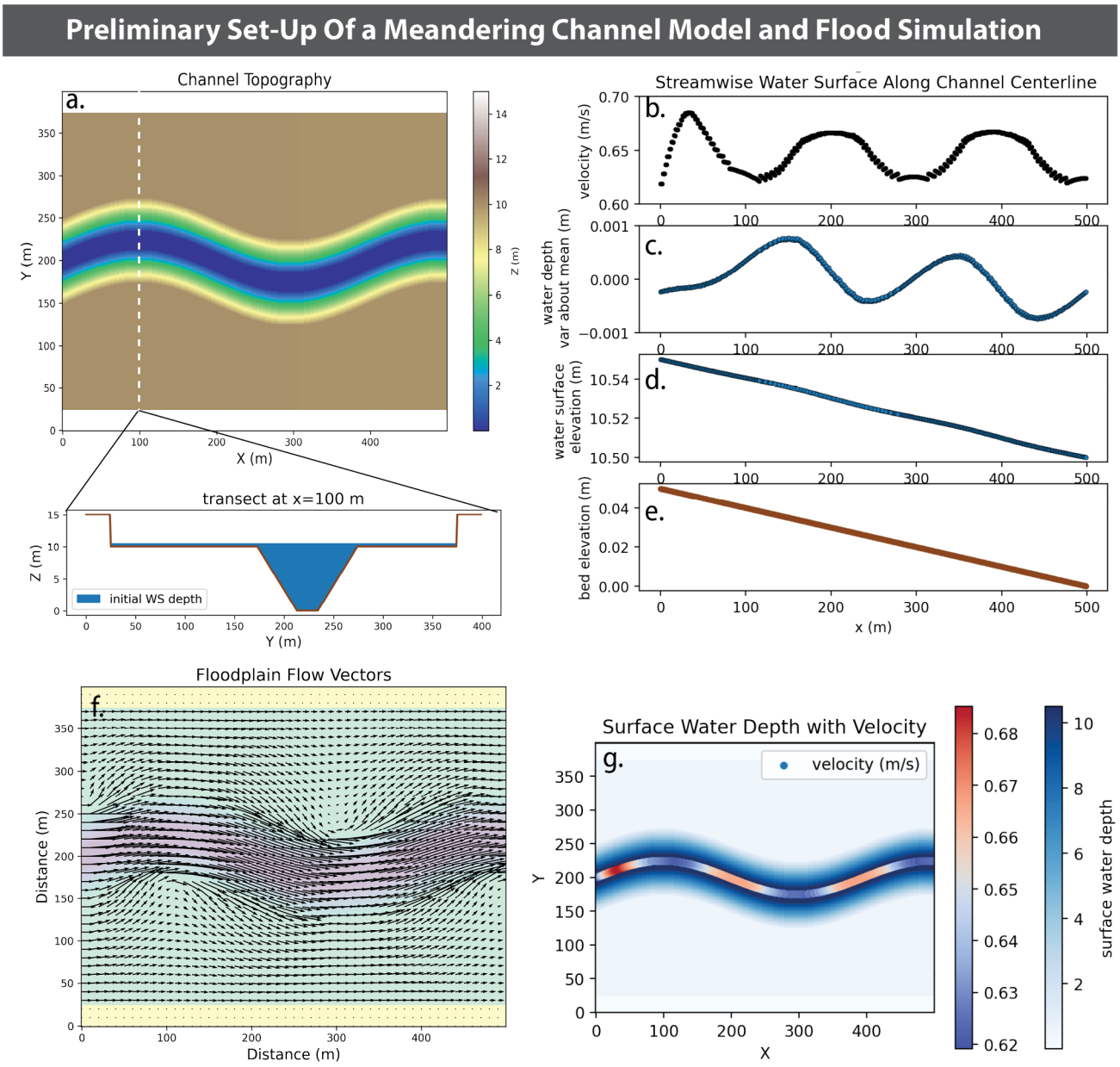

Figure 5.1: *Preliminary set-up of a compound, meandering channel model and flood simulation designed to test questions raised in Part II (Chapter 3): **(a)** planform channel topography designed in Landlab (Barnhart et al., 2020; Hobley et al., 2017) with cross-sectional inset showing compound channel and floodplain; **(b-d)**: hydraulic characteristics along the main-channel centerline during a steady, overbank flow simulation showing meander-scale variation in velocity, water-depth and water surface elevation; **(f)**: flow vectors from steady overbank flow simulation show floodplain-channel flow exchange; **(g)**: planform map of simulated water depth with centerline colored by velocity (m/s)*

BIBLIOGRAPHY

Adams, J. M., N. M. Gasparini, D. E. Hobley, G. E. Tucker, E. W. Hutton, S. S. Nudurupati, and E. Istanbulluoglu, The landlab v1. 0 overlandflow component: a python tool for computing shallow-water flow across watersheds, *Geoscientific Model Development*, *10*(4), 1645–1663, 2017.

AghaKouchak, A., et al., Climate extremes and compound hazards in a warming world, *Annual Review of Earth and Planetary Sciences*, *48*, 519–548, 2020.

Ahrendt, S., A. R. Horner-Devine, B. D. Collins, J. A. Morgan, and E. Istanbulluoglu, Channel conveyance variability can influence flood risk as much as streamflow variability in western Washington State, *Water Resources Research*, *58*(6), e2021WR031,890, 2022.

Anderson, S. W., and K. L. Jaeger, Coarse sediment dynamics in a large glaciated river system: Holocene history and storage dynamics dictate contemporary climate sensitivity, *GSA Bulletin*, 2020.

Anderson, S. W., and C. P. Konrad, Downstream-propagating channel responses to decadal-scale climate variability in a glaciated river basin, *Journal of Geophysical Research: Earth Surface*, *124*(4), 902–919, 2019.

Anderson, S. W., and J. Pitlick, Using repeat lidar to estimate sediment transport in a steep stream, *Journal of Geophysical Research: Earth Surface*, *119*(3), 621–643, 2014.

Anderson, S. W., M. K. Keith, C. S. Magirl, J. R. Wallick, M. C. Mastin, and J. R. Foreman, Geomorphic response of the North Fork Stillaguamish River to the State Route 530 landslide near Oso, Washington, *Tech. rep.*, US Geological Survey, 2017.

Anderson, S. W., C. P. Konrad, E. E. Grossman, and C. A. Curran, Sediment storage and transport in the Nooksack River basin, northwestern Washington, 2006–15, *Tech. rep.*, US Geological Survey, 2019.

Andrews, E. D., Downstream effects of flaming gorge reservoir on the Green River, Colorado and Utah, *Geological Society of America Bulletin*, *97*(8), 1012–1023, 1986.

Arkesteijn, L., A. Blom, M. J. Czapiga, V. Chavarrías, and R. J. Labeur, The quasi-equilibrium longitudinal profile in backwater reaches of the engineered alluvial river: A space-marching method, *Journal of Geophysical Research: Earth Surface*, *124*(11), 2542–2560, 2019.

Arkesteijn, L., A. Blom, and R. J. Labeur, A rapid method for modeling transient river response under stochastic controls with applications to sea level rise and sediment nourishment, *Journal of Geophysical Research: Earth Surface*, *126*(12), e2021JF006,177, 2021.

Arnell, N. W., and S. N. Gosling, The impacts of climate change on river flood risk at the global scale, *Climatic Change*, *134*(3), 387–401, doi:10.1007/s10584-014-1084-5, 2016.

Aslan, A., W. J. Autin, and M. D. Blum, Causes of river avulsion: insights from the late Holocene avulsion history of the Mississippi River, USA, *Journal of Sedimentary Research*, *75*(4), 650–664, 2005.

Barnhart, K. R., et al., Landlab v2. 0: a software package for earth surface dynamics, *Earth Surface Dynamics*, *8*(2), 379–397, 2020.

Biedenharn, D. S., C. M. Elliott, and C. C. Watson, *The WES stream investigation and streambank stabilization handbook*, Citeseer, 1997.

Bijker, E., Sedimentation in channels and trenches, in *Coastal Engineering 1980*, pp. 1708–1718, 1980.

Blench, T., Mobile-bed fluviology, 1969.

Blom, A., Planform changes and overbank flow in meandering rivers: the river Allier, 1997.

Blom, A., E. Viparelli, and V. Chavarrías, The graded alluvial river: Profile concavity and downstream fining, *Geophysical Research Letters*, *43*(12), 6285–6293, 2016.

Blom, A., L. Arkesteijn, V. Chavarrías, and E. Viparelli, The equilibrium alluvial river under variable flow and its channel-forming discharge, *Journal of Geophysical Research: Earth Surface*, *122*(10), 1924–1948, doi:10.1002/2017JF004213, 2017.

Booth, A. M., S. R. LaHusen, A. R. Duvall, and D. R. Montgomery, Holocene history of deep-seated landsliding in the North Fork Stillaguamish River valley from surface roughness analysis, radiocarbon dating, and numerical landscape evolution modeling, *Journal of Geophysical Research: Earth Surface*, *122*(2), 456–472, 2017.

Booth, D. B., Glaciofluvial infilling and scour of the Puget Lowland, Washington, during ice-sheet glaciation, *Geology*, *22*(8), 695–698, 1994.

Boyd, K., P. Pittman, A. Nelson, and T. Thatcher, Lower Nooksack Geomorphic Assessment, *Tech. rep.*, Prepared for Whatcom County Flood Control Zone District, 2019.

Brewer, P., and J. Lewin, Planform cyclicity in an unstable reach: complex fluvial response to environmental change, *Earth Surface Processes and Landforms: The Journal of the British Geomorphological Group*, *23*(11), 989–1008, 1998.

Brooke, S., A. J. Chadwick, J. Silvestre, M. P. Lamb, D. A. Edmonds, and V. Ganti, Where rivers jump course, *Science*, *376*(6596), 987–990, 2022.

Bryant, M., P. Falk, and C. Paola, Experimental study of avulsion frequency and rate of deposition, *Geology*, *23*(4), 365–368, 1995.

Buffin-Bélanger, T., S. Demers, and A. Montané, Hydrogeomorphology: Recognition and evolution of the flood phenomenon, in *Floods*, pp. 167–191, Elsevier, 2017.

Bull, W. B., Alluvial fans, *Journal of Geological Education*, *16*(3), 101–106, 1968.

Cameron, V. J., The late quarternary geomorphic history of the sumas valley, 1989.

Cannon, S. H., J. E. Gartner, R. C. Wilson, J. C. Bowers, and J. L. Laber, Storm rainfall conditions for floods and debris flows from recently burned areas in southwestern Colorado and southern California, *Geomorphology*, *96*(3-4), 250–269, 2008.

Castro, J. M., and P. L. Jackson, Bankfull discharge recurrence intervals and regional hydraulic geometry relationships: Patterns in the Pacific Northwest, USA, *JAWRA Journal of the American Water Resources Association*, *37*(5), 1249–1262, 2001.

Chou, C., J. C. Chiang, C.-W. Lan, C.-H. Chung, Y.-C. Liao, and C.-J. Lee, Increase in the range between wet and dry season precipitation, *Nature Geoscience*, *6*(4), 263–267, 2013.

Chowdhury, M. K., A. Blom, C. Y. Arbós, M. C. Verbeek, M. H. Schropp, and R. M. Schielen, Semicentennial response of a bifurcation region in an engineered river to peak flows and human interventions, *Water Resources Research*, p. e2022WR032741, 2023.

Church, M., and R. Ferguson, Morphodynamics: Rivers beyond steady state, *Water Resources Research*, *51*(4), 1883–1897, 2015.

Coe, D., Floodplain visualization using lidar-derived relative elevation models, *Poster presented at Digital Mapping Techniques, Tallahassee, FL*, 2016.

Collier, M., R. H. Webb, and J. C. Schmidt, *Dams and rivers: a primer on the downstream effects of dams*, vol. 1126, US Department of the Interior, US Geological Survey, 1996.

Collins, B. D., and D. R. Montgomery, The legacy of Pleistocene glaciation and the organization of lowland alluvial process domains in the Puget Sound region, *Geomorphology*, *126*(1-2), 174–185, 2011.

Collins, B. D., S. E. Dickerson-Lange, S. Schanz, and S. Harrington, Differentiating the effects of logging, river engineering, and hydropower dams on flooding in the Skokomish River, Washington, USA, *Geomorphology*, *332*, 138–156, 2019.

Coombs, H. A., Mt. Baker, a cascade volcano, *Bulletin of the Geological Society of America*, *50*(10), 1493–1510, 1939.

Cornwall, W., Flood maps missed mark; Pacific homeowners got soaked, *The Seattle Times*, 2009.

Corringham, T. W., and D. R. Cayan, The effect of El Niño on flood damages in the western United States, *Weather, Climate, and Society*, *11*(3), 489–504, doi:10.1175/WCAS-D-18-0071.1, 2019.

Costa, A., P. Molnar, L. Stutenbecker, M. Bakker, T. A. Silva, F. Schlunegger, S. N. Lane, J.-L. Loizeau, and S. Girardclos, Temperature signal in suspended sediment export from an alpine catchment, *Hydrology and Earth System Sciences*, *22*(1), 509–528, 2018.

Czapiga, M. J., A. Blom, and E. Viparelli, Efficacy of longitudinal training walls to mitigate riverbed erosion, *Water Resources Research*, p. e2022WR033072, 2022.

Czuba, J. A., C. R. Czuba, C. S. Magirl, and F. D. Voss, *Channel-conveyance capacity, channel change, and sediment transport in the lower Puyallup, White, and Carbon Rivers, western Washington*, US Department of the Interior, US Geological Survey, 2010.

Czuba, J. A., C. S. Magirl, C. R. Czuba, C. A. Curran, K. H. Johnson, T. D. Olsen, H. K. Kimball, and C. C. Gish, Geomorphic analysis of the river response to sedimentation downstream of Mount Rainier, Washington, *Open-File Report*, pp. i–134, 2012.

Davidson, S., and B. Eaton, Beyond regime: A stochastic model of floods, bank erosion, and channel migration, *Water Resources Research*, *54*(9), 6282–6298, 2018.

De Almeida, G. A. M., and J. F. Rodríguez, Understanding pool-riffle dynamics through continuous morphological simulations, *Water Resources Research*, *47*(1), 2011.

Diakakis, M., E. Nikolopoulos, S. Mavroulis, E. Vassilakis, and E. Korakaki, Observational evidence on the effects of mega-fires on the frequency of hydrogeomorphic hazards. the case of the Peloponnese fires of 2007 in Greece, *Science of the total environment*, *592*, 262–276, 2017.

Dinehart, R. L., Evolution of coarse gravel bed forms: Field measurements at flood stage, *Water Resources Research*, *28*(10), 2667–2689, 1992.

Dury, G., Magnitude–frequency analysis and channel morphometry, *Fluvial geomorphology. NY State Univ. Publ. Geomorphol*, pp. 91–121, 1973.

East, A. E., K. J. Jenkins, P. J. Happe, J. A. Bountry, T. J. Beechie, M. C. Mastin, J. B. Sankey, and T. J. Randle, Channel-planform evolution in four rivers of Olympic National Park, Washington, USA: The roles of physical drivers and trophic cascades, *Earth Surface Processes and Landforms*, *42*(7), 1011–1032, 2017.

Engelund, F., and E. Hansen, A monograph on sediment transport in alluvial streams, *Technical University of Denmark ostervoldgade 10, Copenhagen K.*, 1967.

Erskine, W. D., Geomorphic controls on historical channel planform changes on the lower Pages River, Hunter Valley, Australia, *Australian Geographer*, *42*(3), 289–307, 2011.

Ervine, D., B. Willetts, R. Sellin, and M. Lorena, Factors affecting conveyance in meandering compound flows, *Journal of Hydraulic Engineering*, *119*(12), 1383–1399, 1993.

Etzelmüller, B., et al., Permafrost in monitored unstable rock slopes in Norway–new insights from temperature and surface velocity measurements, geophysical surveying, and ground temperature modelling, *Earth Surface Dynamics*, *10*(1), 97–129, 2022.

Falcone, J. A., GAGES-II: Geospatial attributes of gages for evaluating streamflow, *Tech. rep.*, US Geological Survey, 2011.

FEMA, Recommended procedures for flood velocity data development, *Tech. rep.*, Federal Emergency Management Agency Department of Homeland Security, 2012.

Fischer, E. M., and R. Knutti, Anthropogenic contribution to global occurrence of heavy-precipitation and high-temperature extremes, *Nature climate change*, *5*(6), 560–564, 2015.

Gaeuman, D., J. C. Schmidt, and P. R. Wilcock, Complex channel responses to changes in stream flow and sediment supply on the lower Duchesne River, Utah, *Geomorphology*, *64*(3-4), 185–206, 2005.

Gearon, J. H., and D. A. Edmonds, Investigating hypotheses for river avulsion using space-borne lidar, in *AGU Fall Meeting Abstracts*, vol. 2022, pp. EP16B–04, 2022.

Gendaszek, A. S., C. S. Magirl, and C. R. Czuba, Geomorphic response to flow regulation and channel and floodplain alteration in the gravel-bedded Cedar River, Washington, USA, *Geomorphology*, *179*, 258–268, doi:10.1016/j.geomorph.2012.08.017, 2012.

Gershunov, A., et al., Precipitation regime change in western North America: The role of atmospheric rivers, *Scientific reports*, *9*(1), 1–11, 2019.

Gessler, D., B. Hall, M. Spasojevic, F. Holly, H. Pourtaheri, and N. Raphelt, Application of 3d mobile bed, hydrodynamic model, *Journal of Hydraulic Engineering*, *125*(7), 737–749, 1999.

Gilbert, G. K., *Hydraulic-mining debris in the Sierra Nevada*, 105, US Government Printing Office, 1917.

Gilles, D., and M. Moore, Review of hydraulic flood modeling software used in Belgium, The Netherlands, and The United Kingdom, *International Perspectives in Water Resource Management*, *15*, 2010.

Gillett, N. P., et al., Human influence on the 2021 british columbia floods, *Weather and Climate Extremes*, *36*, 100,441, 2022.

Google, (August 10, 2021). Everson, Washington State, USA, *Google Earth: Maxar Technologies (retrieved from:http://www.earth.google.com)*, 2021.

Google, (February, 2022). Everson, Washington State, USA, *Google Earth (retrieved from:http://www.earth.google.com)*, 2022.

Grant, G. E., The geomorphic response of gravel-bed rivers to dams: perspectives and prospects, *In: Church, M.; Biron, PM; Roy, AG, eds. Gravel-bed rivers: processes, tools, environments. Chichester, UK: John Wiley & Sons, Ltd*, pp. 165–181, 2012.

Green, S. J., Pacific mayor blames corps for flooding, *The Seattle Times*, 2009.

Guan, M., J. L. Carrivick, N. G. Wright, P. A. Sleigh, and K. E. Staines, Quantifying the combined effects of multiple extreme floods on river channel geometry and on flood hazards, *Journal of Hydrology*, *538*, 256–268, 2016.

Gurnell, A., K. Tockner, P. Edwards, and G. Petts, Effects of deposited wood on biocomplexity of river corridors, *Frontiers in Ecology and the Environment*, *3*(7), 377–382, 2005.

Halpert, M., A. Barnston, M. L'Heureux, and E. Becker, El Niño and La Niña: Frequently asked questions, 2016.

Hamed, K., and A. R. Rao, *Flood frequency analysis*, CRC press, 2019.

Handwerger, A. L., E. J. Fielding, M.-H. Huang, G. L. Bennett, C. Liang, and W. H. Schulz, Widespread initiation, reactivation, and acceleration of landslides in the northern California Coast Ranges due to extreme rainfall, *Journal of Geophysical Research: Earth Surface*, *124*(7), 1782–1797, 2019.

Hansen, K., L. Dauphin, and J. Stevens, Severe Flooding in the Pacific Northwest, 2021.

Harmar, O. P., N. J. Clifford, C. R. Thorne, and D. S. Biedenharn, Morphological changes of the Lower Mississippi River: geomorphological response to engineering intervention, *River Research and Applications*, *21*(10), 1107–1131, 2005.

Harrell, J., Where and When Does Streamflow Regulation Significantly Affect Climate Change Outcomes in the Columbia River Basin? , Master's thesis, The University of Washington, 2021.

Havinga, H., Towards sustainable river management of the Dutch Rhine River, *Water*, *12*(6), 1827, 2020.

Helsel, D. R., and R. M. Hirsch, *Statistical methods in water resources*, vol. 49, Elsevier, 1992.

Hicks, D. M., M. McSaveney, and T. Chinn, Sedimentation in proglacial ivory lake, southern alps, new zealand, *Arctic and Alpine Research*, *22*(1), 26–42, 1990.

Hobley, D. E., J. M. Adams, S. S. Nudurupati, E. W. Hutton, N. M. Gasparini, E. Istanbulluoglu, and G. E. Tucker, Creative computing with landlab: an open-source toolkit for building, coupling, and exploring two-dimensional numerical models of earth-surface dynamics, *Earth Surface Dynamics*, *5*(1), 21–46, 2017.

Hodgkins, G., R. Dudley, S. A. Archfield, and B. Renard, Effects of climate, regulation, and urbanization on historical flood trends in the United States, *Journal of Hydrology*, *573*, 697–709, 2019.

Hoekstra, G., B.c., washington state working on nooksack river cross-border flooding solutions, *Vancouver Sun*, 2022.

Howard, A. D., Equilibrium and time scales in geomorphology: Application to sand-bed alluvial streams, *Earth Surface Processes and Landforms*, *7*(4), 303–325, 1982.

Hu, Z., X. Chen, D. Chen, J. Li, S. Wang, Q. Zhou, G. Yin, and M. Guo, "dry gets drier, wet gets wetter": A case study over the arid regions of central Asia, *International Journal of Climatology*, *39*(2), 1072–1091, 2019.

Jemberie, A. A., N. Pinter, and J. W. Remo, Hydrologic history of the Mississippi and Lower Missouri Rivers based upon a refined specific-gauge approach, *Hydrological Processes: An International Journal*, *22*(22), 4436–4447, 2008.

Jerolmack, D. J., and C. Paola, Shredding of environmental signals by sediment transport, *Geophysical Research Letters*, *37*(19), 2010.

Jongman, B., P. J. Ward, and J. C. Aerts, Global exposure to river and coastal flooding: Long term trends and changes, *Global Environmental Change*, *22*(4), 823–835, doi:10.1016/j.gloenvcha.2012.07.004, 2012.

Julien, P. Y., and G. J. Klaassen, Sand-dune geometry of large rivers during floods, *Journal of hydraulic engineering*, *121*(9), 657–663, 1995.

Kahraman, A., E. J. Kendon, S. C. Chan, and H. J. Fowler, Quasi-stationary intense rainstorms spread across europe under climate change, *Geophysical Research Letters*, *48*(13), e2020GL092,361, 2021.

Kahya, E., and J. A. Dracup, US streamflow patterns in relation to the El Niño/Southern Oscillation, *Water Resources Research*, *29*(8), 2491–2503, 1993.

Karimaee Tabarestani, M., and A. Zarrati, Sediment transport during flood event: a review, *International Journal of Environmental Science and Technology*, *12*, 775–788, 2015.

Kelly, J. M., P. Scarpino, H. Berry, J. Syvitski, and M. Meybeck, *Rivers of the Anthropocene*, University of California Press, 2017.

Kempe, Y., Tensions rise as Whatcom contemplates this flood prevention strategy, *The Bellingham Herald*, 2021.

Kjelstrom, L., Methods for estimating selected flow-duration and flood-frequency characteristics at ungaged sites in central idaho, *Water-Resources Investigations Report*, *94*, 4120, 1998.

Kleinhans, M. G., R. I. Ferguson, S. N. Lane, and R. J. Hardy, Splitting rivers at their seams: bifurcations and avulsion, *Earth surface processes and landforms*, *38*(1), 47–61, 2013.

Knutson, T. R., et al., Tropical cyclones and climate change, *Nature geoscience*, *3*(3), 157–163, 2010.

Konrad, C., H. Berge, R. Fuerstenberg, K. Steff, T. Olsen, and J. Guyenet, Channel dynamics in the Middle Green River, washington, from 1936 to 2002, *Northwest Science*, *85*(1), 1–14, 2011.

Kovanen, D., and O. Slaymaker, The paraglacial geomorphology of the Fraser Lowland, southwest British Columbia and northwest Washington, *Geomorphology*, *232*, 78–93, 2015.

Kovanen, D. J., R. A. Haugerud, and D. J. Easterbrook, Geomorphic map of western Whatcom County, Washington, *Tech. rep.*, US Geological Survey, 2020.

LaHusen, S. R., A. R. Duvall, A. M. Booth, and D. R. Montgomery, Surface roughness dating of long-runout landslides near Oso, Washington (USA), reveals persistent postglacial hillslope instability, *Geology*, *44*(2), 111–114, 2016.

Lancaster, S. T., and N. E. Casebeer, Sediment storage and evacuation in headwater valleys at the transition between debris-flow and fluvial processes, *Geology*, *35*(11), 1027–1030, doi:10.1130/G239365A.1, 2007.

Lane, E., The importance of fluvial geomorphology in hydraulic engineering: American society of civil engineers, *Proceedings, Journal of Hydraulics Divisions*, *81745*, 17, 1955.

Lauer, J. W., E. Viparelli, and H. Piégay, Morphodynamics and sediment tracers in 1-D (MAST-1D): 1-D sediment transport that includes exchange with an off-channel sediment reservoir, *Advances in Water Resources*, *93*, 135–149, 2016.

Le Coz, J., B. Renard, L. Bonnifait, F. Branger, and R. Le Boursicaud, Combining hydraulic knowledge and uncertain gaugings in the estimation of hydrometric rating curves: A Bayesian approach, *Journal of Hydrology*, *509*, 573–587, 2014.

Lee, S.-Y., A. F. Hamlet, and E. E. Grossman, Impacts of climate change on regulated streamflow, hydrologic extremes, hydropower production, and sediment discharge in the Skagit river basin, *Northwest Science*, *90*(1), 23–43, 2016.

Leggat, M. S., P. N. Owens, T. A. Stott, B. J. Forrester, S. J. Déry, and B. Menounos, Hydrometeorological drivers and sources of suspended sediment flux in the pro-glacial zone of the retreating Castle Creek Glacier, Cariboo Mountains, British Columbia, Canada, *Earth Surface Processes and Landforms*, *40*(11), 1542–1559, 2015.

Leonard, E. M., The relationship between glacial activity and sediment production: evidence from a 4450-year varve record of neoglacial sedimentation in hector lake, alberta, canada, *Journal of Paleolimnology*, *17*, 319–330, 1997.

Leopold, L. B., M. Gordon Wolman, and J. P. Miller, Fluvial processes in geomorphology, *Tech. rep.*, 1964.

Lesser, G. R., J. v. Roelvink, J. Van Kester, and G. Stelling, Development and validation of a three-dimensional morphological model, *Coastal engineering*, *51*(8-9), 883–915, 2004.

Li, Y., D. B. Wright, and P. K. Byrne, The Influence of Tropical Cyclones on the Evolution of River Conveyance Capacity in Puerto Rico, *Water Resources Research*, *56*(9), e2020WR027,971, 2020.

Lian, X., et al., Multifaceted characteristics of dryland aridity changes in a warming world, *Nature Reviews Earth & Environment*, *2*(4), 232–250, 2021.

Liang, C., M. Jaksa, B. Ostendorf, and Y. Kuo, Influence of river level fluctuations and climate on riverbank stability, *Computers and Geotechnics*, *63*, 83–98, 2015.

Lisle, T. E., Channel recovery from recent large floods in north coastal california: rates and processes, in *Proceedings of a symposium on watershed rehabilitation in Redwood National Park and other pacific coastal areas. Napa, CA: John Muir Institute, Center for Natural Resource Studies*, pp. 153–160, 1981.

Lisle, T. E., and S. Hilton, Fine bed material in pools of natural gravel bed channels, *Water Resources Research*, *35*(4), 1291–1304, 1999.

Lisle, T. E., J. M. Nelson, J. Pitlick, M. A. Madej, and B. L. Barkett, Variability of bed mobility in natural, gravel-bed channels and adjustments to sediment load at local and reach scales, *Water Resources Research*, *36*(12), 3743–3755, 2000.

Liu, C., Y. Shan, X. Liu, K. Yang, and H. Liao, The effect of floodplain grass on the flow characteristics of meandering compound channels, *Journal of Hydrology*, *542*, 1–17, 2016.

Lundquist, J. D., et al., Yosemite Hydroclimate Network: Distributed stream and atmospheric data for the Tuolumne River watershed and surroundings, *Water Resources Research*, *52*(9), 7478–7489, 2016.

Mackin, H. J., Concept of the graded river, *Geological Society of America Bulletin*, *59*(5), 463–512, 1948.

Magilligan, F. J., E. Buraas, and C. Renshaw, The efficacy of stream power and flow duration on geomorphic responses to catastrophic flooding, *Geomorphology*, *228*, 175–188, 2015.

Major, J. J., S. Zheng, A. Mosbrucker, K. R. Spicer, T. Christianson, and C. R. Thorne, Multidecadal geomorphic evolution of a profoundly disturbed gravel bed river system—a complex, nonlinear response and its impact on sediment delivery, *Journal of Geophysical Research: Earth Surface*, *124*(5), 1281–1309, 2019.

Mantua, N. J., S. R. Hare, Y. Zhang, J. M. Wallace, and R. C. Francis, A Pacific interdecadal climate oscillation with impacts on salmon production, *Bulletin of the american Meteorological Society*, *78*(6), 1069–1080, 1997.

Martin, Y., and D. Ham, Testing bedload transport formulae using morphologic transport estimates and field data: lower Fraser River, British Columbia, *Earth Surface Processes and Landforms: The Journal of the British Geomorphological Research Group*, *30*(10), 1265–1282, 2005.

Masteller, C. C., N. J. Finnegan, J. M. Turowski, E. M. Yager, and D. Rickenmann, History-dependent threshold for motion revealed by continuous bedload transport measurements in a steep mountain stream, *Geophysical Research Letters*, *46*(5), 2583–2591, 2019.

Mastin, M. C., C. P. Konrad, A. G. Veilleux, and A. E. Tecca, Magnitude, frequency, and trends of floods at gaged and ungaged sites in Washington, based on data through water year 2014, *Tech. rep.*, US Geological Survey, 2016.

Maudlin, M. R., and A. M. Stark, Analysis of nooksack river delta progradation into bellingham bay, washington using archival data sources [abs.], in *Geological Society of America, Cordilleran Section, 103rd Annual Meeting, Paper*, pp. 16–2, 2007.

May, C., et al., Impacts, Risks, and Adaptation in the United States: Fourth National Climate Assessment, Volume II, doi:10.7930/NCA4.2018.CH24, 2018.

Menounos, B., Anomalous early 20th century sedimentation in proglacial Green Lake, British Columbia, Canada, *Canadian Journal of Earth Sciences*, *43*(6), 671–678, 2006.

Menounos, B., and J. J. Clague, Reconstructing hydro-climatic events and glacier fluctuations over the past millennium from annually laminated sediments of Cheakamus Lake, southern Coast Mountains, British Columbia, Canada, *Quaternary Science Reviews*, *27*(7-8), 701–713, 2008.

Meyer-Peter, E., and R. Müller, Formulas for bed-load transport, in *IAHSR 2nd meeting, Stockholm, appendix 2*, IAHR, 1948.

Miall, A. D., A review of the braided-river depositional environment, *Earth-Science Reviews*, *13*(1), 1–62, 1977.

Michaelis, A. C., A. Gershunov, A. Weyant, M. A. Fish, T. Shulgina, and F. M. Ralph, Atmospheric river precipitation enhanced by climate change: A case study of the storm that contributed to California's Oroville Dam crisis, *Earth's Future*, *10*(3), e2021EF002,537, 2022.

Milhous, R. T., Sediment transport in a gravel-bottomed stream, 1973.

Milliman, J. D., K. Farnsworth, P. Jones, K. Xu, and L. Smith, Climatic and anthropogenic factors affecting river discharge to the global ocean, 1951–2000, *Global and planetary change*, *62*(3-4), 187–194, 2008.

Mohr, S., et al., A multi-disciplinary analysis of the exceptional flood event of july 2021 in central Europe–part 1: Event description and analysis, *Natural Hazards and Earth System Sciences*, *23*(2), 525–551, 2023.

Morgan, J., N. Kumar, A. R. Horner-Devine, W. Ni, S. Ahrendt, E. Istanbulluoblu, and E. Schwat, Modeling dynamic flood-risk at the event-timescale due to sediment transport and morphoydnamics, in prep.

Morgan, J. A., N. Kumar, A. R. Horner-Devine, S. Ahrendt, E. Istanbullouglu, and C. Bandaragoda, The use of a morphological acceleration factor in the simulation of large-scale fluvial morphodynamics, *Geomorphology*, *356*, 107,088, 2020.

Mote, P. W., Trends in snow water equivalent in the Pacific Northwest and their climatic causes, *Geophysical Research Letters*, *30*(12), 2003.

Mote, P. W., S. Li, D. P. Lettenmaier, M. Xiao, and R. Engel, Dramatic declines in snowpack in the western US, *Npj Climate and Atmospheric Science*, *1*(1), 1–6, 2018.

Moyo, E. N., and S. S. Nangombe, Southern Africa's 2012–13 violent storms: role of climate change, *Procedia Iutam*, *17*, 69–78, 2015.

Murray, V., and K. L. Ebi, IPCC special report on managing the risks of extreme events and disasters to advance climate change adaptation (SREX), 2012.

Nanson, G., and J. Croke, A genetic classification of floodplains, *Geomorphology*, *4*(6), 459–486, 1992.

Nardi, L., and M. Rinaldi, Spatio-temporal patterns of channel changes in response to a major flood event: the case of the Magra river (central–northern Italy), *Earth Surface Processes and Landforms*, *40*(3), 326–339, 2015.

Nederland, E., Actueel Hoogtebestand Nederland, versie 4, data retrieved from, https://hub.arcgis.com/maps/esrinl-content::ahn4-download-kaartbladen-1/about, 2021.

Neiman, P. J., L. J. Schick, F. M. Ralph, M. Hughes, and G. A. Wick, Flooding in western Washington: The connection to atmospheric rivers, *Journal of Hydrometeorology*, *12*(6), 1337–1358, 2011.

Nelson, A., and K. Dubé, Channel response to an extreme flood and sediment pulse in a mixed bedrock and gravel-bed river, *Earth Surface Processes and Landforms*, *41*(2), 178–195, 2016.

NOAA, National Weather Service advanced hydrologic prediction service.

Observatory, Y. V., How might the devastating june 2022 floods in and around Yellowstone National Park influence sesimic and hydrothermal activity?, 2022.

Ockelford, A., S. Woodcock, and H. Haynes, The impact of inter-flood duration on non-cohesive sediment bed stability, *Earth Surface Processes and Landforms*, *44*(14), 2861–2871, 2019.

Olson, P. L., N. T. Legg, T. B. Abbe, M. A. Reinhart, J. K. Radloff, et al., A methodology for delineating planning-level channel migration zones., *Tech. rep.*, Washington (State). Dept. of Ecology, 2014.

Paarlberg, A. J., C. M. Dohmen-Janssen, S. J. Hulscher, P. Termes, and R. Schielen, Modelling the effect of time-dependent river dune evolution on bed roughness and stage, *Earth Surface Processes and Landforms*, *35*(15), 1854–1866, 2010.

Parker, G., Transport of gravel and sediment mixtures, in *Sedimentation engineering: Processes, measurements, modeling, and practice*, pp. 165–251, 2008.

Parker, G., C. Paola, K. X. Whipple, and D. Mohrig, Alluvial fans formed by channelized fluvial and sheet flow. i: Theory, *Journal of Hydraulic engineering*, *124*(10), 985–995, 1998.

Patel, K., A. Coletta, J. Samenow, and L. Karklis, First fires, now floods: British columbia and washington reeling from atmospheric river, *The Washington Post*, 2021.

Payne, A. E., et al., Responses and impacts of atmospheric rivers to climate change, *Nature Reviews Earth & Environment*, *1*(3), 143–157, 2020.

Petley, D., The Hallett Peak rockslide in Rocky Mountain National Park, 2022.

Pfeiffer, A. M., and N. J. Finnegan, Regional variation in gravel riverbed mobility, controlled by hydrologic regime and sediment supply, *Geophysical Research Letters*, *45*(7), 3097–3106, 2018.

Pfeiffer, A. M., B. D. Collins, S. W. Anderson, D. R. Montgomery, and E. Istanbulluoglu, River bed elevation variability reflects sediment supply, rather than peak flows, in the uplands of Washington State, *Water Resources Research*, *55*(8), 6795–6810, 2019.

Pfeiffer, A. M., S. Morey, H. M. Karlsson, E. M. Fordham, and D. R. Montgomery, Survival of the strong and dense: Field evidence for rapid, transport-dependent bed material abrasion of heterogeneous source lithology, *Journal of Geophysical Research: Earth Surface*, *127*(6), e2021JF006,455, 2022.

Phillips, C. B., and D. J. Jerolmack, Self-organization of river channels as a critical filter on climate signals, *Science*, *352*(6286), 694–697, 2016.

Piégay, H., et al., Remotely sensed rivers in the Anthropocene: State of the art and prospects, *Earth Surface Processes and Landforms*, *45*(1), 157–188, 2020.

Pilgrim, D. H., and I. Cordery, Rainfall temporal patterns for design floods, *Journal of the Hydraulics Division*, *101*(1), 81–95, 1975.

Pinter, N., and R. A. Heine, Hydrodynamic and morphodynamic response to river engineering documented by fixed-discharge analysis, Lower Missouri River, USA, *Journal of Hydrology*, *302*(1-4), 70–91, doi:10.1016/j.jhydrol.2004.06.039, 2005.

Pittman, P., Lower Nooksack Geomorphic Assessment: Appendix A, Geologic and Geomorphic History, *Tech. rep.*, Prepared for Whatcom County Flood Control Zone District, 2019.

Pittman, P., M. Maudlin, and B. Collins, Evidence of a major late holocene river avulsion, in *Geological Society of America Abstracts with Programs*, vol. 35, p. 334, 2003.

Plink-Björklund, P., Morphodynamics of rivers strongly affected by monsoon precipitation: Review of depositional style and forcing factors, *Sedimentary Geology*, *323*, 110–147, 2015.

Poff, N. L., Rivers of the Anthropocene?, *Frontiers in Ecology and the Environment*, *12*(8), 427–427, 2014.

Ralph, F. M., M. D. Dettinger, M. M. Cairns, T. J. Galarneau, and J. Eylander, Defining "atmospheric river": How the glossary of meteorology helped resolve a debate, *Bulletin of the American Meteorological Society*, *99*(4), 837–839, 2018.

Read, L., and R. M. Vogel, Reliability, return periods, and risk under nonstationarity, *Journal of the American Water Resources Association*, *5*(3), 2–2, doi:10.1111/j.1752-1688.1969.tb04897.x, 1969.

Redolfi, M., Free alternate bars in rivers: Key physical mechanisms and simple formation criterion, *Water Resources Research*, *57*(12), e2021WR030,617, 2021.

Reid, I., L. E. Frostick, and J. T. Layman, The incidence and nature of bedload transport during flood flows in coarse-grained alluvial channels, *Earth Surface Processes and Landforms*, *10*(1), 33–44, 1985.

Reyer, C. P., et al., Climate change impacts in Latin America and the Caribbean and their implications for development, *Regional Environmental Change*, *17*, 1601–1621, 2017.

Rhoads, B., *River Dynamics Chapter 5–Sediment Transport Dynamics in Rivers*, Cambridge University Press, 2020.

Rijkswaterstaat, WAQUA/TRIWAQ: technical documentation. simona report 99-01, *Tech. rep.*, Rijkswaterstaat, 2015.

Rumsby, B. T., and M. G. Macklin, Channel and floodplain response to recent abrupt climate change: the Tyne basin, northern England, *Earth Surface Processes and Landforms*, *19*(6), 499–515, 1994.

Saltveit, S. J., Å. Brabrand, and J. E. Brittain, Rivers need floods: Management lessons learnt from the regulation of the Norwegian salmon river, Suldalslågen, *River Research and Applications*, *35*(8), 1181–1191, 2019.

Sauer, V. B., Standards for the analysis and processing of surface-water data and information using electronic methods, *Tech. rep.*, US Geological Survey, 2002.

Schielen, R. M. J., P. Jesse, and L. Botwidt, On the use of flexible spillways to control the discharge ratio of the Rhine in the Netherlands: hydraulic and morphological observations, *Netherlands journal of Geosciences*, *86*(1), 77–88, 2007.

Scholten, M., and J. Stout, Dataprotocol Baseline 5.2.2, data retrieved from, https://iplo.nl/thema/water/applicaties-modellen/watermanagementmodellen/baseline/?utm_source=hdwater&utm_medium=link&utm_campaign=applicatiesmodellen, 2013.

Schumm, S. A., The fluvial system, 1977.

Scott, D. N., and B. D. Collins, Frequent mass movements from glacial and lahar terraces, controlled by both hillslope characteristics and fluvial erosion, are an important sediment source to Puget Sound rivers, *Water Resources Research*, *57*(4), e2020WR028,389, 2021.

Searcy, K., James, Flow-duration curves; manual of hydrology: Part 2. low flow techniques, *Tech. rep.*, US Geological Survey, 1959.

Sellin, R., D. Ervine, and B. Willetts, Behaviour of meandering two-stage channels., *Proceedings of the Institution of Civil Engineers-Water Maritime and Energy*, *112*(2), 176–178, 1995.

Shields, A., Application of similarity principles and turbulence research to bed-load movement (translated), 1936.

Sholtes, J. S., S. E. Yochum, J. A. Scott, and B. P. Bledsoe, Longitudinal variability of geomorphic response to floods, *Earth Surface Processes and Landforms*, *43*(15), 3099–3113, 2018.

Šilhán, K., Dendrogeomorphological analysis of landslides on the undercut river terrace bank (a case study in czech republic), *Landslides*, *19*(3), 621–635, 2022.

Simons, D. B., E. V. Richardson, and W. L. Haushild, *Some effects of fine sediment on flow phenomena*, US Geological Survey, 1963.

Slater, L., To what extent have changes in channel capacity contributed to flood hazard trends in england and wales?, *Earth Surface Processes and Landforms*, *41*(8), 1115–1128, 2016.

Slater, L., and M. B. Singer, Imprint of climate and climate change in alluvial riverbeds: Continental United States, 1950-2011, *Geology*, *41*(5), 595–598, doi:10.1130/G34070.1, 2013.

Slater, L., M. B. Singer, and J. W. Kirchner, Hydrologic versus geomorphic drivers of trends in flood hazard, *Geophysical Research Letters*, *42*(2), 370–376, 2015.

Slater, L., A. Khouakhi, and R. Wilby, River channel conveyance capacity adjusts to modes of climate variability, *Scientific reports*, *9*(1), 1–10, 2019.

Slingerland, R., and N. D. Smith, River avulsions and their deposits, *Annu. Rev. Earth Planet. Sci.*, *32*, 257–285, 2004.

Sofia, G., and E. Nikolopoulos, Floods and rivers: a circular causality perspective, *Scientific reports*, *10*(1), 1–17, 2020.

Stover, S., and D. Montgomery, Channel change and flooding, Skokomish River, Washington, *Journal of Hydrology*, *243*(3-4), 272–286, 2001.

Te Linde, A., J. Aerts, A. Bakker, and J. Kwadijk, Simulating low-probability peak discharges for the rhine basin using resampled climate modeling data, *Water resources research*, *46*(3), 2010.

Thomas, H., and T. Nisbet, An assessment of the impact of floodplain woodland on flood flows, *Water and Environment Journal*, *21*(2), 114–126, 2007.

Todić, F., centerline (python): Version 1.0.1, https://centerline.readthedocs.io/en/latest/index.html, 2014.

Toebes, G. H., and A. A. Sooky, Hydraulics of meandering rivers with flood plains, *Journal of the Waterways and Harbors Division*, *93*(2), 213–236, 1967.

Tucker, D. S., K. M. Scott, E. E. Grossman, and S. Linneman, Mount Baker lahars and debris flows, ancient, modern, and future, *Field Guides*, *38*, 33–52, 2014.

Turowski, J. M., E. M. Yager, A. Badoux, D. Rickenmann, and P. Molnar, The impact of exceptional events on erosion, bedload transport and channel stability in a step-pool channel, *Earth Surface Processes and Landforms*, *34*(12), 1661–1673, 2009.

Underwood, K. L., D. M. Rizzo, M. M. Dewoolkar, and M. Kline, Analysis of reach-scale sediment process domains in glacially-conditioned catchments using self-organizing maps, *Geomorphology*, *382*, 107,684, 2021.

USGS, 1/3rd arc-second Digital Elevation Models (DEMs) - USGS National Map 3DEP Downloadable Data Collection, *Tech. rep.*, U.S. Geological Survey, 2017.

USGS-NWIS, National weather information system: Web interface, data retreived from https://waterdata.usgs.gov/nwis.

UW Geomorphological Research Group, Mosaicked 30-meter data for western (zone 10) Washington.

Van Denderen, P., and M. Van Hoek, Wavelet Application: Help Documentation, *Tech. rep.*, Rijkswaterstaat, 2022.

Van Denderen, R., M. Van Hoek, N. Van der Sleen, M. Reneerkens, and R. Schielen, An interactive atlas of river morphodynamics, *Abstract from NCR days*, 2022a.

Van Denderen, R. P., Bed level changes in the Waal during floods, Master's thesis, Technical University of Delft, Delft, The Netherlands, 2014.

Van Denderen, R. P., E. Kater, L. H. Jans, and R. M. Schielen, Disentangling changes in the river bed profile: The morphological impact of river interventions in a managed river, *Geomorphology*, *408*, 108,244, 2022b.

Van Steeter, M. M., and J. Pitlick, Geomorphology and endangered fish habitats of the upper Colorado River: 1. historic changes in streamflow, sediment load, and channel morphology, *Water Resources Research*, *34*(2), 287–302, 1998.

Vanderklippe, N., Could Canada hold the U.S. liable for billions in b.c. flood damage?, *The Globe and Mail*, 2021.

Vogel, R. M., C. Yaindl, and M. Walter, Nonstationarity: Flood magnification and recurrence reduction factors in the United States, *Journal of the American Water Resources Association*, *47*(3), 464–474, doi:10.1111/j.1752-1688.2011.00541.x, 2011.

WA-DNR, LiDAR Portal, 2023.

Wagner, A. M., K. E. Bennett, G. E. Liston, C. A. Hiemstra, and D. Cooley, Multiple indicators of extreme changes in snow-dominated streamflow regimes, Yakima River Basin region, USA, *Water*, *13*(19), 2608, 2021.

Ward, P. J., et al., A global framework for future costs and benefits of river-flood protection in urban areas, *Nature Climate Change*, *7*(9), 642–646, doi:10.1038/nclimate3350, 2017.

Warmink, J. J., M. Straatsma, F. Huthoff, M. J. Booij, and S. J. Hulscher, Uncertainty of design water levels due to combined bed form and vegetation roughness in the Dutch River Waal, *Journal of flood risk management*, *6*(4), 302–318, 2013.

Wasko, C., R. Nathan, L. Stein, and D. O'Shea, Evidence of shorter more extreme rainfalls and increased flood variability under climate change, *Journal of Hydrology*, *603*, 126,994, 2021.

Weibull, W., A statistical theory of strength of materials, *IVB-Handl.*, 1939.

Wilcock, P. R., and S. T. Kenworthy, A two-fraction model for the transport of sand/gravel mixtures, *Water Resources Research*, *38*(10), 12–1, 2002.

Wilcock, P. R., G. M. Kondolf, W. G. Matthews, and A. F. Barta, Specification of sediment maintenance flows for a large gravel-bed river, *Water Resources Research*, *32*(9), 2911–2921, 1996.

Winsemius, H. C., et al., Global drivers of future river flood risk, *Nature Climate Change*, *6*(4), 381–385, doi:10.1038/nclimate2893, 2016.

Wohl, E., Rivers in the landscape: Science and management, 2014.

Wohl, E., Rivers in the Anthropocene: The US perspective, *Geomorphology*, *366*, 106,600, 2020.

Wolman, M. G., and J. P. Miller, Magnitude and frequency of forces in geomorphic processes, *The Journal of Geology*, *68*(1), 54–74, 1960.

Wolman, M. G., L. B. Leopold, et al., *River flood plains: some observations on their formation*, vol. 282, US Government Printing Office Washington, DC, 1957.

Xiong, J., S. Guo, J. Chen, and J. Yin, A reexamination of the dry gets drier and wet gets wetter paradigm over global land: insight from terrestrial water storage changes, *Hydrology and Earth System Sciences Discussions*, pp. 1–20, 2022.

Yang, J., R. D. Townsend, and B. Daneshfar, Applying the HEC-RAS model and GIS techniques in river network floodplain delineation, *Canadian Journal of Civil Engineering*, *33*(1), 19–28, 2006.

Yang, T., J. Ding, D. Liu, X. Wang, and T. Wang, Combined use of multiple drought indices for global assessment of dry gets drier and wet gets wetter paradigm, *Journal of Climate*, *32*(3), 737–748, 2019.

Ylla Arbós, C., A. Blom, E. Viparelli, M. Reneerkens, R. Frings, and R. Schielen, River response to anthropogenic modification: Channel steepening and gravel front fading in an incising river, *Geophysical Research Letters*, *48*(4), e2020GL091,338, 2021.

Ylla Arbós, C., A. Blom, C. Sloff, and R. Schielen, Centennial channel response to climate change in an engineered river, *Geophysical Research Letters*, *50*(8), e2023GL103,000, 2023.

Yochum, S. E., J. S. Sholtes, J. A. Scott, and B. P. Bledsoe, Stream power framework for predicting geomorphic change: The 2013 Colorado Front Range flood, *Geomorphology*, *292*, 178–192, 2017.

Yousefi, S., S. Mirzaee, S. Keesstra, N. Surian, H. R. Pourghasemi, H. R. Zakizadeh, and S. Tabibian, Effects of an extreme flood on river morphology (case study: Karoon River, Iran), *Geomorphology*, *304*, 30–39, 2018.

Zagonjolli, M., 5th generation WAQUA subdomain models of Rijntakken, *Tech. rep.*, Deltares, 2015.